UNIVERSITA' DEGLI STUDI DI TRIESTE

UNIVERSITA' DEGLI STUDI DI TRIESTE

DIPARTIMENTO DI SCIENZE DELLA VITA

XXI° Ciclo del Dottorato di Ricerca in
SCIENZE BIOMOLECOLARI

NEW MOLECULAR INSIGHTS ABOUT HEPATOCELLULAR CARCINOMA BEHAVIOUR AND THE CONTROL OF CELL PROGRESSION

Settore scientifico-disciplinare BIO/11

Dottorando

DANIELE BAIZ

Coordinatore del Collegio Docenti
Chiar.mo prof. FRANCO VITTUR – UNIV. STUDI TRIESTE

Tutore/Supervisore
Chiar.mo prof. BRUNA SCAGGIANTE – UNIV. STUDI TRIESTE

Relatore
Chiar.mo prof. BRUNA SCAGGIANTE – UNIV. STUDI TRIESTE

Correlatore
Chiar.mo prof. GABRIELE GRASSI – UNIV. STUDI TRIESTE

ACKNOWLEDGEMENTS

I am extremely grateful to Prof. Gabriele Grassi and Prof. Bruna Scaggiante for allowing me to work under their enthusiastic guidance and for sharing their expertise in cell and molecular biology. I also thank Prof. Gabriele Pozzato for his entusiastic support regarding bortezomib project, Prof. Claudio Tiribelli and Dr. Licio Collavin. for their supervision and for their inspiring ideas.

I would like to express my sincere gratitude to Prof. Franco Vittur for his support during all the entire process.

I would like to express all my gratitude to all my colleagues, in particular to Dr. Barbara Dapas, for her important suggestions and for the fruitful discussions. Special credits must be given to Dr. Rossella Farra, and Dr. Francesco Agostini.

I am grateful to Dr. Nicola Fiotti to have introduced me to microarray technology.

There are many others who helped me in many ways through these three years, and even if I would love to, it is impossible for me to mention them all now.

Finally, my heartfelt thanks to my parents, and especially to my wife, to whom this thesis is dedicated, for her constant and important support and understanding during these challenging years.

RIASSUNTO

Il carcinoma epatocellulare (HCC) rappresenta la terza causa di morte per cancro nel mondo, con una stima di 564,000 nuovi casi nel 2000 e con un numero di decessi dello stesso ordine [1]. Nonostante l'alcoolizzazione, la chemo-emobilizzazione o l'ablazione termica, le recidive locali sono la regola e l'aspettativa di vita breve. Il trapianto di un fegato sano costituisce il migliore approccio terapeutico, anche perchè le fasi avanzate di questo tipo di tumore, caratterizzate da una pronunciata ipervascolarizzazione e chemio-resistenza, hanno quasi sempre una prognosi infausta.

Il fattore eucariotico di elongazione (eEF1A) è una proteina che gioca un ruolo determinante nel processo di traduzione. E' una GTP-binding protein, la cui funzione principale infatti è quella di reclutare l'amminoacil-tRNA e di trasportarlo sul sito A del ribosoma; per far ciò necessita di uno scambiatore di nucleotidi, eEF1B, e una molecola di GTP, che una volta idrolizzata permetterà il rilascio dell'amminoacil-tRNA sul ribosoma. eEF1A è codificata da solo due geni attivamente trascritti, rispettivamente EEF1A1 ed EEF1A2. Il primo mappa sul cromosoma 6q14.1, mentre il secondo sul cromosoma 20q13.3. Possiedono un'identità del 78% circa, mentre l'omologia di sequenza tra le due proteine è di circa il 92%. Nei Mammiferi eEF1A1 è espressa ubiquitariamente tranne nel tessuto scheletrico, cardiaco, nel cervello e nell'aorta, dove compare invece eEF1A2. eEF1A ha inoltre altre funzioni, definite non canoniche, in quanto è presente nei processi biochimici che regolano il citoscheletro, modulando la sua organizzazione durante il ciclo cellulare, in quanto ha due siti di legame per l'actina, uno all'N- e l'altro al C-terminale.

Sono state prese in considerazione due linee cellulari tumorali: le HepG2, le e le JHH6, che rappresentano i*n vitro* rispettivamente un modello di carcinoma epatocellulare ben differenziato e uno indifferenziato, onde capire quale possa esser il ruolo di eEF1A1 ed eEF1A2 nel carcinoma epatocellulare.

Gli esperimenti di Real Time PCR indicano che si ha iperespressione di EEF1A1 e l'attivazione genica ed iperespressione di EEF1A2. I livelli di mRNA di eEF1A, paragonati a quelli del fegato normale, risultano infatti aumentati in entrambe le linee tumorali. L'iperespressione di questi geni dipende solo in parte dall' amplificazione genica, in quanto si riscontra un modesto aumento nel numero dei geni. La maggior espressione di entrambe le forme di eEF1A nelle JHH6 trova conferma anche nei western blotting, dove si evidenzia un incremento di eEF1A nella linea JHH6 rispetto alle HepG2.

Nonostante gli alti livelli espressi di questi due geni, i dati in nostro possesso indicano che eEF1A non conferisce alle linee tumorali JHH6 e HepG2 una protezione da apoptosi indotta dall'assenza di siero, nè influenza la proliferazione delle cellule sub-confluenti. Alti livelli di eEF1A sono invece correlabili con il mantenimento nel ciclo cellulare delle JHH6, rispetto alle HepG2, in condizioni di confluenza. Infatti, il saggio della senescenza associata a β-gal indica che già dopo due giorni dalla confluenza, la linea HepG2 va in senescenza in modo maggiore rispetto alla linea JHH6. Dopo quattro giorni dalla confluenza, le HepG2 sono quasi totalmente senescenti, mentre le JHH6 non mostrano significativa attività di X-gal.

Si possono fare diverse ipotesi per dare una spiegazione a questo fenomeno, una delle quali potrebbe essere che nella linea JHH6 i livelli più alti di eEF1A1 influenzerebbero l'organizzazione del citoscheletro e quelli di eEF1A2 del ciclo cellulare conferendo una

maggior agressività a queste cellule sia in termini di motilità, che in termini di maggior resistenza a rimanere nel ciclo in condizioni estreme.

Il bortezomib è un derivato dipeptidilico dell'acido boronico e fa parte di una nuova classe di antineoplastici definiti come "inibitori del proteasoma 26S". Il proteasoma 26S è un complesso multienzimatico responsabile della degradazione via ubiquitina di proteine connesse con il ciclo cellulare, soppressori tumorali, oncogeni o inibitori correlati. Il bortezomib è il primo inibitore del proteasoma ad aver dimostrato una concreta efficacia terapeutica contro diverse neoplasie, tra cui alcune forme di leucemia mieloide, il mieloma multiplo (per cui ha già preso il via la sperimentazione clinica), i tumori della prostata, colon, polmone, ovaia, pancreas ed il melanoma. Non esistono tuttavia dati sulla sua possibile applicazione nei tumori epatici, nonchè attraverso quale/i meccanismo/i possa agire tale molecola. Le tre linee cellulari prese come modello di epatocarcinoma *in vitro*, sono state la linea HepG2, la linea HuH7 e la linea JHH6 che presentano un fenotipo simil-epatocitario per la prima, poco differenziato per la seconda ed epiteliode indifferenziata per la terza. Questo ci ha permesso di valutare se gli effetti del bortezomib potevano esser diversi in base al grado di differenziazione delle cellule tumorali epatiche.

I dati in nostro possesso indicano che il bortezomib agisce sul proteasoma 20S (subunità catalitica del proteasoma 26S) nelle linee di epatocarcinoma considerate e riduce il numero di cellule vitali con un meccanismo dose-dipendente. Il suo meccanismo d'azione nelle linee da noi esaminate si esplica a livello del ciclo cellulare che viene alterato, innescando solo in minor parte la morte cellulare programmata. La risultante è quindi un effetto di blocco della proliferazione più evidente nelle HepG2 e nelle HuH7,

rispetto alle JHH6 (anche se l'andamento dell'inibizione del proteasoma 20S sembra esser molto simile).

ABSTRACT

Hepatocellular carcinoma (HCC) is the most frequent type of liver cancer and the fifth leading cause of cancer-related death worldwide. Various aetiologies have been related to HCC development, but the most relevant being chronic hepatitis B virus (HBV) and hepatitis C virus (HCV) infections, chronic alcohol consumption and, in certain geographical areas, aflatoxin B1 food contamination. Approximately 10% of HCC patients show no signs of hepatitis virus infection, alcoholic history or other defined causes, such as genetic hemochromatosis or α_1-antitripsin deficiency. Although such environmental risk factors have been clearly defined, the distinct molecular events that occur during HCC development are still not fully understood.

We investigated the oncogenic role of the two forms of eukaryotic Elongation Factor 1A (eEF1A1/2) in the biology of HCC, as they have been recently proposed as important players in the process of oncogenic transformation and progression. The tumorogenic potential of eEF1A1 is supported by the observation that its over-expression correlates with increased metastatic potential in mammary adenocarcinoma. The ectopic expression of eEF1A2 induces the transformation towards a malignant phenotype of mouse and rat fibroblast and its expression in a human ovarian cell line that does not express eEF1A2 confers a more aggressive neoplastic phenotype compared to the parental cell line. Finally, amplification of the genome region encoding for eEF1A2 protein has been found in breast, colon and ovary tumors.

Results in the HCC cell lines HepG2, HuH7 and JHH6, indicated that EEF1A1 and, in JHH6 only, EEF1A2 are over-expressed when compared to normal liver tissue and this only in part depends on gene amplification. Moreover, the increased nuclear-

enriched/cytoplasmic protein ratio of eEF1A and the marked raise of both gene expression detected in JHH6 do not relate with apoptosis resistance. Finally, we observed that the increased of eEF1A expression is associated with an higher proliferation capacity in the undifferentiated JHH6 under sub-optimal growth conditions only.

Despite major efforts to improve diagnosis and treatment of HCC, therapeutic options remain limited. The main therapeutic strategies consists either of surgical resection of the tumor or of organ transplantation. However, most patients reach the late stages of the disease with liver cirrhosis, a condition for which surgery may no longer be indicated. Moreover, liver transplantation is limited by the number of donors. Other treatments such as alcohization, chemo-embolization or thermal ablation, do not prevent local recurrences and the life expectancy is short. Thus, the discovery of new therapeutic approaches is of clear clinical relevance.

Bortezomib is a boronic acid dipeptide derivative belonging to a new class of anti-cancer drugs, defined as 26S proteasome inhibitors. 26S proteasome is a multicatalytic complex involved in ubiquitinated proteins degradation, and bortezomib exerts its specific activity inhibiting the chymotrypsin – like activity of 26S proteasome. *In vitro*, many tumour cell lines have been shown to be susceptible to bortezomib-induced cell cycle arrest or cell death, while *in vivo* phase II and III clinical trials have been conducted in multiple myeloma and non-Hodgkin's lymphoma affected patients, demonstrating increased survival rate in bortezomib-treated patients compared to controls.

Despite the broad anti-cancer potential of bortezomib, little informations are available with regard to its effects on HCC. For these reasons, bortezomib effects on hepatocellular carcinoma cells was investigated.

Our data show the mechanisms regulating cell toxicity and proliferation inhibition effects of bortezomib on the HCC cell lines JHH6 and HuH7, expanding the knowledge on HepG2. The different phenotypes, hepatocyte-like for HepG2, low differentiated for HuH7 and undifferentiated for JHH6, together with the less overall effect of bortezomib on JHH6, suggests that *in vivo* not all HCC forms may respond similarly to bortezomib treatment. Despite this fact, the potent pro apoptotic effect reported, the cytotoxic and anti-proliferative actions here described together with the *in vitro* observed negligible toxicity on normal human hepatocytes, make of bortezomib an attractive candidate for future experimentation in animal models, alone or in combination with specific molecular-targeted drugs, such as siRNA, possibly leading to a novel treatment for HCC.

INDEX OF CONTENTS

INDEX OF PICTURES

INDEX OF TABLES

Introduction

1.1 The Hepatocellular Carcinoma

1.1.1 Distribution of HCC

Hepatocellular carcinoma (HCC) is among the most frequent type of liver cancer worldwide. At present, approximately 550000 new patients are diagnosed with HCC each year worldwide. However, regional differences in the incidence of HCC are significant (Fig. 1). The highest prevalence is found in southeast Asia and in the sub-saharian Africa, mostly due to the high rates of chronic viral hepatitis B and C (HBV and HCV), a high risk factors for HCC development. Additional causes linked to HCC are abuse of alcohol consumption, in certain geographical areas aflatoxin B1 food contamination, genetic hemocromatosis or α_1-antitripsin deficiency [1-4].

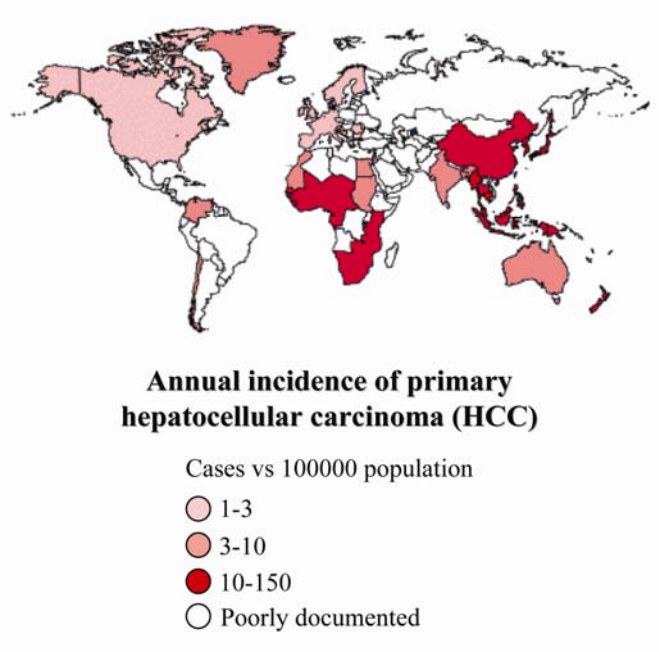

Figure 1. Distribution of hepatocellular carcinoma.

As evidenced, southeast Asia and sub-saharian Africa have the highest incident of HCC.

1.1.2 Hepatitis virus B and C

HBV and HCV represent a major risk factor for developing of hepatocellular carcinoma.

HBV (Fig. 2) infection is associated with about 40% of all HCC cases worldwide and most of the HBV-related HCCs contain viral DNA sequences integrated in human genome. Consequences of random and variable integrations reported are translocation, inverted duplication and recombination [5]. As consequence of these genomic alterations, some cellular regulatory genes could get lost.

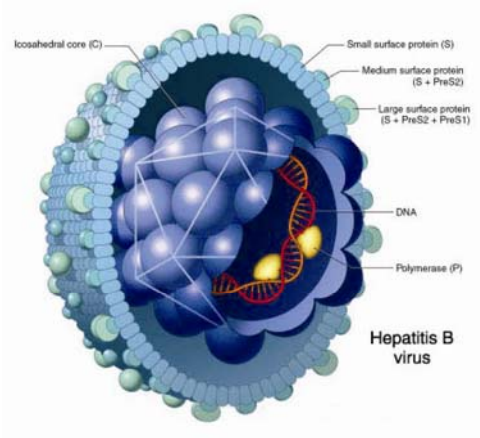

Figure 2. Hepatitis B virus model.

Hepatitis B virus (HBV) is a member of the*Hepadnavirus* family. The virus particle consists of an outer lipid envelope and an icosahedral nucleocapsid core composed of protein. The nucleocapsid encloses the viral DNA and a DNA polymerase that has reverse transcriptase activity. The outer envelope contains embedded proteins which are involved in viral binding of, and entry into, susceptible cells. The virus is one of the smallest enveloped animal viruses with a diameter of 42 nm.

It was reported that the HBx viral gene seems to play a more causal role in HBV-related HCC, because it is the most commonly integrated viral gene [6, 7]. HBx protein acts as transcriptional transactivator of viral genes, *via* the modulation of RNA polymerase II and III; moreover, it affects the cellular DNA repair system. HBx protein acts also as co-transcription factor for the major histocompatibility complex (MHC), deregulates cell cycle checkpoint controls and oncogenes like c-myc, c-jun/fos. These effects may alter host gene expression and lead to development of hepatocellular carcinoma. [6].

Compared to HBV-related hepatocarcinogenesis, much less is known about HCV-related liver damage (Fig. 3A and 3B). None of the different parts of the HCV genome is integrated into the host genome.

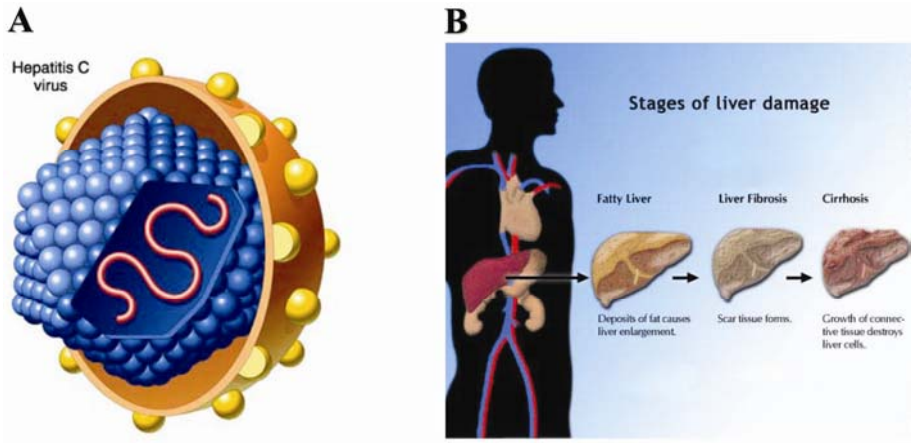

Figure 3.

A) Hepatitis C virus model.

Hepatitis C virus (HCV) is a small (55-65 nm in size), enveloped, positive sense single strand RNA virus in the family *Flaviviridae*. The structure of the hepatitis C virus consists of a core of genetic material (RNA), surrounded by an icosahedral protective shell of protein, and further encased in a lipid (fatty) envelope of cellular origin. Two viral envelope glycoproteins, E1 and E2, are embedded in the lipid envelope.

B) Cirrhosis development.

Cirrhosis is a consequence of chronic liver disease characterized by replacement of liver tissue by fibrous scar tissue as well as regenerative nodules (lumps that occur as a result of a process in which damaged tissue is regenerated), leading to progressive loss of liver function. Macroscopically, the liver may be initially enlarged, but with progression of the disease, it becomes smaller. Its surface is irregular, the consistency is firm and the colour is often yellow (if associates steatosis). Microscopically, cirrhosis is characterized by regeneration nodules, surrounded by fibrous septa. In these nodules, regenerating hepatocytes are disorderly disposed. Portal tracts, central veins and the radial pattern of hepatocytes are absent. Fibrous septa are important and may present inflammatory infiltrate (lymphocytes, macrophages)

It was demonstrated that HCV-related core protein indirectly activate the TNF-α receptor, the Raf-1 kinase and NF-κB pathways leading to inhibition of TNF-α-induced and Fas-mediated apoptosis [8-10]. These events might explain the development of liver carcinogenesis.

To gain better insight into HCV-related hepatocarcinogenesis, the microarray technology has been used in several studies. Honda *et al.* [11] and Shackel *et al.* [12] analyzed HCV cirrhosis and showed an up-regulation of pro-inflammatory, pro-apoptotic, and pro-proliferative genes, which might reflect groups of genes being involved in HCV-related cirrhosis during progression to HCC. Dou *et al.* [13] analyzed gene expression profiles of the HCV genotypes 1b, 2a, and 4d core proteins in HepG2 and HuH7 cells. The authors found that each core protein has its own expression profile and that each of them seems to be implicated in HCV replication and oncogenesis [13, 14].

1.1.3 Genomic instability of HCC

Recent studies have revealed a common genomic instability in human HCC. Conventional and array-based comparative genomic hybridization (aCGH) have been identified frequent DNA copy number gains at 1q, 6p, 8q, 17q, and 20q and losses at 1p, 4q, 8p, 13q, 16q, and 17p in HCC. Although target genes such as *RB1* (13q14) and *TP53* (17p13) have been identified and validated, the most part of altered loci remains unknown. Several aCGH studies have tried to identify chromosomal aberrations specifically related to HCC aetiology [15].

1.1.4 The Wnt pathway and HCC

The Wnt signalling pathway has been studied extensively with respect to cancer development and differentiation [16-19]. Several lines of evidence support an essential role of the Wnt/β-catenin signalling pathway in HCC. These include an increased

expression and nuclear accumulation of β-catenin as a feature of an activated Wnt signalling pathway [16, 20, 21]. Up to 62% of all HCC were shown to display such a deregulation of β-catenin. In addition, a multivariate analysis has demonstrated poorer prognosis and higher rate of tumour recurrence in patients with nuclear accumulation of β-catenin [20, 21].

Further attention was drawn to Wnt-/β-catenin-signalling when oncogenic β-catenin mutations were demonstrated to promote also the development of HCC. These mutations prevent β-catenin from being phosphorylated and thus prevent its degradation, resulting in activation of Wnt-/β-catenin signalling [22-24]. In addition, mutations of Axin1, a negative regulator of the Wnt signalling pathway, have also been reported to be highly prevalent in human HCC and transfection of wild type Axin1 lead to reconstitution of Wnt signalling and apoptosis in cancer cells [25, 26]. At a lower frequency, Axin2 mutations may contribute to HCC as well [27]. A liver-specific disruption of the APC gene in mice resulted in an activation of the Wnt-/β-catenin pathway and also in the development of HCC [28].

1.1.5 The Transforming Growth Factor β and HCC

Elevated expression levels of TGFβ in HCC tissues have been found by means of Northern blot and immunohistochemistry [29-31]. Expression of TGF-β1 in HCC tissue was correlated with poorer histological differentiation [31]. In addition, serum and urine TGFβ levels have been shown to correlate with poorer prognosis and increased tumour angiogenesis [32-34]. Furthermore, it has recently been described in several tumour

entities that during tumour progression [35, 36]. TGFβ activity continues to be increased due to autostimulation of the *Tgfb1* gene and due to transcriptional activation by Ras and other effectors, as well as by the action of proteases that activate the latent TGFβ in the extracellular matrix [37, 38].

1.1.6 Ras family and HCC

Overexpression of Ras and members of the signalling pathway such as $p21^{waf1/cip1}$ have been demonstrated in HCC [39, 40]. The three human ras genes (H-ras, N-ras and K-ras) encode for four proteins that function as small guanosine triphosphate (GTP) binding proteins, H-Ras, N-Ras, K-Ras4A and K-Ras4B [41-44]. The two forms of K-Ras only differ in their C-terminal 25 amino acids due to alternative splicing. Ras proteins are localized at the inner surface of the plasma membrane, where they serve as molecular switch to transduce extracellular signals into the cytoplasm to control signal transduction pathways that influence cell growth, differentiation and apoptosis [45]. Ras proteins can be activated by a wide range of extracellular proteins. For example, Ras proteins become activated following triggering of receptor tyrosine kinases such as the epidermal growth factor receptor (EGFR) [46].

Single amino acid substitutions at N-ras codon 12, H-ras codon 13 or K-ras codon 61, that unmask Ras transforming potential, create mutant proteins that are insensitive to GAP (Ras p120 **G**TPase **A**ctivation **P**rotein) stimulation [47]. Consequently, these oncogenic Ras mutant proteins are locked in the active, GTP-bound state, leading to constitutive, deregulated activation of Ras function. Likewise, inhibitors of the Ras pathway were

reported to be down-regulated in HCC [48]. Besides overexpression of Ras in HCC, mutations of the Ras proto-oncogenes, locking Ras in the active state, have been identified. The most commonly investigated mutations were the N-Ras codon 61 [49-51], the H-Ras codon 12 [52] and the K-Ras codon 12 mutation [53-55].

Ras mutations were continuously observed in HCC induced by various chemical agents in rats. These chemicals inducing HCC were N-nitrosomorpholine (NNM) [56], a combination of bleomycin and 1-nitropyrene [53], methyl (acetoxymethyl) nitrosamine [57], acetylaminofluorene (AAF) [140], 3-methyl-(dimethylamino) azobenzene [58], and nitroglycerine [59]. In accordance with these data originating from murine HCC models, tumour tissue of workers exposed to vinyl chloride were demonstrated to contain a significant level of Ras mutations, supporting evidence for a role of Ras mutations in HCC [60, 61]. As a consequence of the overexpression of the Ras pathway in HCC and in order to identify novel therapeutic targets for the treatment of HCC, various groups have lately studied regulation of the pathway by antisense RNA. Thereby, it has been reported that the antisense treatment for H-Ras significantly inhibited hepatocarcinogenesis and was able to reconstitute apoptosis [56, 62, 63]. In addition, novel therapeutic approaches using multikinase inhibitors such as sorafenib which targets Raf kinase in patients with advanced HCC, have displayed a moderate therapeutic efficacy as a single-agent and may now be evaluated for combination treatment with other anticancer agents [64].

1.1.7 The role of Retinoblastoma protein in HCC

Although a vast amount of data has been accumulated on the role of Retinoblastoma protein (Rb) in cancer differentiation for several cancer entities, only limited insight is available on a role of Rb in HCC differentiation.

The tumour suppressor retinoblastoma protein, is critical for the development of several cancer types. Rb is the target for phosphorylation by several kinases. In normal cell signalling, Rb prevents cell division and cell cycle progression [65]. Bound to the transcription factor E2F, Rb acts as a growth suppressor and prevents progression through the cell cycle [66]. Rb inhibits cell cycle progression only in the hypo-phosphorylated state, binding the transcription factor E2F [66].

Before entering S-phase, complexes of a cyclin-dependent kinases (CDK) and cyclins phosphorylate Rb [65-69]. Subsequently, phosphorylation of Rb results in the dissociation of E2F-DP from Rb [65, 66]. Free E2F can then activate cell cycle factors, leading to progression of the cell cycle (Fig. 4). Thus, cells with mutated Rb are subject to reduced control in cell cycle progression one of the hit required for the development of cancer.

Rb has been demonstrated to be inactivated in human HCC cell lines and in 28% of HCCs [70]. Simultaneously, additional members of the Rb network also have significantly aberrant expression in HCC. For example cyclin D1/CdK4, which inactivates Rb by phosphorylation, is over-expressed in 58% of HCCs [71]. Furthermore, the $p16^{ink4a}$ protein, a regulator of Rb activity through inhibition of CdK4, is absent in 34% of HCCs [72]. Together, these data suggest that disruption of the Rb regulatory pathway is common in HCC carcinogenesis.

1.2 The cell cycle

1.2.1 Cell cycle phases

The cell cycle consists of four distinct phases: G_1 phase, S phase (synthesis), G_2 phase (collectively known as interphase) and M phase (mitosis). M phase is itself composed of two tightly coupled processes: mitosis, in which the chromosomes are divided between the two daughter cells, and cytokinesis, in which the cytoplasm divides forming distinct cells. Activation of each phase is dependent on the proper progression and completion of the previous one. Cells that have temporarily or reversibly stopped dividing are said to have entered in a state of quiescence, called G_0 phase. Although the various stages of interphase are not usually morphologically distinguishable, each phase of the cell cycle has a distinct set of specialized biochemical processes that prepare the cell for initiation of cell division. Regulation of the cell cycle involves ordered and directional processes crucial to the survival of a cell, including the detection and repair of genetic damages as well as the prevention of uncontrolled cell division [73].

1.2.2 Cell cycle regulators

Two key classes of regulatory molecules, cyclins and cyclin-dependent kinases (CdKs), determine the cell progression through the cell cycle [74, 75]. Cyclins form the regulatory subunits and CdKs the catalytic subunits of an activated heterodimer; cyclins have no catalytic activity and CdKs are inactive in the absence of a cyclin partner. When activated by a bound cyclin, CdKs activates target proteins to orchestrate coordinated entry into the next phase of the cell cycle. CdKs are constitutively expressed in cells whereas cyclins are

synthesised at specific stages of the cell cycle, in response to various molecular signals. Cyclin D is the first cyclin produced in the cell cycle, in response to extracellular signals (eg. growth factors) [76, 77]. Cyclin D binds to existing CdK4, forming the active cyclin D-CdK4 complex. Cyclin D-CdK4 complex in turn phosphorylates the retinoblastoma protein (pRB) [78]. The hyperphosphorylated pRB released active E2F/DP complex. Activation of E2F results in transcription of various genes like cyclin D, cyclin E, cyclin A, CdKs, etc. [79]. Cyclin E thus produced binds to CdK2, forming the cyclin E-CdK2 complex, which pushes the cell from G_1 to S phase (G_1/S transition). Cyclin B along with CdK1 forms the cyclin B-CdK1 complex, which initiates the G_2/M transition [73, 80, 81].

1.2.3 Cell cycle inhibitors

Two families of genes, the INK4/ARF (*In*hibitor of *K*inase 4/*A*lternative *R*eading *F*rame) and the CIP/KIP inhibit the progression of the cell cycle [70, 82, 83]. The INK4/ARF family include $p16^{ink4a}$, which binds to CdK4 and arrests the cell cycle in G_1 phase, and $p14^{arf}$ which prevents p53 degradation. The CIP/KIP family includes the cell cycle inhibitors $p21^{waf1/cip1}$, $p27^{kip1}$ and $p57^{kip2}$. They inhibit cell cycle in G_1/S phase, by binding to, and inactivating, cyclin-CdK complexes. $p21^{waf1/cip1}$ can be activated also by p53, while $p27^{kip1}$ is activated by Transforming Growth Factor β (TGF β) [80]. A summary of cell cycle is reported in Figure 4.

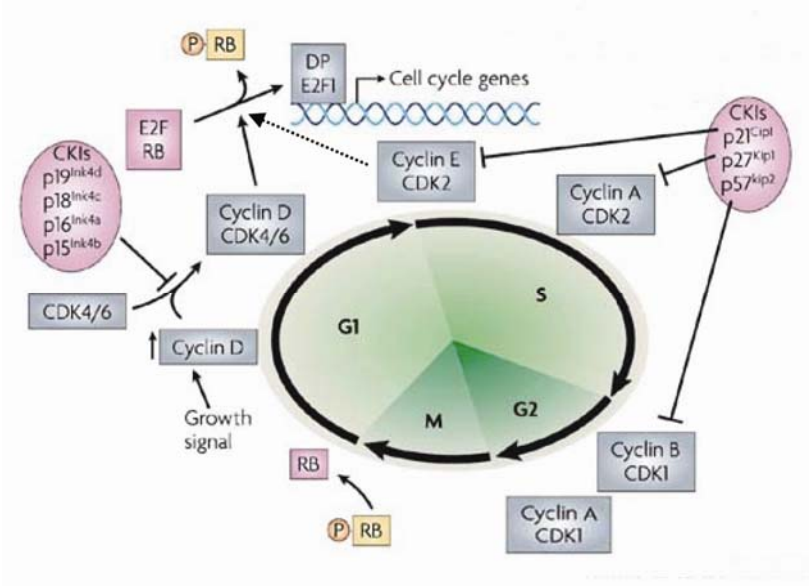

Figure 4. Cell cycle summary and related factors.

Here are reported the main factors related to cell cycle activation (Cyclin D, CdK 4/6, E2F), progression (Cyclin E, cyclin E, cyclin A, CdK 1/2, E2F) and inhibition ($p16^{ink4a}$, $p21^{waf1/cip1}$, $p27^{kip1}$, Rb).

1.3 The Eukaryotic Elongation Factor 1A

1.3.1 Role in protein elongation

The eukaryotic elongation factor 1A (eEF1A, eEF1α) catalyzes the first step of the elongation cycle [84, 85] It carries the aminoacyl-tRNA (aa-tRNA) on the A site of the ribosome which contains the growing polypeptide chain as peptidyl-tRNA in the P site. The aa-tRNA is carried on the ribosome as a ternary complex eEF1A-GTP-(aa-tRNA) and, following the hydrolysis of GTP, the eEF1A-GDP leaves the ribosome. This event allows the correct positioning of aa-tRNA in the A site of the ribosome in response to a correct codon-anticodon recognition. The second step of the elongation cycle involves the regeneration of the inactive GDP-bound form of eEF1A into the active GTP-bound form through an exchange reaction catalysed by the exchange factor 1Bα (eEF1Bα). After the formation of a new peptide bond catalysed by the ribosomal peptidyltransferase, a

peptidyl-tRNA is present on the A site of the ribosome and a deacylated tRNA in the P site (ribosome in pre-translocative state). In the third step of the elongation cycle, translocation, the elongated peptidyl-tRNA moves from the A site to the P site of the ribosome. The reaction is catalysed by the elongation factor 2. Following the hydrolysis of GTP, the complex eEF2-GDP leaves the ribosome, thus ending the translocation reaction. The elongation cycle is so completed and the machinery is ready to initiate a new cycle (Fig. 5) [86].

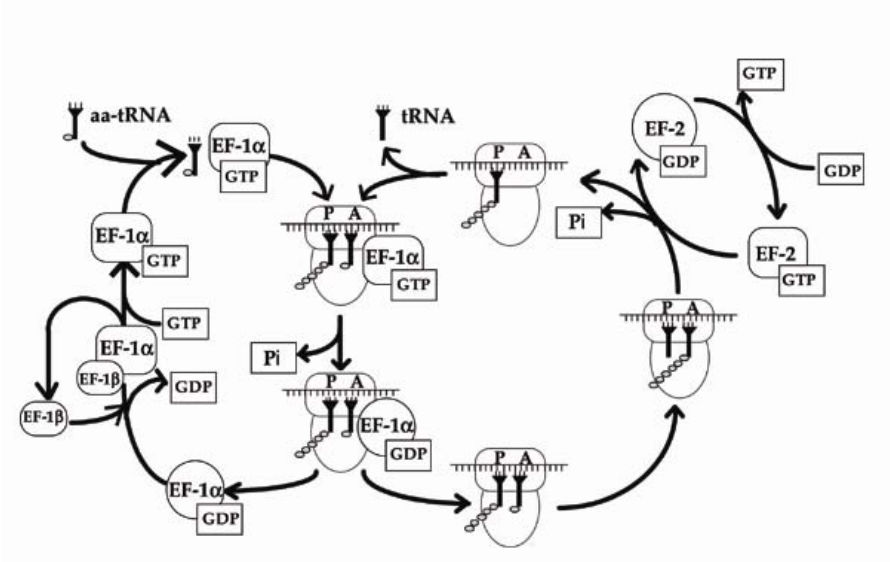

Figure 5. Protein synthesis elongation cycle.

Role of eEF1A, eEF1Bα and eEF2 in the first, second and third step of the elongation cycle, respectively.

aa-tRNA=aminoacyl-tRNA, EF-1α=elongation factor 1A, EF-1β=elongation factor 1Bα; EF-2=elongation factor 2, A and P=ribosomal A and P site

1.3.2 eEF1A1 and eEF1A2

In mammals several eEF1A-genes are present, but only two forms, termed eEF1A1 and eEF1A2, are actively transcribed. Human EEF1A1 has been mapped on chromosome 6q14, while human EEF1A2 has been mapped on 20q13.3 [87]. The two proteins are 92%

identical at the aminoacid level and display equal activities in an *in vitro* translation assay [88]. However, eEF1A1 is constitutively expressed in all known tissues except for skeletal muscle, whereas eEF1A2 expression appears to be limited to skeletal muscle, heart, brain and aorta [88, 89]. The transcription of eEF1A2 occurs concomitantly with a down-regulation of eEF1A1, indicating that eEF1A2 takes over the function of eEF1A1 in protein syntesis in a tissue-specific manner [90, 91].

1.3.3 Non-canonical functions of eEF1A and cancer

Beside the central role in protein translation, eEF1A is implicated in several biochemical processes including the interaction with the cytoskeleton [92, 93], apoptosis and cell proliferation. With regard to apoptosis, it has been shown that eEF1A2 ectopic over-expression protects muscle cells from caspase-3 induced apoptosis [94], and its absence in mice results in an increased muscle cell apoptosis [95]. eEF1A1 protects also against apoptosis induced by IL-3 withdrawal [96], and the acquisition of cisplatinum resistance in human head and neck cancer cell line is associated to eEF1A1 over-expression [97]. eEF1A interconnection with cell proliferation derives from the observations that eEF1A levels directly correlates to cell cycling rate [98-100]. Additionally, redistribution from the cytoplasm to the nucleus of eEF1A was observed in proliferating compared to starved cells [92].

The eEF1A ability to modulate apoptosis and cell growth has strictly linked this protein with cancer. Recently, eEF1A has been implicated in the process of oncogenic transformation. The tumorogenic potential of eEF1A1 has been proposed following the observation that its over-expression correlates with increased metastatic potential in

mammary adenocarcinoma [101]. The ectopic expression of eEF1A2 induces the transformation towards a malignant phenotype of mouse and rat fibroblast [102] and its expression in a human ovarian cell line that does not express eEF1A2 confers a more aggressive neoplastic phenotype compared to the parental cell line [103]. Finally, amplification of the genome region encoding for eEF1A2 protein has been found in breast, colon and ovary tumors [104-106].

1.4 The ubiquitin-proteasome pathway

1.4.1 Introduction

The ubiquitin-proteasome pathway is the primary mechanism for the disposal of damaged or unwanted proteins in the cells of eukaryotic organisms. Elimination of targeted regulatory proteins *via* this pathway is fundamental for the control of many essential cell functions, including cell cycle progression, gene transcription, signal transduction, inflammatory processes and apoptosis. The ubiquitin-proteasome protein degradation pathway (UPP) consists of ubiquitin, a three-enzyme ubiquitination complex, the intracellular protein ubiquitination targets, and the proteasome that is the organelle of protein degradation. The ubiquitination machinery is present both in the cytosol and in the nucleus [107, 108].

1.4.2 The UPP cascade

The ubiquitin-activating enzyme, E1, initiates ubiquitin ligation by adenylating ubiquitin [109, 110]. One ATP molecule is expended for each E1-ubiquitin linkage. The ubiquitin

molecule is transferred to the ubiquitin-conjugated enzyme E2, which transiently carries ubiquitin. E2 works in conjunction with the ubiquitin E3 ligase, which is responsible for conferring substrate specificity on the reaction. E3 mediates the transfer of ubiquitin to an internal lysine of the target protein. The first conjugated ubiquitin serves as a basal information for a polyubiquitin chain, which constitutes the protein degradation signal. The polyubiquitinated target protein undergoes proteolytic cleavage by the proteasome, which is a large, cylindrical multisubunit complex. The hierarchical organization of the ubiquitin-proteasome enzymatic conjugation cascade places a single E1 enzyme at the top, that activates ubiquitin for all subsequent downstream reactions and all E2 enzymes [110]. At the next stage, there are many E2 ubiquitin-conjugated enzymes that have defined but with a broad specificity. The last phase of ubiquitination is mediated by the E3 family of ubiquitin ligases, which is largely responsible for target protein specificity. Each E2 interacts with several E3s and each E3 targets with several substrates based on the shared recognition motifs. Each E3 can interact with more than one E2 and some substrates can be targeted by more than one E3 (Fig. 6) [111].

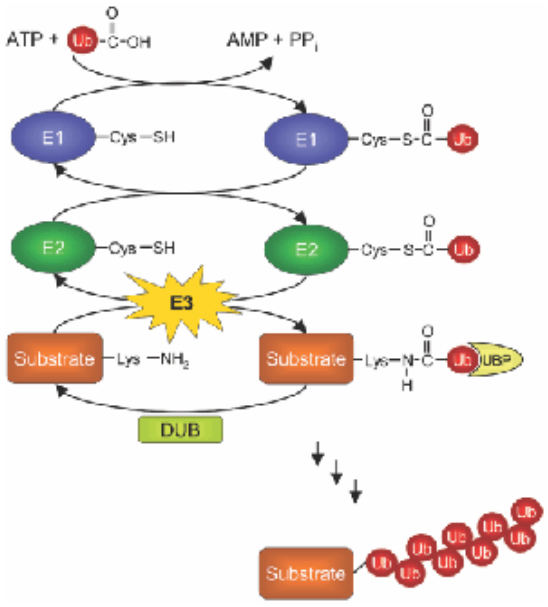

Figure 6. The ubiquitin E1-E2-E3 enzymatic cascade.

A ubiquitin-activating enzyme (E1) binds ubiquitin in an adenosine triphosphate (ATP)-dependent step. Ubiquitin is then transferred to a ubiquitin-conjugated enzyme (E2). A ubiquitin ligase (E3) helps transfer ubiquitin to the target substrate.

AMP=adenosine monophosphate
PP_i=pyrophosphate
Ub=ubiquitin

1.4.3 The 26S proteasome

1.4.3.1 Structure

The 26S proteasome is a multisubunits protein complex and is the site for ATP-dependent degradation of ubiquitin-tagged proteins [112-114]. The structure and function of the proteasome are highly conserved from archaebacteria to eukaryotes [115, 116].

The 26S proteasome is essentially a hollow cylinder-shaped particle formed by two major subunits that can assemble in an ATP-dependent manner [117, 118]. The 20S catalytic component contains multiple proteolytic sites, while the 19S regulatory components contain multiple ATPases and a binding site for ubiquitin concatamers (Fig. 7) [119].

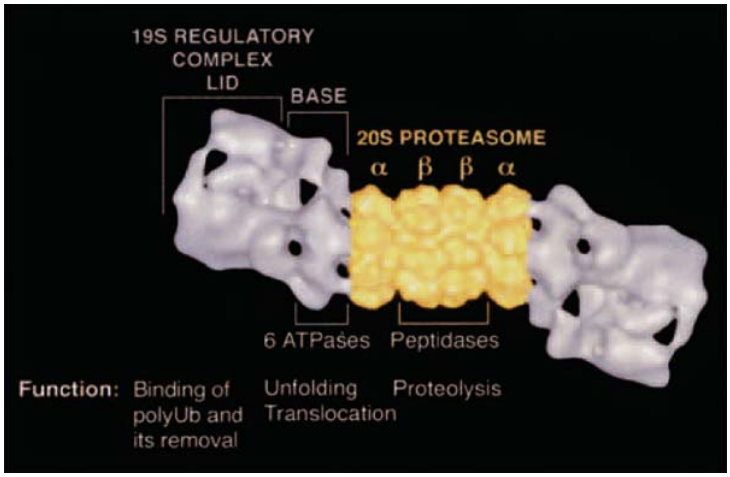

Figure 7. Structure of 26S proteasome.

The 19S regulatory particles attach to the outer surface of the 20S core particle. The 20S core particle contains four heptameric rings (two outer identical α rings and two inner identical β rings). The β rings of the 20S subunit harbour catalytic activity, and the 19S regulatory subunits function in substrate recognition, binding, and unfolding.

ATP=adenosine triphosphate
polyUb=polyubiquitination

The 20S subunit is the core of the 26S proteasome and it is formed by four heptameric protein rings harbouring catalytic sites that face into the hollow centre of the ring structure [118, 120]. The 20S catalytic-β-subunits contain trypsin (β2), chymotrypsin (β5) and post-glutamyl peptide hydrolase (β1)-like activities. The two α-rings sandwich the β-rings. The amino terminus of the α-subunits blocks the access to the proteolytic chamber, so the inner

cavity of the proteasome is only available through the narrow pores on both ends of the cylinder [121].

The 19S regulatory components assemble at each pore of the 20S subunit to form the 26S proteasome. The 19S subunits act as a gate agent limiting the entry of targeted proteins into the proteasome. The 19S subunits are also essential for proteolytic activity because the 20S subunit alone is inactive [111, 122]. A single 19S regulatory particle is composed of two substructures, a lid and base, involved in substrate selection, preparation and protein translocation into the catalytic chamber for degradation [122, 123]. Each 19S particle is composed of numerous subunits, including six ATPases, that most likely provide the energy necessary for substrate unfolding required before entry into the 20S chamber [124]. The outer-lid subcomplex of the 19S component is involved in the recognition and ubiquitin chain processing before substrate translocation and degradation [125, 126].

1.4.3.2 Degradation of Ub-proteins by 26S proteasome

Proteins are degraded in a processive manner by the proteasome; thus, a single protein is hydrolyzed to final products before the next substrate enters [127]. This ordered process contrasts to the activity of cytosolic proteases that cleave proteins once before dissociating from their substrates. The average length of the cleavage products in the proteasome varies from six to ten aminoacids; complete hydrolysis to individual aminoacids, occurs in the cytosol (Fig. 8) [128].

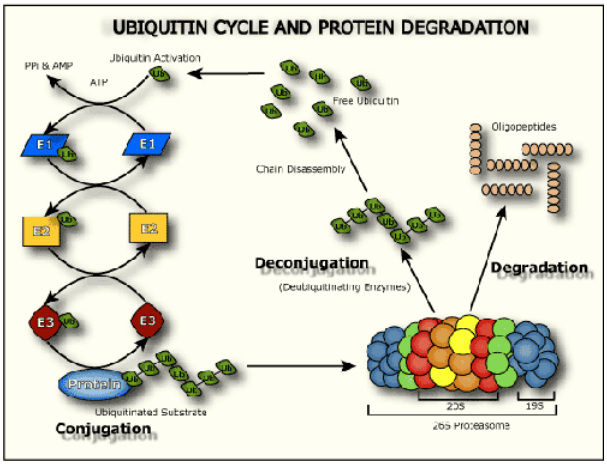

Figure 8. The ubiquitin-proteasome pathway.
Proteins marked with a polyubiquitin chain by the E1-E2-E3 enzymatic cascade are targeted for degradation by the proteasome. Proteins degraded through proteasome average six to ten aminoacids in length, and eventual hydrolysis to individual aminoacids occurs in the cytosol.

1.4.4 26S proteasome inhibitors

Because the 26S proteasome occupies a critical position in the regulation of cellular processes, its inhibition is under investigation as a potential anticancer therapy. The dideptide boronic acid analogue bortezomib (Fig. 9A and 9B) is the first proteasome inhibitor to be evaluated in human studies [129-133].

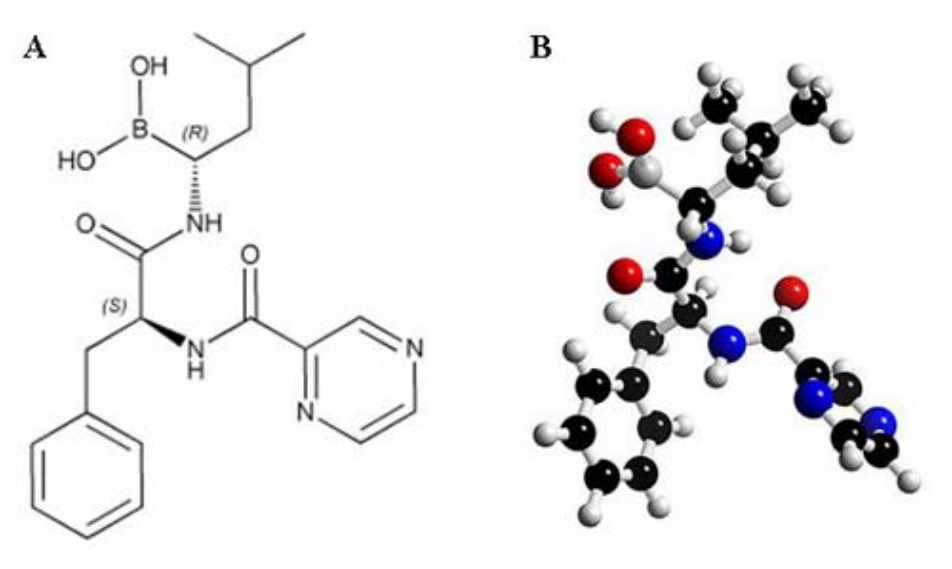

Figure 9. Bortezomib formula.

A) [(1R)-3-methyl-1-[[(2S)-1-oxo-3-phenyl-2-[(pyrazinylcabonyl) amino]propyl]amino]butyl]boronic acid.
B) Tridimensional model of bortezomib structure.

The first compound with documented effects on proteasomal function was identified as non-peptidic Streptomyces metabolite lactacystin. Its intermediate clasto-lactacystin β-lactone interferes with the β5-subunit (chymotrypsin-like activity) irreversibly by selective modification of amino-terminal threonine residues and reversibly with the β1-subunit (peptidylglutamyl-like activity) and β2-subunit (trypsin-like activity) [134, 135]. In the course of further characterizations of proteasome structure with x-ray crystallography, more selective and potent proteasome inhibitors were synthesized [136, 137]. They included tripeptide aldheydes, which inhibit reversibly β2- and β5- subunit by forming hemiacetal adducts with the active site of β-subunits. Moreover, they also inhibit thiol proteases like calpains and cathepsin B and display metabolic instability due to their configuration, so that poor specificity and bioavailability limit their utility *in vivo*. The next generation of proteasome inhibitors included boronic acid dipeptides like bortezomib, which are capable of building stable, but reversible, tetrahedrical intermediates with the amino-threonine residues of the catalytically active core complex of the 26S proteasome [136]. Bortezomib blocks the proteasome with a K_i value of 0,6 nM [138], with a restoration of proteasome activity within 24 hours [131]. This explains their slow dissociation from the proteasome in comparison to the aldehydes, the 1000-fold potency and the high sensitivity for chymotrypsin-like activities of the 26S proteasome. High selectivity, stability and low toxicity profile due to the reversibility of the proteasome inhibition, allowed bortezomib to enter clinical trials.

1.4.5 Bortezomib affects cell cycle progression and apoptosis

Cell division might be divided into 3 steps: DNA replication, mitosis and cytokinesis. In the G_1/S phase of the cell cycle, the sister chromatids are separated and synthesis of the

complimentary DNA takes place. The ordered processing of only one round of DNA replication in each cell cycle requires exactly coordinated levels of positive and negative regulators, such as cyclins, cyclin-dependent kinases (CDK), CDK-cyclin complexes and cyclin-dependend kinase inhibitors of the Cip/Kip and INK4 families [139].

The G_2/M phase of the cell cycle is responsible for proper localization of doubled chromosomes along kinetochore microtubules, division of sister chromatides and nuclear division. Cyclin B activates CDK1 and thus produces an active mitotic CDK-cyclin complex that promotes the entry into the prophase and consecutively the formation of mitotic spindle. Furthermore, the CDK-complex activates the anaphase-promoting complex/cyclosone (APC/C), which acts as a E3 ubiquitin ligase. APC catalyses the ubiquitination and thus initiates degradation of cyclin A and B, in order to ensure the completion of mitosis and re-enter into the next cell cycle [140]. Proteasome inhibition leads to stabilization and accumulation of both promoters and suppressors of the cell cycle. As a consequence, the cell receives aberrant signals thus getting arrested and activating the apoptotic program.

Apoptosis is a highly conserved process that ensures the tissue development during embryonic organogenesis, postembryonic organ growth and development [141]. A complex network of molecular events governs the activation of enzymatic DNA-fragmentation managed by caspases. The DNA degradation ultimately results in apoptosis. The direct mechanism of the 26S proteasome to generate anti-apoptotic signals and to promote survival is based on the observation that proteasome degrades pro-apoptotic proteins like Bax and Bid [142]. They both are members of the Bcl-2 family of apoptosis-regulating proteins localized in the outer mitochondrial membrane and regulate mitochondrial release of cytochrome c, which is a *sine qua non* condition for the execution

of apoptosis. Stabilization of Bax and the disruption of the Bax/Bcl-2 balance, enhances the mitochondrial apoptosis in tumour cells [143]. Table 1 reports target proteins of 26S proteasome.

Table 1. Target proteins of 26S proteasome.

Class of protein	Proteins	Functions
Apoptosis	Bax, IAPs, MDM2	Promotion of apoptosis
	Bcl-2	Inhibition of apoptosis
Cyclins	Cyclin A	Cell cycle regulation during S and M phases
	Cyclin B	Cell cycle regulation during M phase
	Cyclin D	Cell cycle regulation during G_1 phase
	Cyclin E	Cell cycle regulation during G_1-S transition
Cyclins dependent kinase inhibitors	$p21^{waf1/cip1}$	Cell cycle regulation
	$p27^{kip1}$	
Inhibitors of transcriptional factors	I-κB	Inhibition of transcriptional factor NF-κB
Oncogenes	c-Fos/c-Jun, c-Myc	Transcription factors
	B-catenin	Transcription regulator
Transcriptional factors	E2A	Cellular growth and differentiation
	E2F	Regulation of cell cycle genes
	STAT	Transcription of cytokine-inducible genes
Tumor suppressor proteins	p53	Apoptosis, cell cycle arrest, senescence
	Rb	Repressor of transcriptional factor E2F

1.4.6 Bortezomib and Nuclear Factor-kappa B pathway

Proteasome inhibitors drew clinical interest as potential antineoplastic agents owing to their ability to down-regulate the nuclear factor-kappa B (NF-κB) pathway, resulting in an anti-apoptotic and survival signals in neoplastic cells [144]. NF-κB is one of crucial

transcription initiators of various genes involved in cell proliferation and inflammation. Inactive NF-κB is found in cytoplasm, bound to its inhibitor IκB. IκB is a proteasomal substrate, which, after phosphorylation and ubiquitination, is degraded by the proteasome. Following IκB degradation, free NF-κB translocates into the nucleus promoting transcription of cytokines, growth factors and growth factor receptors (Fig. 10) [145, 146]. NF-κB activation is observed in many malignant cells undergoing radio- or chemotherapy. The molecular mechanism involved in chemosensitization due to proteasome inhibition includes the inhibition of aberrant NF-κB activation. Specific inhibition of NF-κB sensitized cells to chemotherapy, demonstrating that NF-κB is a target for circumventing drug resistance [133].

Since proteasome inhibition has been shown to block NF-κB activation, this strategy has been examined in various preclinical studies in order to disrupt tumour drug resistance and enhance chemosensitivity. Bortezomib-induced reduction of NF-κB activation led to diminished transcription of anti-apoptotic molecules [147], as well as pro-survival cytokines.

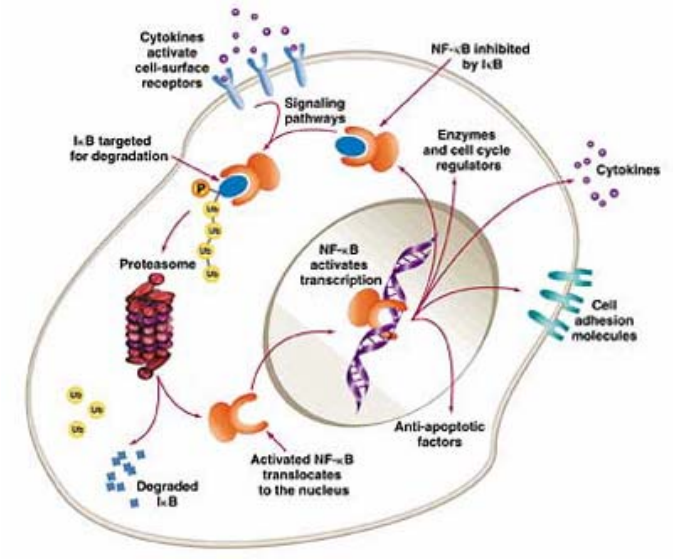

Figure 10. NF-κB pathway.

Degradation of NF-κB inhibithor, IκB, by ubiquitin-proteasome pathway activates NF-κB that translocates into the nucleus promoting transcription of cytokines, cell adhesion molecules, anti-apoptotic and cell cycle related factors.

1.4.7 Potential therapeutic value of bortezomib

In several *in vitro* and *in vivo* experiments many tumour cell lines have been shown to be susceptible to bortezomib-induced cell cycle arrest or cell death [148]. Pre-clinical studies have repeatedly demonstrated a selective susceptibility of transformed cells to proteasome inhibition [149]. Several group have explored the molecular basis by which proteasome inhibitors selectively mediate apoptosis in malignant cells and found that actively proliferating cells were more susceptible to proteasome inhibitor-mediated apoptosis than quiescent cells [150].

In human Bcr/Abl+ leukaemia cells resistant to imantinib (STI-1571, a protein kinase inhibitor), bortezomib induced synergistic apoptosis, when administered with cyclin-dependen kinase inhibitor flavopiridol [151], further demonstrating the chemosensitizing effects of bortezomib.

Exposure to bortezomib inhibits growth and causes apoptosis in cultured PC-3 prostate cancer cells [152]; bortezomib increased also the potency of camptothecin-11 (CPT-11) and radiation against colon tumour xenograft [153]; in addition, it enhanced the antitumour effect of gemcitabine and CPT-11 against pancreatic tumour xenograft [154]. Finally, bortezomib exerts a pro-apoptotic effect by decreasing the levels of XIAP protein, a member of the inhibitor of apoptosis (IAP) family, in ovarian carcinoma cells [155].

Non-Hodgkin's lymphoma (NHL) cells also appear to be affected by bortezomib. The agent has been shown to cause cell cycle arrest and rapid induction of apoptosis in mantle cell lymphoma (MCL) and primary effusion lymphoma (PEL) cells. As NF-kB is constitutively active in both these tumour types, inhibition of the NF-kB pathway by bortezomib may contribute to the apoptotic activity [149, 156]. In addition, bortezomib has been shown to induce apoptosis through the up-regulation of $p21^{waf1/cip1}$, $p27^{kip1}$ and

p53 in PEL cell lines [157]. The effectiveness of bortezomib in PEL cells is particularly significant, because these tumours, a rare subtype of NHL, are relatively resistant to standard cytotoxic chemotherapy [158]. Activity has also been demonstrated in cell samples derived from patients with MCL and patients with follicular lymphoma (FL). Using a primary culture system, bortezomib was found to be effective in cells from both NHL subtypes; MCL cells were significantly more sensitive to bortezomib than FL cells [159].

Expression of cell cycle regulators has been identified in bortezomib studies as an early effect of proteasome inhibition; this is followed by down-regulation of cyclin D1 expression and subsequent cell cycle arrest [156]. Bortezomib also demonstrated *in vivo* activity in MCL, suppressing cell growth and preventing the development of tumours in human MCL-xenografted mice [160]. Additionally, bortezomib has demonstrated potent inhibition of adult T-leukemia/lymphoma (ATLL) cell growth in *in vitro* and xenograft murine models [161]. The efficacy of bortezomib in several subtypes of NHL has been demonstrated in phase II clinical trials. A number of studies on bortezomib, both as a single agent and in combination with dexamethasone and doxorubicin, are ongoing or planned. Interim results indicate that bortezomib is well tolerated and active in NHL, with some durable response rates of 18-60% in FL and 39-56% in MCL. There is also preliminary evidence of drug activity in other subtypes of NHL, including marginal zone lymphoma (MZL) and Waldenström's macroglobulinemia (WM) [162-164].

In multiple myeloma cell lines and freshly isolated patient myeloma cells, bortezomib could induce apoptosis irrespective of p53 status and despite $p21^{waf1/cip1}$ and $p27^{kip1}$ induction, by inhibiting the mitogen-activated protein-kinase growth signalling and NF-κB signalling. NF-κB is constitutively active in myeloma cell lines and patient myeloma

samples [165]. Treatment of myeloma cell lines and patient samples with bortezomib resulted in growth inhibition, even in drug-resistant cell lines and correlates with I-κB stabilization and decrease of NF-κB activity. Interestingly, bone marrow stroma-mediated production of interleukin-6, a cytokine that plays an important role in myelomagenesis and whose transcription is up-regulated by NF-κB, was attenuated by bortezomib, demonstrating that proteasome inhibitors may achieve the anti-myeloma effects in part through modulation of the bone marrow microenvironment [166]. Bortezomib potently sensitizes myeloma cells to doxorubicin and melphalan, even in cases with confirmed resistance to these drugs by inhibiting genotoxic stress response pathways and thereby restoring sensitivity to DNA-damage induced by chemotherapeutic agents [167].

1.4.8 Multiple Myeloma treatment with bortezomib

Recently, phase III trial for treatment of refractory multiple myeloma (MM) patients was performed. The study evaluated bortezomib and dexamethasone therapy in patients with MM relapsed after 1-3 prior therapies, and results revealed a highly significant difference in response rates (38% for bortezomib/18% for dexamethasone), benefit in time to progression and overall survival for patients who received bortezomib [168]. Bortezomib has now been approved by the United States Food and Drug Administration and the European Medicine Evaluation Agency for patients with relapsed or refractory multiple myeloma.

In conclusion, bortezomib is the first proteasome inhibitor to enter human clinical trials, and results indicate that this drug may be particularly useful in anticancer therapy.

1.5 RNA interference pathway

RNA interference (RNAi) is a post-transcriptional gene-silencing phenomenon that occurs in eukaryotic organisms. It is involved in development regulation, genome maintenance and immune response to viral and transposon expansion [169, 170]. It was most notably described in *Caenorhabditis elegans* by Andrew Fire, Craig Mello and their colleagues in 1998 and represents an exciting development in the field of nucleic acid–based therapeutics [171].

The RNAi response is initiated when the guest cell encounters a long host dsDNA molecule-derived and it can be divided into two distinct steps. The first, called the assembly phase, comprises the recognition of a long dsRNA molecule and its processing by the RNase III-like enzyme Dicer into fragments of 19-21 nucleotides, termed short interfering RNAs (siRNAs). siRNAs are then incorporated into the RNA-induced silencing complex (RISC), a ribonucleoprotein composed of an Argonaute protein and a single-stranded guide RNA. The selection of the RNA strand that will be incorporated is governed by the thermodynamic profile of the siRNA duplex termini.

In the second phase, also known as the effector phase, ATP-activated RISC uses this single-stranded RNA molecule as a guide to cleave complementary mRNAs. The cleavage products are released and degraded, leaving the siRNA-RISC complex to survey and further deplete the available pool of target mRNAs. Although RISC-mediated target RNA cleavage is very studied, the final steps of the assembly process of RISC are still a matter of debate, especially how the “guide” strand is separated from the passenger strand (Fig. 11) [172, 173].

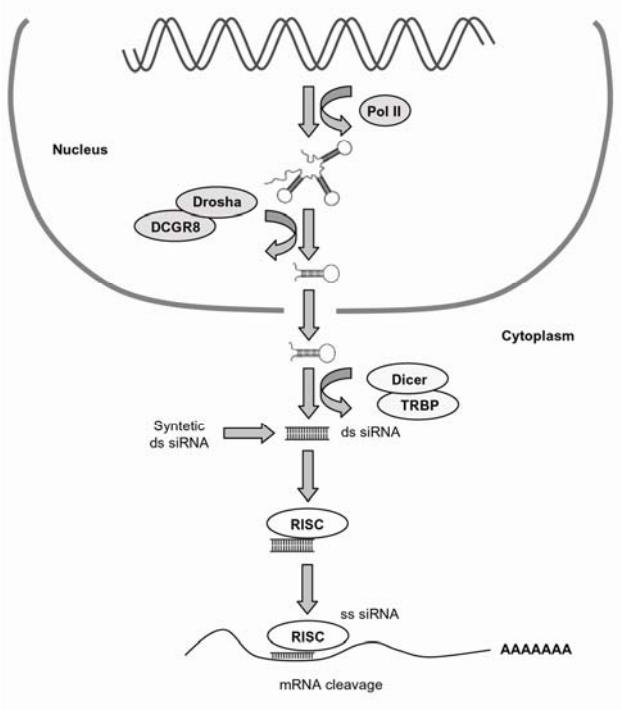

Figure 11. RNA interference pathway

In 2001 it was demonstrated that synthetic duplexes mimicking natural siRNAs, could be introduced into cultured mammalian cells to elicit sequence-specific inhibition of target mRNA, without the induction of interferon response [174, 175]. Additional studies have shown that the silencing effect is relatively stable and persist through several cell divisions. For these reasons, RNAi is considered a valuable tool for systematic gene function analysis, able to bypass the difficulties associated with creating multigene knockdown combinations [176]. As example, Sorkina *et al,* in order to identify proteins that partecipate in chlatrin-mediated endocytosis, have been depleted simultaneously thirteen endocytic proteins in HeLa cells, using highly efficient siRNAs [177]. They have been demonstrated that the specific and efficient gene silencing by siRNA could be used as an approach to functionally analyze the entire cellular machineries, such as the clathrin-coated pit [178].

In therapeutics, siRNAs hold promise as precise, target-specific silencers of desease-related genes and human pathogens [179, 180]. Inhibition of anti-angiogenetic or pro-apoptotic factors in endothelial cells seems to have a great potential for the treatment of ischemic diseases, promoting angiogenesis or inhibiting apoptosis [181]. On the other side, the advantage of silencing several important angiogenic factors may be in future a useful tool for treatment of tumors in which angiogenesis contribute to drug resistance, as in hepatocellular carcinoma (HCC) which is dependent on neovascularization. Inhibition of factors that are required for angiogenesis should therefore be effective in countering the growth of this cancer [182]. Wei *et al.* have also demonstrated that siRNA-mediated knockdown of hTERT (catalytic and rate-limiting subunit of telomerase activity), enhance the sensitivity of hepatocellular carcinoma cells to cisplatin, causing much greater extent of apoptosis. In this sense, one of the new siRNAs applications could be as "therapeutic enhancers" [183]. The enormous therapeutic potential of RNAi-based specific gene silencing has prompted enthusiasm for advancement of novel therapies for difficult to treat diseases, such as HCC. Developments have been exiting and clinical trials are now in progress for treatment. Use of gene silencing to treat HCC faces difficulties, because hepatocarcinogenesis is a multistep process with heterogeneous molecular mechanisms that drive hepatocyte transformation to malignancy. However, published data are promising that desease-specific siRNAs, in combination with advancements in conjugate chemistries may soon yield a new of therapeutic reagents.

1.6 Aim of the thesis

Hepatocellular carcinoma (HCC) is one of the most frequent type of liver cancer and is the fifth leading cause of cancer-related death worldwide. Although many environmental risk factors have been defined, the distinct molecular events that occur during HCC development are still not fully understood. Moreover, despite major efforts to improve diagnosis and treatment of HCC, available therapeutic options remain very limited in efficacy.

We investigated the oncogenic role of eEF1A1 and eEF1A2 factors in the biology of hepatocellular carcinoma, suggesting the possibility that eEF1A forms might become a relevant markers related to HCC tumor phenotype.

The tumorogenic potential of eEF1A1 has been proposed following the observation that its over-expression correlates with increased metastatic potential in mammary adenocarcinoma [101]. The ectopic expression of eEF1A2 induces the transformation towards a malignant phenotype of mouse and rat fibroblast [102] and its expression in a human ovarian cell line confers a more aggressive neoplastic phenotype compared to the parental cell line [103]. Finally, amplification of the genome region encoding for eEF1A2 protein has been found in breast, colon and ovary tumors [104-106].

Bortezomib is a boronic acid dipeptide derivative and takes part in a new class of anti-cancer drugs, defined as 26S proteasome inhibitors. *In vitro*, many tumour cell lines have been shown to be susceptible to bortezomib-induced cell cycle arrest or cell death, while *in vivo* phase II and III clinical trial have been conducted in multiple myeloma and non-Hodgkin's lymphoma affected patients [149, 168], revealing increased of survival for bortezomib-treated patients compared to controls.

Despite the broad anti-cancer potential of bortezomib, few informations are available so far with regard to its effects on hepatocellular carcinoma (HCC) [88, 93, 184], particularly on cell proliferation. It should be noted that in HCC patients, despite alcoholization, chemo-embolization or thermal ablation, the local tumor recurrences are the rule and life expectancy is short. Thus the identification of novel anti-HCC drugs is of utmost clinical relevance.

In this study, we report the evaluation of the cytotoxic and anti-proliferative effects of bortezomib in three human hepatic cell lines with a different phenotype, hepatocyte-like for HepG2, low differentiated for HuH7 and undifferentiated for JHH6 [185, 186] based on albumin expression, a known marker of hepatic differentiation.

Our data show that, despite a certain phenotype-dependent effect, bortezomib exerts potent cytotoxic and anti-proliferative effects on the three cell lines, supporting the rationale for a future use as anti-HCC agent.

1.7 REFERENCES

1. Motola-Kuba, D., et al., *Hepatocellular carcinoma. An overview.* Ann Hepatol, 2006. **5**(1): p. 16-24.
2. McGlynn, K.A. and W.T. London, *Epidemiology and natural history of hepatocellular carcinoma.* Best Pract Res Clin Gastroenterol, 2005. **19**(1): p. 3-23.
3. Srivatanakul, P., H. Sriplung, and S. Deerasamee, *Epidemiology of liver cancer: an overview.* Asian Pac J Cancer Prev, 2004. **5**(2): p. 118-25.
4. Teo, E.K. and K.M. Fock, *Hepatocellular carcinoma: an Asian perspective.* Dig Dis, 2001. **19**(4): p. 263-8.
5. Staib, F., et al., *TP53 and liver carcinogenesis.* Hum Mutat, 2003. **21**(3): p. 201-16.
6. Wang, X.W., et al., *Hepatitis B virus X protein inhibits p53 sequence-specific DNA binding, transcriptional activity, and association with transcription factor ERCC3.* Proc Natl Acad Sci U S A, 1994. **91**(6): p. 2230-4.
7. Hofseth, L.J., et al., *Nitric oxide-induced cellular stress and p53 activation in chronic inflammation.* Proc Natl Acad Sci U S A, 2003. **100**(1): p. 143-8.
8. You, L.R., et al., *Hepatitis C virus core protein interacts with cellular putative RNA helicase.* J Virol, 1999. **73**(4): p. 2841-53.
9. Marusawa, H., et al., *Hepatitis C virus core protein inhibits Fas- and tumor necrosis factor alpha-mediated apoptosis via NF-kappaB activation.* J Virol, 1999. **73**(6): p. 4713-20.
10. Block, T.M., et al., *Molecular viral oncology of hepatocellular carcinoma.* Oncogene, 2003. **22**(33): p. 5093-107.
11. Honda, M., et al., *Differential gene expression between chronic hepatitis B and C hepatic lesion.* Gastroenterology, 2001. **120**(4): p. 955-66.
12. Shackel, N.A., et al., *Insights into the pathobiology of hepatitis C virus-associated cirrhosis: analysis of intrahepatic differential gene expression.* Am J Pathol, 2002. **160**(2): p. 641-54.
13. Dou, J., et al., *Preliminary analysis of gene expression profiles in HepG2 cell line induced by different genotype core proteins of HCV.* Cell Mol Immunol, 2006. **3**(3): p. 227-33.
14. Dou, J., P. Liu, and X. Zhang, *Cellular response to gene expression profiles of different hepatitis C virus core proteins in the Huh-7 cell line with microarray analysis.* J Nanosci Nanotechnol, 2005. **5**(8): p. 1230-5.
15. Moinzadeh, P., et al., *Chromosome alterations in human hepatocellular carcinomas correlate with aetiology and histological grade--results of an explorative CGH meta-analysis.* Br J Cancer, 2005. **92**(5): p. 935-41.
16. Willert, K. and K.A. Jones, *Wnt signaling: is the party in the nucleus?* Genes Dev, 2006. **20**(11): p. 1394-404.
17. Johnson, M.L. and N. Rajamannan, *Diseases of Wnt signaling.* Rev Endocr Metab Disord, 2006. **7**(1-2): p. 41-9.

18. Kelleher, F.C., D. Fennelly, and M. Rafferty, *Common critical pathways in embryogenesis and cancer.* Acta Oncol, 2006. **45**(4): p. 375-88.
19. Janssens, N., M. Janicot, and T. Perera, *The Wnt-dependent signaling pathways as target in oncology drug discovery.* Invest New Drugs, 2006. **24**(4): p. 263-80.
20. Inagawa, S., et al., *Expression and prognostic roles of beta-catenin in hepatocellular carcinoma: correlation with tumor progression and postoperative survival.* Clin Cancer Res, 2002. **8**(2): p. 450-6.
21. Wong, C.M., S.T. Fan, and I.O. Ng, *beta-Catenin mutation and overexpression in hepatocellular carcinoma: clinicopathologic and prognostic significance.* Cancer, 2001. **92**(1): p. 136-45.
22. Hsu, H.C., et al., *Beta-catenin mutations are associated with a subset of low-stage hepatocellular carcinoma negative for hepatitis B virus and with favorable prognosis.* Am J Pathol, 2000. **157**(3): p. 763-70.
23. Mao, T.L., et al., *Expression of mutant nuclear beta-catenin correlates with non-invasive hepatocellular carcinoma, absence of portal vein spread, and good prognosis.* J Pathol, 2001. **193**(1): p. 95-101.
24. Terris, B., et al., *Close correlation between beta-catenin gene alterations and nuclear accumulation of the protein in human hepatocellular carcinomas.* Oncogene, 1999. **18**(47): p. 6583-8.
25. Devereux, T.R., et al., *CTNNB1 mutations and beta-catenin protein accumulation in human hepatocellular carcinomas associated with high exposure to aflatoxin B1.* Mol Carcinog, 2001. **31**(2): p. 68-73.
26. Huang, H., et al., *Beta-catenin mutations are frequent in human hepatocellular carcinomas associated with hepatitis C virus infection.* Am J Pathol, 1999. **155**(6): p. 1795-801.
27. Taniguchi, K., et al., *Mutational spectrum of beta-catenin, AXIN1, and AXIN2 in hepatocellular carcinomas and hepatoblastomas.* Oncogene, 2002. **21**(31): p. 4863-71.
28. Colnot, S., et al., *Liver-targeted disruption of Apc in mice activates beta-catenin signaling and leads to hepatocellular carcinomas.* Proc Natl Acad Sci U S A, 2004. **101**(49): p. 17216-21.
29. Matsuzaki, K., et al., *Autocrine stimulatory mechanism by transforming growth factor beta in human hepatocellular carcinoma.* Cancer Res, 2000. **60**(5): p. 1394-402.
30. Abou-Shady, M., et al., *Transforming growth factor betas and their signaling receptors in human hepatocellular carcinoma.* Am J Surg, 1999. **177**(3): p. 209-15.
31. Idobe, Y., et al., *Expression of transforming growth factor-beta 1 in hepatocellular carcinoma in comparison with the non-tumor tissue.* Hepatogastroenterology, 2003. **50**(49): p. 54-9.
32. Song, B.C., et al., *Transforming growth factor-beta1 as a useful serologic marker of small hepatocellular carcinoma.* Cancer, 2002. **94**(1): p. 175-80.
33. Tsai, J.F., et al., *Clinical relevance of transforming growth factor-beta 1 in the urine of patients with hepatocellular carcinoma.* Medicine (Baltimore), 1997. **76**(3): p. 213-26.

34. Tsai, J.F., et al., *Elevated urinary transforming growth factor-beta1 level as a tumour marker and predictor of poor survival in cirrhotic hepatocellular carcinoma.* Br J Cancer, 1997. **76**(2): p. 244-50.
35. Massague, J., *TGF-beta signal transduction.* Annu Rev Biochem, 1998. **67**: p. 753-91.
36. Ito, N., et al., *Positive correlation of plasma transforming growth factor-beta 1 levels with tumor vascularity in hepatocellular carcinoma.* Cancer Lett, 1995. **89**(1): p. 45-8.
37. Akhurst, R.J. and R. Derynck, *TGF-beta signaling in cancer--a double-edged sword.* Trends Cell Biol, 2001. **11**(11): p. S44-51.
38. Wakefield, L.M. and A.B. Roberts, *TGF-beta signaling: positive and negative effects on tumorigenesis.* Curr Opin Genet Dev, 2002. **12**(1): p. 22-9.
39. Jagirdar, J., et al., *ras oncogene p21 expression in hepatocellular carcinoma.* J Exp Pathol, 1989. **4**(1): p. 37-46.
40. Nonomura, A., et al., *Immunohistochemical detection of ras oncogene p21 product in liver cirrhosis and hepatocellular carcinoma.* Am J Gastroenterol, 1987. **82**(6): p. 512-8.
41. Boguski, M.S. and F. McCormick, *Proteins regulating Ras and its relatives.* Nature, 1993. **366**(6456): p. 643-54.
42. Barbacid, M., *ras genes.* Annu Rev Biochem, 1987. **56**: p. 779-827.
43. Bourne, H.R., L. Wrischnik, and C. Kenyon, *Ras proteins. Some signal developments.* Nature, 1990. **348**(6303): p. 678-9.
44. Quilliam, L.A., et al., *Guanine nucleotide exchange factors: activators of the Ras superfamily of proteins.* Bioessays, 1995. **17**(5): p. 395-404.
45. Satoh, T. and Y. Kaziro, *Ras in signal transduction.* Semin Cancer Biol, 1992. **3**(4): p. 169-77.
46. Reuther, G.W. and C.J. Der, *The Ras branch of small GTPases: Ras family members don't fall far from the tree.* Curr Opin Cell Biol, 2000. **12**(2): p. 157-65.
47. Clark, G.J., et al., *Differential antagonism of Ras biological activity by catalytic and Src homology domains of Ras GTPase activation protein.* Proc Natl Acad Sci U S A, 1993. **90**(11): p. 4887-91.
48. Schuierer, M.M., et al., *Raf kinase inhibitor protein is downregulated in hepatocellular carcinoma.* Oncol Rep, 2006. **16**(3): p. 451-6.
49. Challen, C., et al., *Infrequent point mutations in codons 12 and 61 of ras oncogenes in human hepatocellular carcinomas.* J Hepatol, 1992. **14**(2-3): p. 342-6.
50. Tsuda, H., et al., *Low incidence of point mutation of c-Ki-ras and N-ras oncogenes in human hepatocellular carcinoma.* Jpn J Cancer Res, 1989. **80**(3): p. 196-9.
51. Takada, S. and K. Koike, *Activated N-ras gene was found in human hepatoma tissue but only in a small fraction of the tumor cells.* Oncogene, 1989. **4**(2): p. 189-93.
52. Cerutti, P., et al., *Mutagenesis of the H-ras protooncogene and the p53 tumor suppressor gene.* Cancer Res, 1994. **54**(7 Suppl): p. 1934s-1938s.

53. Bai, F., et al., *Codon 64 of K-ras gene mutation pattern in hepatocellular carcinomas induced by bleomycin and 1-nitropyrene in A/J mice.* Teratog Carcinog Mutagen, 2003. **Suppl 1**: p. 161-70.
54. Boix-Ferrero, J., et al., *K-ras Gene Mutations in Liver Carcinomas from a Mediterranean Area of Spain.* Int J Surg Pathol, 2000. **8**(4): p. 267-270.
55. Soman, N.R. and G.N. Wogan, *Activation of the c-Ki-ras oncogene in aflatoxin B1-induced hepatocellular carcinoma and adenoma in the rat: detection by denaturing gradient gel electrophoresis.* Proc Natl Acad Sci U S A, 1993. **90**(5): p. 2045-9.
56. Baba, M., et al., *Ha-ras mutations in N-nitrosomorpholine-induced lesions and inhibition of hepatocarcinogenesis by antisense sequences in rat liver.* Int J Cancer, 1997. **72**(5): p. 815-20.
57. Watatani, M., et al., *Infrequent activation of K-ras, H-ras, and other oncogenes in hepatocellular neoplasms initiated by methyl(acetoxymethyl)nitrosamine, a methylating agent, and promoted by phenobarbital in F344 rats.* Cancer Res, 1989. **49**(5): p. 1103-9.
58. Li, H., et al., *Low frequency of ras activation in 2-acetylaminofluorene- and 3'-methyl-4-(dimethylamino)azobenzene-induced rat hepatocellular carcinomas.* Cancer Lett, 1991. **56**(1): p. 17-24.
59. Yamamoto, S., et al., *Rapid induction of more malignant tumors by various genotoxic carcinogens in transgenic mice harboring a human prototype c-Ha-ras gene than in control non-transgenic mice.* Carcinogenesis, 1996. **17**(11): p. 2455-61.
60. Weihrauch, M., et al., *High prevalence of K-ras-2 mutations in hepatocellular carcinomas in workers exposed to vinyl chloride.* Int Arch Occup Environ Health, 2001. **74**(6): p. 405-10.
61. Weihrauch, M., et al., *Frequent k- ras -2 mutations and p16(INK4A)methylation in hepatocellular carcinomas in workers exposed to vinyl chloride.* Br J Cancer, 2001. **84**(7): p. 982-9.
62. Liao, Y., et al., *Apoptosis of human BEL-7402 hepatocellular carcinoma cells released by antisense H-ras DNA--in vitro and in vivo studies.* J Cancer Res Clin Oncol, 1997. **123**(1): p. 25-33.
63. Liao, Y., et al., *Modulation of apoptosis, tumorigenesity and metastatic potential with antisense H-ras oligodeoxynucleotides in a high metastatic tumor model of hepatoma: LCI-D20.* Hepatogastroenterology, 2000. **47**(32): p. 365-70.
64. Abou-Alfa, G.K., et al., *Phase II study of sorafenib in patients with advanced hepatocellular carcinoma.* J Clin Oncol, 2006. **24**(26): p. 4293-300.
65. Das, S.K., et al., *Fucoxanthin induces cell cycle arrest at G0/G1 phase in human colon carcinoma cells through up-regulation of p21WAF1/Cip1.* Biochim Biophys Acta, 2005. **1726**(3): p. 328-35.
66. Munger, K. and P.M. Howley, *Human papillomavirus immortalization and transformation functions.* Virus Res, 2002. **89**(2): p. 213-28.
67. Korenjak, M. and A. Brehm, *E2F-Rb complexes regulating transcription of genes important for differentiation and development.* Curr Opin Genet Dev, 2005. **15**(5): p. 520-7.
68. Bartkova, J., et al., *Deregulation of the RB pathway in human testicular germ cell tumours.* J Pathol, 2003. **200**(2): p. 149-56.

69. Bartkova, J., et al., *Deregulation of the G1/S-phase control in human testicular germ cell tumours.* APMIS, 2003. **111**(1): p. 252-65; discussion 265-6.
70. Azechi, H., et al., *Disruption of the p16/cyclin D1/retinoblastoma protein pathway in the majority of human hepatocellular carcinomas.* Oncology, 2001. **60**(4): p. 346-54.
71. Joo, M., et al., *Cyclin D1 overexpression in hepatocellular carcinoma.* Liver, 2001. **21**(2): p. 89-95.
72. Hui, A.M., et al., *Inactivation of p16INK4 in hepatocellular carcinoma.* Hepatology, 1996. **24**(3): p. 575-9.
73. Schafer, K.A., *The cell cycle: a review.* Vet Pathol, 1998. **35**(6): p. 461-78.
74. Hartwell, L., et al., *Cell cycle checkpoints, genomic integrity, and cancer.* Cold Spring Harb Symp Quant Biol, 1994. **59**: p. 259-63.
75. Hartwell, L.H. and T.A. Weinert, *Checkpoints: controls that ensure the order of cell cycle events.* Science, 1989. **246**(4930): p. 629-34.
76. Adnane, J., Z. Shao, and P.D. Robbins, *Cyclin D1 associates with the TBP-associated factor TAF(II)250 to regulate Sp1-mediated transcription.* Oncogene, 1999. **18**(1): p. 239-47.
77. Siegert, J.L., et al., *Cyclin D1 suppresses retinoblastoma protein-mediated inhibition of TAFII250 kinase activity.* Oncogene, 2000. **19**(50): p. 5703-11.
78. Buchkovich, K., L.A. Duffy, and E. Harlow, *The retinoblastoma protein is phosphorylated during specific phases of the cell cycle.* Cell, 1989. **58**(6): p. 1097-105.
79. Duronio, R.J., et al., *E2F-induced S phase requires cyclin E.* Genes Dev, 1996. **10**(19): p. 2505-13.
80. Taylor, W.R. and G.R. Stark, *Regulation of the G2/M transition by p53.* Oncogene, 2001. **20**(15): p. 1803-15.
81. Porter, T.R., et al., *Contribution of cyclin d1 (CCND1) and E-cadherin (CDH1) polymorphisms to familial and sporadic colorectal cancer.* Oncogene, 2002. **21**(12): p. 1928-33.
82. Bloom, J., et al., *Proteasome-mediated degradation of p21 via N-terminal ubiquitinylation.* Cell, 2003. **115**(1): p. 71-82.
83. Sgambato, A., et al., *Multiple functions of p27(Kip1) and its alterations in tumor cells: a review.* J Cell Physiol, 2000. **183**(1): p. 18-27.
84. Moldave, K., *Eukaryotic protein synthesis.* Annu Rev Biochem, 1985. **54**: p. 1109-49.
85. Kaziro, Y., et al., *Structure and function of signal-transducing GTP-binding proteins.* Annu Rev Biochem, 1991. **60**: p. 349-400.
86. Dever, T.E., M.J. Glynias, and W.C. Merrick, *GTP-binding domain: three consensus sequence elements with distinct spacing.* Proc Natl Acad Sci U S A, 1987. **84**(7): p. 1814-8.
87. Lund, A., et al., *Assignment of human elongation factor 1alpha genes: EEF1A maps to chromosome 6q14 and EEF1A2 to 20q13.3.* Genomics, 1996. **36**(2): p. 359-61.
88. Knudsen, S.M., et al., *Tissue-dependent variation in the expression of elongation factor-1 alpha isoforms: isolation and characterisation of a cDNA encoding a novel variant of human elongation-factor 1 alpha.* Eur J Biochem, 1993. **215**(3): p. 549-54.

89. Kahns, S., et al., *The elongation factor 1 A-2 isoform from rabbit: cloning of the cDNA and characterization of the protein.* Nucleic Acids Res, 1998. **26**(8): p. 1884-90.

90. Lee, S., E. Stollar, and E. Wang, *Localization of S1 and elongation factor-1 alpha mRNA in rat brain and liver by non-radioactive in situ hybridization.* J Histochem Cytochem, 1993. **41**(7): p. 1093-8.

91. Lee, S., et al., *Terminal differentiation-dependent alteration in the expression of translation elongation factor-1 alpha and its sister gene, S1, in neurons.* Exp Cell Res, 1995. **219**(2): p. 589-97.

92. Gangwani, L., et al., *Interaction of ZPR1 with translation elongation factor-1alpha in proliferating cells.* J Cell Biol, 1998. **143**(6): p. 1471-84.

93. Condeelis, J., *Elongation factor 1 alpha, translation and the cytoskeleton.* Trends Biochem Sci, 1995. **20**(5): p. 169-70.

94. Ruest, L.B., R. Marcotte, and E. Wang, *Peptide elongation factor eEF1A-2/S1 expression in cultured differentiated myotubes and its protective effect against caspase-3-mediated apoptosis.* J Biol Chem, 2002. **277**(7): p. 5418-25.

95. Potter, M., A. Bernstein, and J.M. Lee, *The wst gene regulates multiple forms of thymocyte apoptosis.* Cell Immunol, 1998. **188**(2): p. 111-7.

96. Talapatra, S., J.D. Wagner, and C.B. Thompson, *Elongation factor-1 alpha is a selective regulator of growth factor withdrawal and ER stress-induced apoptosis.* Cell Death Differ, 2002. **9**(8): p. 856-61.

97. Johnsson, A., et al., *Identification of genes differentially expressed in association with acquired cisplatin resistance.* Br J Cancer, 2000. **83**(8): p. 1047-54.

98. Scaggiante, B., et al., *Interaction of G-rich GT oligonucleotides with nuclear-associated eEF1A is correlated with their antiproliferative effect in haematopoietic human cancer cell lines.* FEBS J, 2006. **273**(7): p. 1350-61.

99. Cavallius, J., S.I. Rattan, and B.F. Clark, *Changes in activity and amount of active elongation factor 1 alpha in aging and immortal human fibroblast cultures.* Exp Gerontol, 1986. **21**(3): p. 149-57.

100. Duttaroy, A., et al., *Apoptosis rate can be accelerated or decelerated by overexpression or reduction of the level of elongation factor-1 alpha.* Exp Cell Res, 1998. **238**(1): p. 168-76.

101. Edmonds, B.T., et al., *Elongation factor-1 alpha is an overexpressed actin binding protein in metastatic rat mammary adenocarcinoma.* J Cell Sci, 1996. **109 (Pt 11)**: p. 2705-14.

102. Lee, J.M., *The role of protein elongation factor eEF1A2 in ovarian cancer.* Reprod Biol Endocrinol, 2003. **1**: p. 69.

103. Anand, N., et al., *Protein elongation factor EEF1A2 is a putative oncogene in ovarian cancer.* Nat Genet, 2002. **31**(3): p. 301-5.

104. Schlegel, J., et al., *Comparative genomic in situ hybridization of colon carcinomas with replication error.* Cancer Res, 1995. **55**(24): p. 6002-5.

105. Tanner, M.M., et al., *Frequent amplification of chromosomal region 20q12-q13 in ovarian cancer.* Clin Cancer Res, 2000. **6**(5): p. 1833-9.

106. Hodgson, J.G., et al., *Genome amplification of chromosome 20 in breast cancer.* Breast Cancer Res Treat, 2003. **78**(3): p. 337-45.

107. Pickart, C.M., *Mechanisms underlying ubiquitination.* Annu Rev Biochem, 2001. **70**: p. 503-33.

108. Hershko, A. and A. Ciechanover, *The ubiquitin system.* Annu Rev Biochem, 1998. **67**: p. 425-79.

109. Handley, P.M., et al., *Molecular cloning, sequence, and tissue distribution of the human ubiquitin-activating enzyme E1.* Proc Natl Acad Sci U S A, 1991. **88**(1): p. 258-62.

110. Adams, J., *The proteasome: structure, function, and role in the cell.* Cancer Treat Rev, 2003. **29 Suppl 1**: p. 3-9.

111. Thrower, J.S., et al., *Recognition of the polyubiquitin proteolytic signal.* EMBO J, 2000. **19**(1): p. 94-102.

112. Voges, D., P. Zwickl, and W. Baumeister, *The 26S proteasome: a molecular machine designed for controlled proteolysis.* Annu Rev Biochem, 1999. **68**: p. 1015-68.

113. Hough, R., G. Pratt, and M. Rechsteiner, *Ubiquitin-lysozyme conjugates. Identification and characterization of an ATP-dependent protease from rabbit reticulocyte lysates.* J Biol Chem, 1986. **261**(5): p. 2400-8.

114. Zwickl, P., D. Voges, and W. Baumeister, *The proteasome: a macromolecular assembly designed for controlled proteolysis.* Philos Trans R Soc Lond B Biol Sci, 1999. **354**(1389): p. 1501-11.

115. Fujiwara, T., et al., *Proteasomes are essential for yeast proliferation. cDNA cloning and gene disruption of two major subunits.* J Biol Chem, 1990. **265**(27): p. 16604-13.

116. Emori, Y., et al., *Molecular cloning and functional analysis of three subunits of yeast proteasome.* Mol Cell Biol, 1991. **11**(1): p. 344-53.

117. Peters, J.M., W.W. Franke, and J.A. Kleinschmidt, *Distinct 19 S and 20 S subcomplexes of the 26 S proteasome and their distribution in the nucleus and the cytoplasm.* J Biol Chem, 1994. **269**(10): p. 7709-18.

118. Ganoth, D., et al., *A multicomponent system that degrades proteins conjugated to ubiquitin. Resolution of factors and evidence for ATP-dependent complex formation.* J Biol Chem, 1988. **263**(25): p. 12412-9.

119. Kisselev, A.F. and A.L. Goldberg, *Proteasome inhibitors: from research tools to drug candidates.* Chem Biol, 2001. **8**(8): p. 739-58.

120. Lowe, J., et al., *Crystal structure of the 20S proteasome from the archaeon T. acidophilum at 3.4 A resolution.* Science, 1995. **268**(5210): p. 533-9.

121. Wenzel, T. and W. Baumeister, *Conformational constraints in protein degradation by the 20S proteasome.* Nat Struct Biol, 1995. **2**(3): p. 199-204.

122. Glickman, M.H., et al., *A subcomplex of the proteasome regulatory particle required for ubiquitin-conjugate degradation and related to the COP9-signalosome and eIF3.* Cell, 1998. **94**(5): p. 615-23.

123. Larsen, C.N. and D. Finley, *Protein translocation channels in the proteasome and other proteases.* Cell, 1997. **91**(4): p. 431-4.

124. Glickman, M.H., et al., *The regulatory particle of the Saccharomyces cerevisiae proteasome.* Mol Cell Biol, 1998. **18**(6): p. 3149-62.

125. Deveraux, Q., et al., *A 26 S protease subunit that binds ubiquitin conjugates.* J Biol Chem, 1994. **269**(10): p. 7059-61.

126. Deveraux, Q., C. Jensen, and M. Rechsteiner, *Molecular cloning and expression of a 26 S protease subunit enriched in dileucine repeats.* J Biol Chem, 1995. **270**(40): p. 23726-9.

127. Akopian, T.N., A.F. Kisselev, and A.L. Goldberg, *Processive degradation of proteins and other catalytic properties of the proteasome from Thermoplasma acidophilum.* J Biol Chem, 1997. **272**(3): p. 1791-8.

128. Wenzel, T., et al., *Existence of a molecular ruler in proteasomes suggested by analysis of degradation products.* FEBS Lett, 1994. **349**(2): p. 205-9.

129. Shah, S.A., et al., *26S proteasome inhibition induces apoptosis and limits growth of human pancreatic cancer.* J Cell Biochem, 2001. **82**(1): p. 110-22.

130. Cusack, J.C., Jr., et al., *Enhanced chemosensitivity to CPT-11 with proteasome inhibitor PS-341: implications for systemic nuclear factor-kappaB inhibition.* Cancer Res, 2001. **61**(9): p. 3535-40.

131. Adams, J., et al., *Proteasome inhibitors: a novel class of potent and effective antitumor agents.* Cancer Res, 1999. **59**(11): p. 2615-22.

132. Bold, R.J., S. Virudachalam, and D.J. McConkey, *Chemosensitization of pancreatic cancer by inhibition of the 26S proteasome.* J Surg Res, 2001. **100**(1): p. 11-7.

133. Hideshima, T., et al., *The proteasome inhibitor PS-341 inhibits growth, induces apoptosis, and overcomes drug resistance in human multiple myeloma cells.* Cancer Res, 2001. **61**(7): p. 3071-6.

134. An, B., et al., *Novel dipeptidyl proteasome inhibitors overcome Bcl-2 protective function and selectively accumulate the cyclin-dependent kinase inhibitor p27 and induce apoptosis in transformed, but not normal, human fibroblasts.* Cell Death Differ, 1998. **5**(12): p. 1062-75.

135. Fenteany, G., et al., *Inhibition of proteasome activities and subunit-specific amino-terminal threonine modification by lactacystin.* Science, 1995. **268**(5211): p. 726-31.

136. Hough, R., G. Pratt, and M. Rechsteiner, *Purification of two high molecular weight proteases from rabbit reticulocyte lysate.* J Biol Chem, 1987. **262**(17): p. 8303-13.

137. Dick, L.R., et al., *Mechanistic studies on the inactivation of the proteasome by lactacystin in cultured cells.* J Biol Chem, 1997. **272**(1): p. 182-8.

138. Loidl, G., et al., *Bivalency as a principle for proteasome inhibition.* Proc Natl Acad Sci U S A, 1999. **96**(10): p. 5418-22.

139. Shah, I.M., et al., *Early clinical experience with the novel proteasome inhibitor PS-519.* Br J Clin Pharmacol, 2002. **54**(3): p. 269-76.

140. Hershko, A., *Roles of ubiquitin-mediated proteolysis in cell cycle control.* Curr Opin Cell Biol, 1997. **9**(6): p. 788-99.

141. Turnell, A.S., et al., *The APC/C and CBP/p300 cooperate to regulate transcription and cell-cycle progression.* Nature, 2005. **438**(7068): p. 690-5.

142. Hengartner, M.O., *The biochemistry of apoptosis.* Nature, 2000. **407**(6805): p. 770-6.

143. Chang, Y.C., et al., *mdm2 and bax, downstream mediators of the p53 response, are degraded by the ubiquitin-proteasome pathway.* Cell Growth Differ, 1998. **9**(1): p. 79-84.

144. Orlowski, R.Z. and A.S. Baldwin, Jr., *NF-kappaB as a therapeutic target in cancer.* Trends Mol Med, 2002. **8**(8): p. 385-9.

145. Traenckner, E.B., S. Wilk, and P.A. Baeuerle, *A proteasome inhibitor prevents activation of NF-kappa B and stabilizes a newly phosphorylated form of I kappa B-alpha that is still bound to NF-kappa B.* EMBO J, 1994. **13**(22): p. 5433-41.

146. Palombella, V.J., et al., *Role of the proteasome and NF-kappaB in streptococcal cell wall-induced polyarthritis.* Proc Natl Acad Sci U S A, 1998. **95**(26): p. 15671-6.

147. Wang, C.Y., et al., *Control of inducible chemoresistance: enhanced anti-tumor therapy through increased apoptosis by inhibition of NF-kappaB.* Nat Med, 1999. **5**(4): p. 412-7.

148. Teicher, B.A., et al., *The proteasome inhibitor PS-341 in cancer therapy.* Clin Cancer Res, 1999. **5**(9): p. 2638-45.

149. Zavrski, I., et al., *Proteasome: an emerging target for cancer therapy.* Anticancer Drugs, 2005. **16**(5): p. 475-81.

150. Ganten, T.M., et al., *Proteasome inhibition sensitizes hepatocellular carcinoma cells, but not human hepatocytes, to TRAIL.* Hepatology, 2005. **42**(3): p. 588-97.

151. Tan, C. and T.A. Waldmann, *Proteasome inhibitor PS-341, a potential therapeutic agent for adult T-cell leukemia.* Cancer Res, 2002. **62**(4): p. 1083-6.

152. Papandreou, C.N., et al., *Phase I trial of the proteasome inhibitor bortezomib in patients with advanced solid tumors with observations in androgen-independent prostate cancer.* J Clin Oncol, 2004. **22**(11): p. 2108-21.

153. Coquelle, A., et al., *Cell cycle-dependent cytotoxic and cytostatic effects of bortezomib on colon carcinoma cells.* Cell Death Differ, 2006. **13**(5): p. 873-5.

154. Maki, R.G., et al., *A multicenter Phase II study of bortezomib in recurrent or metastatic sarcomas.* Cancer, 2005. **103**(7): p. 1431-8.

155. Kudo, Y., et al., *Reduced expression of p27(Kip1) correlates with an early stage of cancer invasion in oral squamous cell carcinoma.* Cancer Lett, 2000. **151**(2): p. 217-22.

156. Chiarle, R., et al., *Increased proteasome degradation of cyclin-dependent kinase inhibitor p27 is associated with a decreased overall survival in mantle cell lymphoma.* Blood, 2000. **95**(2): p. 619-26.

157. Siddiqi, T. and R.M. Joyce, *A case of HIV-negative primary effusion lymphoma treated with bortezomib, pegylated liposomal doxorubicin, and rituximab.* Clin Lymphoma Myeloma, 2008. **8**(5): p. 300-4.

158. An, J., et al., *Antitumor effects of bortezomib (PS-341) on primary effusion lymphomas.* Leukemia, 2004. **18**(10): p. 1699-704.

159. Tilly, H. and A. Zelenetz, *Treatment of follicular lymphoma: current status.* Leuk Lymphoma, 2008. **49 Suppl 1**: p. 7-17.

160. Wang, M., et al., *Bortezomib is synergistic with rituximab and cyclophosphamide in inducing apoptosis of mantle cell lymphoma cells in vitro and in vivo.* Leukemia, 2008. **22**(1): p. 179-85.

161. Satou, Y., et al., *Proteasome inhibitor, bortezomib, potently inhibits the growth of adult T-cell leukemia cells both in vivo and in vitro.* Leukemia, 2004. **18**(8): p. 1357-63.

162. Paoluzzi, L. and O.A. O'Connor, *Mechanistic rationale and clinical evidence for the efficacy of proteasome inhibitors against indolent and mantle cell lymphomas.* BioDrugs, 2006. **20**(1): p. 13-23.

163. O'Connor, O.A., *Marked clinical activity of the proteasome inhibitor bortezomib in patients with follicular and mantle-cell lymphoma.* Clin Lymphoma Myeloma, 2005. **6**(3): p. 191-9.

164. Strauss, S.J., et al., *Bortezomib therapy in patients with relapsed or refractory lymphoma: potential correlation of in vitro sensitivity and tumor necrosis factor alpha response with clinical activity.* J Clin Oncol, 2006. **24**(13): p. 2105-12.

165. Adams, J., *The proteasome: a suitable antineoplastic target.* Nat Rev Cancer, 2004. **4**(5): p. 349-60.

166. Malara, N., et al., *Simultaneous inhibition of the constitutively activated nuclear factor kappaB and of the interleukin-6 pathways is necessary and sufficient to completely overcome apoptosis resistance of human U266 myeloma cells.* Cell Cycle, 2008. **7**(20): p. 3235-45.

167. Blade, J., et al., *Pegylated liposomal doxorubicin plus bortezomib in relapsed or refractory multiple myeloma: efficacy and safety in patients with renal function impairment.* Clin Lymphoma Myeloma, 2008. **8**(6): p. 352-5.

168. Lee, S.J., et al., *Bortezomib is associated with better health-related quality of life than high-dose dexamethasone in patients with relapsed multiple myeloma: results from the APEX study.* Br J Haematol, 2008. **143**(4): p. 511-9.

169. Berkhout, B. and J. Haasnoot, *The interplay between virus infection and the cellular RNA interference machinery.* FEBS Lett, 2006. **580**(12): p. 2896-902.

170. Cullen, B.R., *Is RNA interference involved in intrinsic antiviral immunity in mammals?* Nat Immunol, 2006. **7**(6): p. 563-7.

171. Fire, A., et al., *Potent and specific genetic interference by double-stranded RNA in Caenorhabditis elegans.* Nature, 1998. **391**(6669): p. 806-11.

172. Lee, Y., et al., *The nuclear RNase III Drosha initiates microRNA processing.* Nature, 2003. **425**(6956): p. 415-9.

173. Grosshans, H. and F.J. Slack, *Micro-RNAs: small is plentiful.* J Cell Biol, 2002. **156**(1): p. 17-21.

174. Elbashir, S.M., et al., *Duplexes of 21-nucleotide RNAs mediate RNA interference in cultured mammalian cells.* Nature, 2001. **411**(6836): p. 494-8.

175. Caplen, N.J., et al., *Specific inhibition of gene expression by small double-stranded RNAs in invertebrate and vertebrate systems.* Proc Natl Acad Sci U S A, 2001. **98**(17): p. 9742-7.

176. Ge, Q., et al., *RNA interference of influenza virus production by directly targeting mRNA for degradation and indirectly inhibiting all viral RNA transcription.* Proc Natl Acad Sci U S A, 2003. **100**(5): p. 2718-23.

177. Sorkina, T., et al., *RNA interference screen reveals an essential role of Nedd4-2 in dopamine transporter ubiquitination and endocytosis.* J Neurosci, 2006. **26**(31): p. 8195-205.

178. Huang, F., et al., *Analysis of clathrin-mediated endocytosis of epidermal growth factor receptor by RNA interference.* J Biol Chem, 2004. **279**(16): p. 16657-61.

179. Banerjea, A., et al., *Inhibition of HIV-1 by lentiviral vector-transduced siRNAs in T lymphocytes differentiated in SCID-hu mice and CD34+ progenitor cell-derived macrophages.* Mol Ther, 2003. **8**(1): p. 62-71.

180. Boden, D., et al., *Promoter choice affects the potency of HIV-1 specific RNA interference.* Nucleic Acids Res, 2003. **31**(17): p. 5033-8.

181. Cho, S.W., et al., *Delivery of small interfering RNA for inhibition of endothelial cell apoptosis by hypoxia and serum deprivation.* Biochem Biophys Res Commun, 2008. **376**(1): p. 158-63.

182. Mulkeen, A.L., et al., *Short interfering RNA-mediated gene silencing of vascular endothelial growth factor: effects on cellular proliferation in colon cancer cells.* Arch Surg, 2006. **141**(4): p. 367-74; discussion 374.

183. Guo, X., et al., *siRNA-mediated inhibition of hTERT enhances chemosensitivity of hepatocellular carcinoma.* Cancer Biol Ther, 2008. **7**(10): p. 1555-60.

184. Bektas, M., et al., *Interactions of eukaryotic elongation factor 2 with actin: a possible link between protein synthetic machinery and cytoskeleton.* FEBS Lett, 1994. **356**(1): p. 89-93.

185. Gross, S.R. and T.G. Kinzy, *Translation elongation factor 1A is essential for regulation of the actin cytoskeleton and cell morphology.* Nat Struct Mol Biol, 2005. **12**(9): p. 772-8.

186. Lichter, P., *Multicolor FISHing: what's the catch?* Trends Genet, 1997. **13**(12): p. 475-9.

Results

2.1 EEF1A expression levels

HepG2 and JHH6 cell lines are here considered models to explore the so far unknown biological role of eEF1A in hepatocellular carcinoma. These two cell lines have a different morphology, hepatocyte-like for HepG2 and undifferentiated for JHH6 [1, 2]. Moreover, albumin mRNA content, a known marker of hepatocyte differentiation, is more then 2 times more expressed in HepG2 than in JHH6, further indicating the higher differentiation grade of HepG2 compared to JHH6. Thus, the different phenotype allows to detect possible correlation between eEF1A and the tumor cell grade.

2.1.1 EEF1A1 and EEF1A2 mRNA levels

The mRNA levels of EEF1A1 and EEF1A2 were analyzed in sub-confluent (70% confluent) HepG2 and JHH6 cells. Total RNA, obtained from normal liver biopsies collected during surgical resection for angioma, was used as control (see [3]). EEF1A1 and EEF1A2 mRNA levels were also evaluated in the HuH7 hepatic cell line [1] which, compared to HepG2 and JHH6, displays an intermediate differentiation grade as evaluated by morphological inspection and albumin expression.

A non-quantitative PCR analysis of the amplified genes is reported in Figure 1 while the quantitative Real Time PCR data are reported in Figure 2A and 2B.

Compared to normal liver tissue (Fig. 2A), significant (*$p<0.05$) 28, 24 and 177 folds increase of EEF1A1 mRNA were detected in HepG2, HuH7 and JHH6 cell line, respectively. In the case of EEF1A2 (Fig. 2B), a marked increase of the mRNA level (205 folds) was observed in JHH6 (*$p<0.001$), while no significant increment in the mRNA levels was found in HepG2 and HuH7. Based on this result, the subsequent

experiments were conducted with the two most phenotipically different hepatic cell line, HepG2 and JHH6.

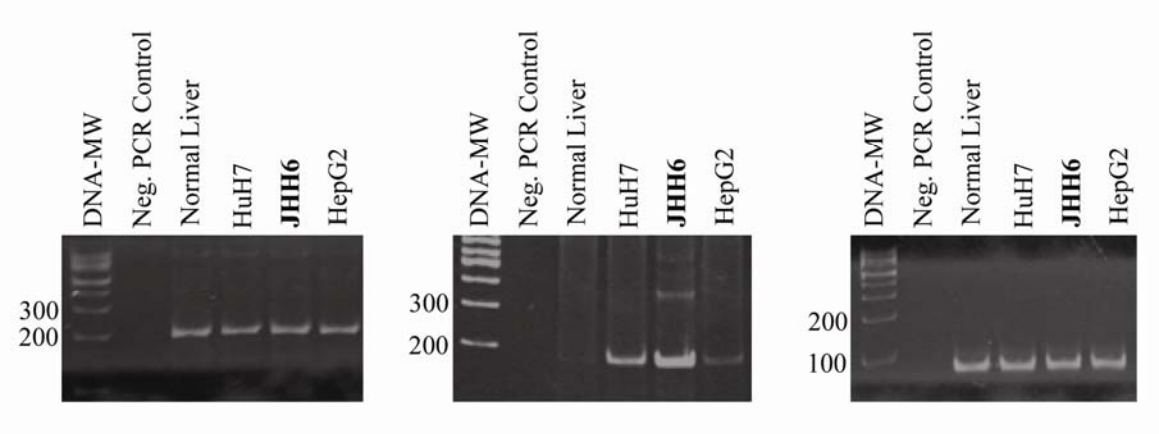

Figure 1. Non-quantitative PCR analysis of EEF1A1, EEF1A2 and 28S genes. DNA-MW=DNA molecular weights (bp).

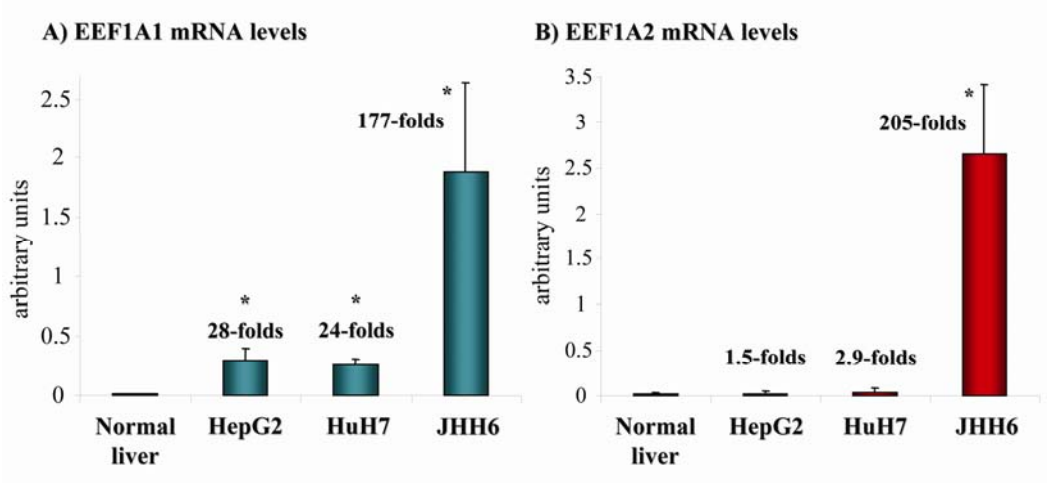

Figure 2. Real Time PCR of EEF1A1 and EEF1A2.

A) EEF1A1 mRNA levels in HepG2 and JHH6 compared with normal liver. Significant folds increase were detected in HepG2 and JHH6 cell lines (*p<0,05).
B) EEF1A2 mRNA levels in HepG2 and JHH6 compared with normal liver. A marked increase of the mRNA level was observed in JHH6 (*p<0,001), while no significant increment in the mRNA levels was found in HepG2.
The results are expressed as means ±SEM, n=3

2.1.2 Gene amplification

To evaluate the contribution of gene amplification to the increased mRNA levels, EEF1A1 and EEF1A2 genes were amplified by 2 specific pairs of primers (see Experimental Procedures). As shown in Figure 3A and 3B, a significant (*p<0.05) amplification rate of both genes was observed in JHH6 compared to normal liver tissue, whereas in HepG2 a significant (*p=0.05) increment was observed for EEF1A2 gene only.

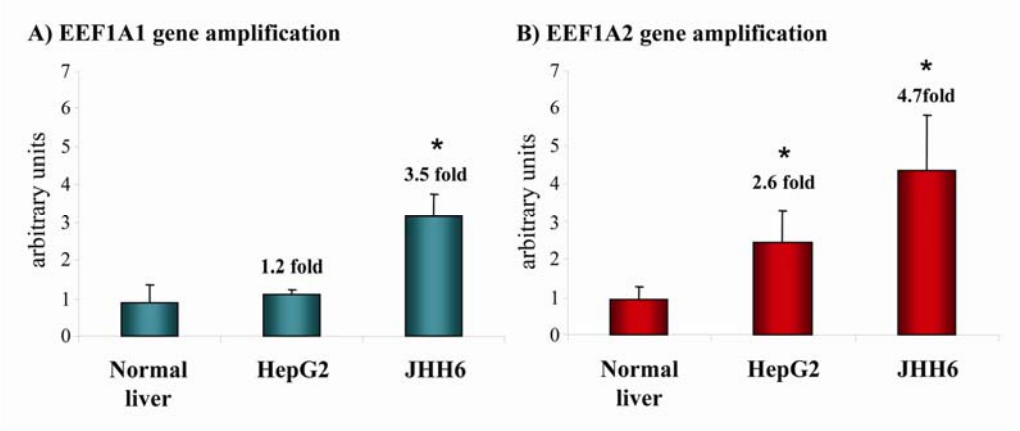

Figure 3. Evaluation of genes amplification in HepG2 and JHH6 cell lines compared to normal liver.

Significant gene amplification of EEF1A1 was observed in JHH6 cell line (A) compared with normal liver (*p<0,05), while a significant gene amplification of EEF1A2 (B) was observed in both HCC cell lines compared with normal liver. The results are expressed as means ±SEM, n=3

2.1.3 Western blot analysis

Western blotting analysis of cytoplasmic and nuclear-enriched eEF1A content was performed, in order to distinguish between eEF1A1 and eEF1A2 proteins in absence of two specific antibodies available. The data are reported in a representative western blot in Figure 4A and summarized as nuclear-enrched versus cytoplasmic ratio in Figure 4B. An increased nuclear-enriched/cytoplasmic ratio for eEF1A protein was observed in JHH6 compared to HepG2 (p=0.038) (Figure 4A).

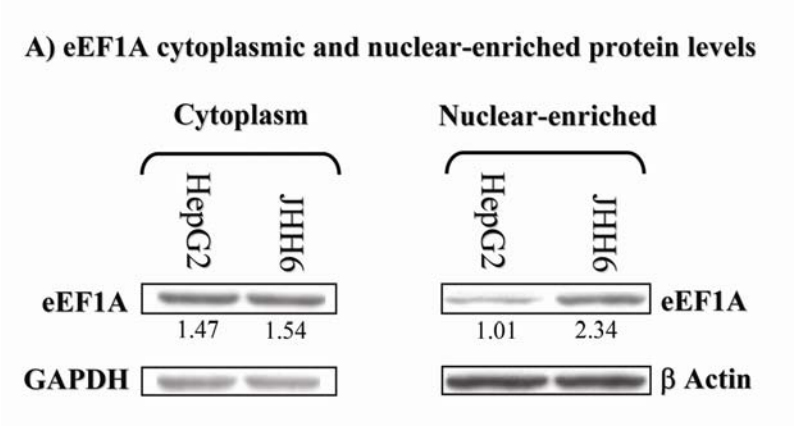

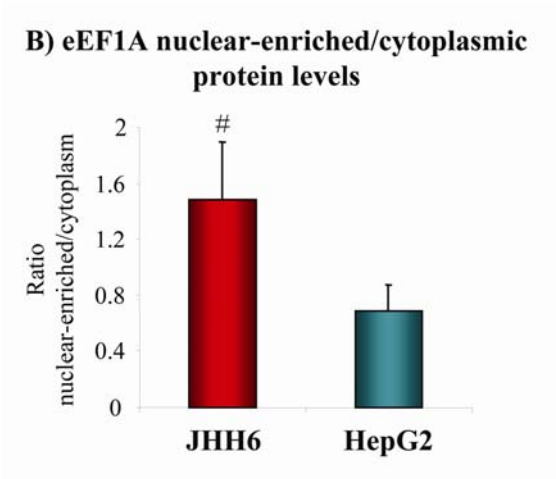

Figure 4

A) On the top a representative western blotting analysis of cytoplasmic and nuclear-enriched eEF1A content in HepG2 and JHH6 cell lines is reported.

B). On the right a summary of nuclear-enriched/cytoplasmic ratio. An increased nuclear-enriched/cytoplasmic ratio for eEF1A protein was observed in JHH6 compared to HepG2 ($p=0.038$). The results are expressed as means ±SEM, n=3

2.1.4 Apopotsis

The capacity of eEF1A1 and eEF1A2 to modulate programmed cell death in relation to the expression levels [4], prompted us to evaluate the apoptotic rate of HepG2 and JHH6 cell lines. In sub-confluent cells (two days after cell plating in complete medium) no differences were detected among HepG2 and JHH6 in the apoptosis rate evaluated by the percent of Annexin V positive cells (see [3]).

The Annexin V test (Fig. 5) is based on the observation that soon after initiating apoptosis, cells translocate the membrane phosphatidylserine (PS) from the inner face of the plasma membrane to the external face. Once on the cell surface, phosphatidylserine can be easily detected by staining with a fluorescent conjugate of Annexin V, a protein

that has an high affinity for PS. By conjugating fluorescein isothiocyanate (FITC) to Annexin V, it is possible to identify and quantitate apoptotic cells on a single-cell basis by flow cytometry. Staining cells simultaneously with FITC-Annexin V (green fluorescence) and the non-vital dye propidium iodide (red fluorescence) allows the discrimination of intact cells (FITC-/PI-), early apoptotic (FITC+/PI-), late apoptotic/necrotic cells (FITC+/PI+) and cell debris (PI+).

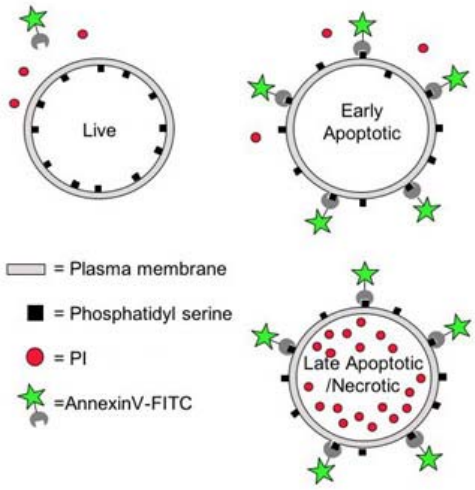

Figure 5. The Annexin V test.

Phosphatidylserine can be easily detected by staining with a fluorescent conjugate of Annexin V, a protein with an high affinity for PS. Annexin V conjugated with fluorescein isothiocyanate (FITC) can identify apoptotic cells on a single-cell basis by flow cytometry. Staining cells with FITC-Annexin V (green fluorescence) and the non-vital dye propidium iodide (red fluorescence) allows the discrimination of living cells, early apoptotic, late apoptotic/necrotic cells and cell debris.

Since the influence of eEF1A on apoptosis induced by serum deprivation has been reported [5-7], we explored the effects of serum removal on the apoptotic rate. No difference was observed between JHH6 and HepG2 after 2 days of starvation in spite of a general increase in Annexin V positive cells as compared to non starved cells. To evaluate the effect of one additional pro-apoptic condition, cells were treated by the known apoptic inducer staurosporin [8, 9]. Once again, no major differences were noted in the amount of apoptotic cells. Notably, in Hela cells, used as control, the amount of Annexin V positive cells, i.e. apoptotic cells, did not substantially change under all the

condition tested. As expected, the percent of Annexin V positive cells was inversely related to the number of cells in both HepG2 and JHH6 cell line (see [3]).

2.1.5 Proliferation

Due to the implication of eEF1A in cell proliferation [6, 10-12], the relation between EEF1A expression-level/subcellular-localization and the proliferative activity was investigated by measuring the amount of different cell cycle inhibitors ($p16^{ink4a}$, $p21^{waf/cip1}$ and $p27^{kip1}$), and mediators of the cell cycle such as cyclins (cyclin E1, cyclin D1, cyclin A). The amount of the transcription factor E2F1 and of the newly synthesized DNA were also investigated. In sub-confluent cells, $p16^{ink4a}$ and $p27^{kip1}$, but not $p21^{waf/cip1}$, are more elevated in HepG2 compared to JHH6 (Fig. 6). On the contrary, no significant difference was observed for the protein levels of cyclin E1, cyclin D1, cyclin A and of the transcription factor E2F1 (see [3]).

In HuH7 cell line (a low differentiated HCC cell line), Maeta *et Al.* [13] have demonstrated that $p16^{ink4a}$ gene promoter is methylated. They also observed that the demethylating agent, 5-aza-2-deoxycytidine (5-Aza-CdR), up-regulated $p16^{ink4a}$ mRNA, increasing p16 protein expression. It clearly decreased the phosphorylation levels of pRb, resulting in a consequent inhibition of HuH7 cells growth.

For this reason it was not possible to detect $p16^{ink4a}$ in HuH7 but also in JHH6 cell line (undifferentiated HCC cell line). A representative western blot of $p16^{ink4a}$ in HepG2, HuH7 and JHH6 cell lines is reported in Figure 7.

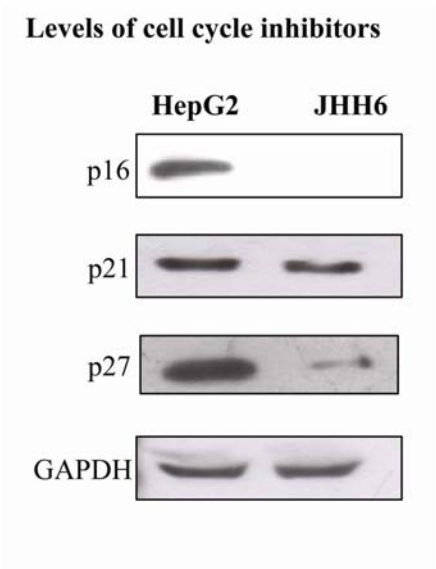

Figure 6. Cell cycle inhibitors.

The relation between EEF1A expression-level/subcellular-localization and the proliferative activity was investigated by measuring the amount of different cell cycle inhibitors ($p16^{ink4a}$, $p21^{waf1/cip1}$ and $p27^{kip1}$), and mediators of the cell cycle. In sub-confluent cells, $p16^{ink4a}$ and $p27^{kip1}$, but not $p21^{waf1/cip1}$, are more elevated in HepG2 compared to JHH6. A representative western blot was reported.

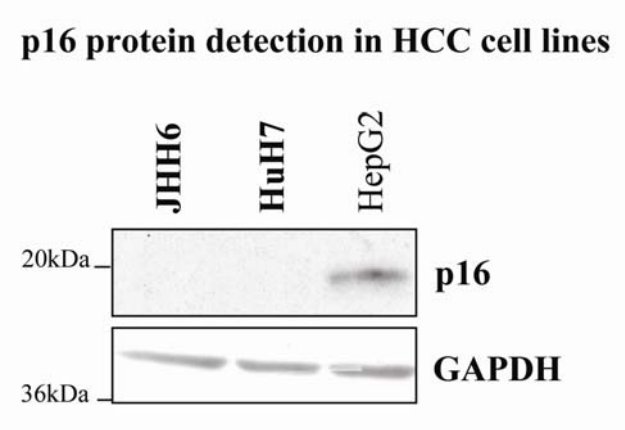

Figure 7. $p16^{ink4a}$ cell cycle inhibitor detection in HCC cell lines.
Detection of $p16^{ink4a}$ in HepG2, HuH7 and JHH6. A representative western blot is reported.

No variation was observed in the proliferative activity as evaluated by bromodeoxyuridine (BrdU) incorporation in HepG2 and JHH6, as reported in Figure 8.

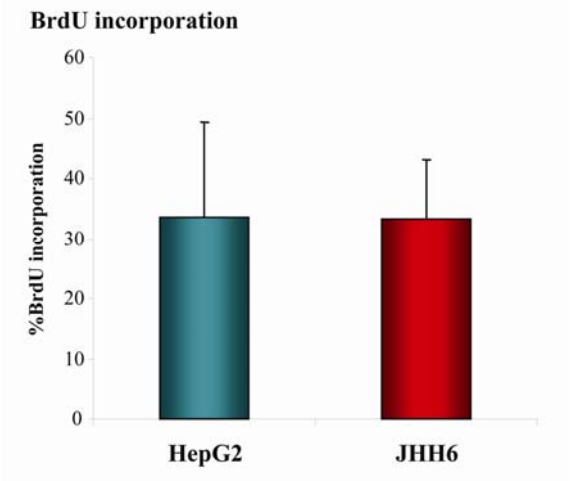

Figure 8.Proliferation assay evaluated by BrdU incorporation.
Regarding to HepG2 and JHH6 cell lines, no variations were observed.

2.1.6 Senescence assay

However, between two and four days after reaching cell confluence, HepG2 (differentiated HCC) exit from the cell cycle more massively than HuH7 (low differentiated HCC) and JHH6 (undifferentiated HCC) cell lines as indicated by the evident staining for the β-gal associated senescence test (see Experimental Procedures) [14]. Data are reported in Figure 9.

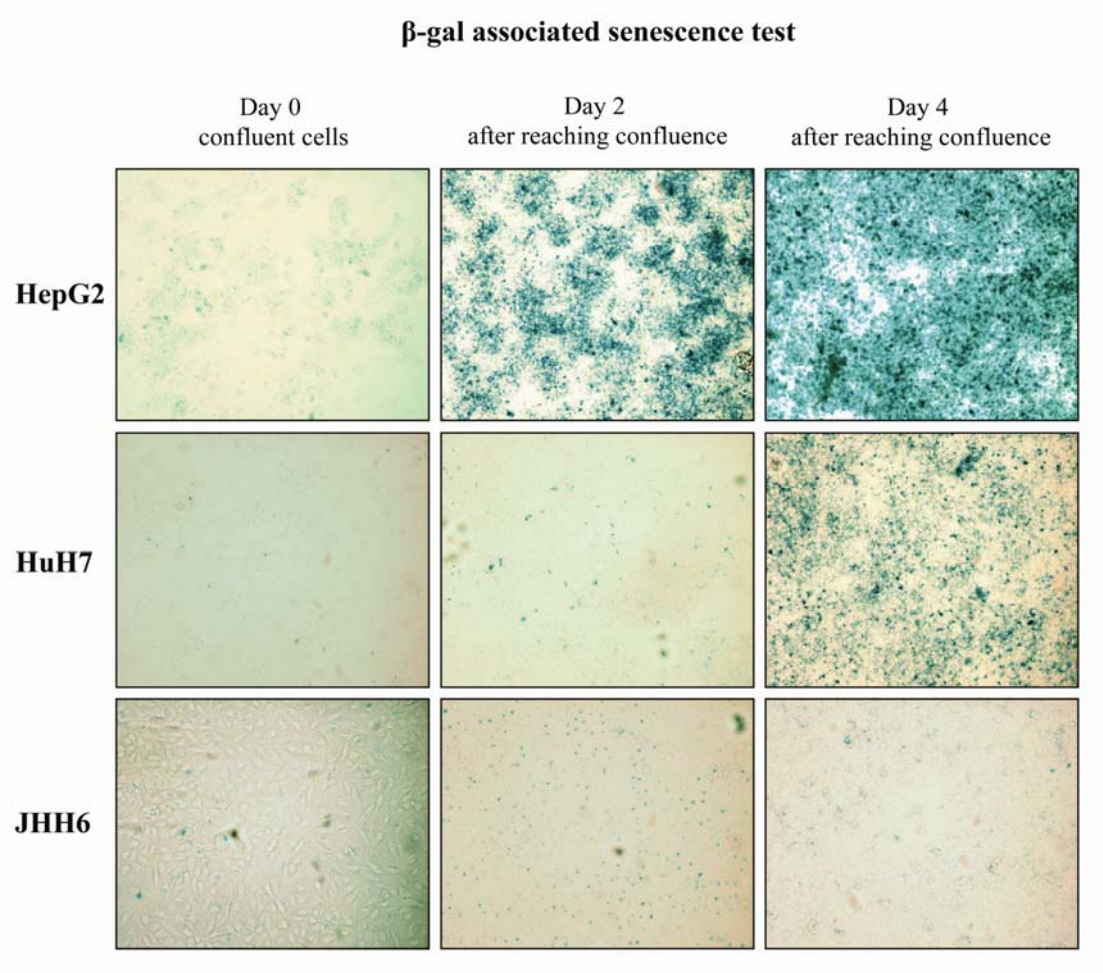

Figure 9. β-gal associated senescence test.

Reported are representative imagines of confluent HepG2, HuH7 and JHH6 cells stained for senescence-associated β-galactosidase and analyzed by microscopy at a 20x magnification.

HuH7 seem to have a similar behaviour like JHH6 at two days after confluence, while at four days JHH6 grow and are not affected by senescence stain like other cell lines. Hela cells did not significantly stain for the senescence associated β-gal test (see [3]).

2.2 Inhibition of 26S proteasome in HCC cell lines by bortezomib

We monitored the effects of bortezomib on HepG2, HuH7 and JHH6, an *in vitro* model of hepatocellular carcinoma. The bortezomib concentrations used were chosen to stay well below the maximal amount/cm^2 recommended for *in vivo* application [15]. Moreover, two days incubation were found to be optimal to study bortezomib effects.

2.2.1 Bortezomib inhibits the 26S proteasome

The first step was first to evaluate that bortezomib inhibits the chymotrypsin – like activity of 26S proteasome in HCC cell lines considered, because there are no data published at regarding. The protocol used was adapted to HCC cell lines from Reinheckel T *et Al.* and Powell SR *et Al*. [16, 17]

Determination of 26S proteasome activity with fluorogenic substrates requires ATP, in order to asses function of the 19S-regulatory particle. Chymotrypsin-like activity was monitored using fluorogenic substrate Suc-LLVY-Amc. Collected cells were suspended in Lysis Buffer (see Experimental Procedures) and immediately disrupted by three freezing/thawing steps through liquid nitrogen, monitoring the cell vitality using trypan blue. 60 μg of protein solution (evaluated by BCA protein staining) was adjusted with

ATP and Suc-LLVY-Amc 26S proteasome substrate, and incubated at 37°C for 45 minutes.

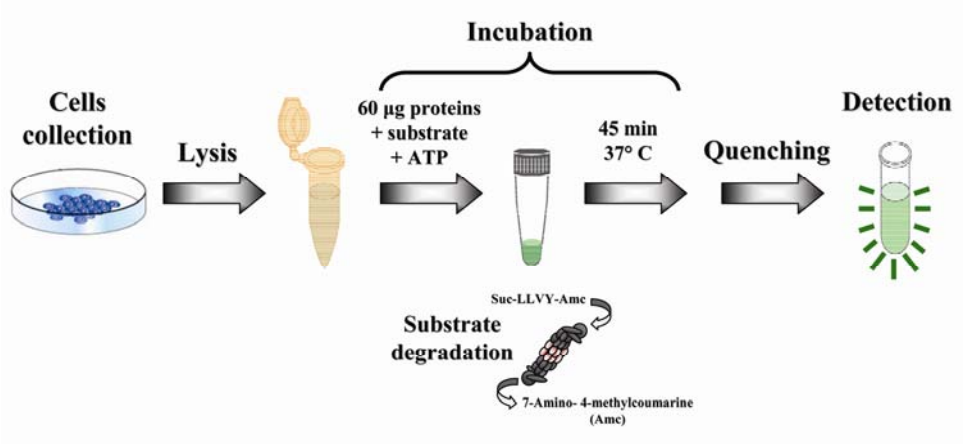

Figure 10. Fluorigenic 26S proteasome Suc-LLVY-Amc substrate reaction.

The reaction was quenched using ice-cold ethanol. Evaluation of chymotrypsin-like activity function of 26S proteasome was conducted analysing fluorescent signal produced by free 7-amino-4-methylcoumarine present in solution, only if 26S proteasome degraded the substrate (Fig. 10). As reported in Figure 11, a dose dependent in 26S proteasome substrate degradation was evident in bortezomib-treated cells

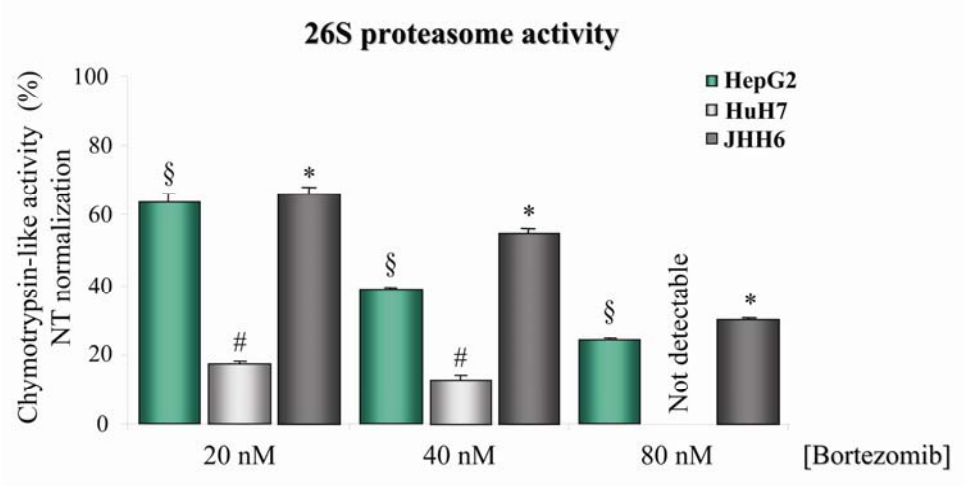

Figure 11. 26S proteasome chymotryptic-like activity inhibition.

Suc-LLVY-Amc substrate decreased of degradation was evident in bortezomib-treated cells compared to controls, confirming the inhibition of the chymotripsyn-like activity of 26S proteasome in all HCC cell lines. The results are expressed as means ±SEM, n=6 (§$p<1x10^{-5}$, #$p<2x10^{-5}$, *$p<1x10^{-5}$, compared to NT)

compared to controls, comparing the fluorescence value of the maximal activity (non-treated cells control) with the fluorescent values of bortezomib-treated cells confirming the inhibition of the chymotripsyn-like activity of 26S proteasome (§p<$1x10^{-5}$ for HepG2, *p<$1x10^{-5}$ JHH6, #p<$2x10^{-5}$ for HuH7, compared to NT). A comparable reduction of 26S proteasome substrate degradation was observed in HepG2 and JHH6 cell lines, while HuH7 were more affected by bortezomib, as evidenced by major decrease of chymotrypsin-like activity.

2.2.2 Effects of bortezomib on cells viability

The incubation of increasing amounts of bortezomib with HepG2, HuH7 and JHH6 resulted in a significant decrease in the number of hepatic cells as evidenced by cell counting (Fig 12) and microscopic inspection (Fig. 13A, 13B and 13C). Notably, in HepG2 and HuH7 the reduction was already evident at 20 nM of bortezomib (*p<0.016, #p<0,0002 respectively), while in JHH6 a significant reduction was evident only at 40 nM (§p<0.05), suggesting a different drug sensitivity.

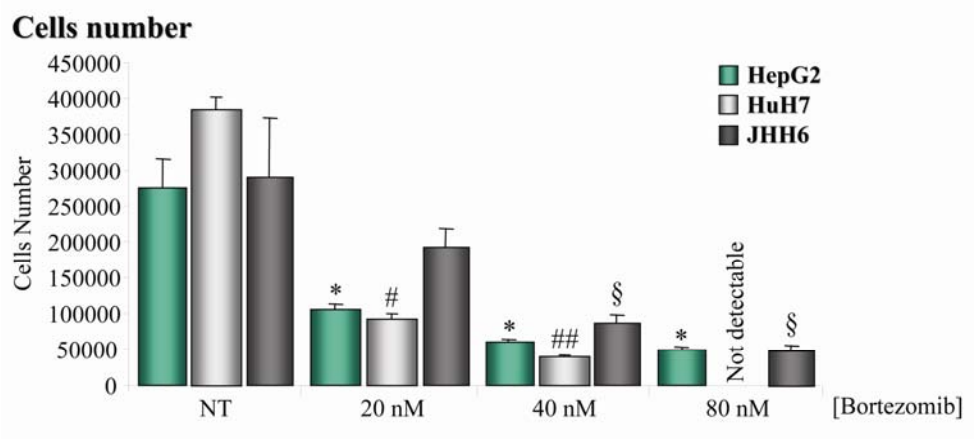

Figure 12. Cell counting.

The reduction of HepG2 and HuH7 cell lines was evident at 20 nM of bortezomib (*p<0.016, #p<0,0002 respectively, compared to NT). A significant reduction of JHH6 was evident only at 40 nM (§p<0.05, compared to NT), while at 80 nM of bortezomib all cell lines were high affected. The results are expressed as means ±SEM, n=4.

An increase of HepG2 and JHH6 floating cells was visible at 80 nM of bortezomib (Fig. 12-III), nevertheless for the HuH7 cell line, the decrease was so high that it was not technically possible to detect living cells, as evidenced in Figure 13B-III.

HepG2 cell line grows in colonies as shown in Figure 13-A-I, as a result of a differentiated phenotype. We evaluated in this HCC cell line the possible effects of bortezomib analysing colonies area and colonies number at low microscopical inspection.

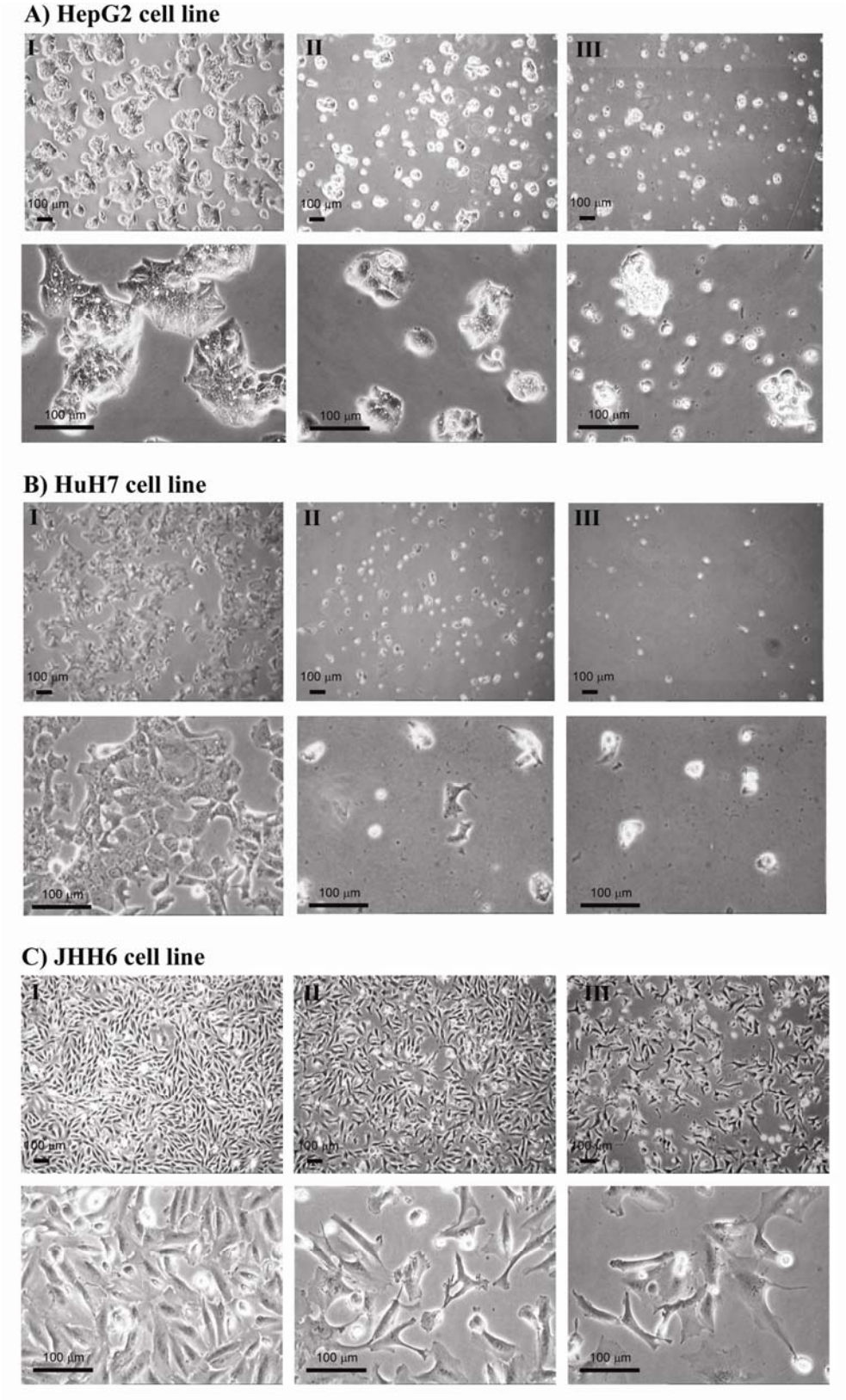

Figure 13. Microscopical inspection of HepG2, HuH7 and JHH6 at two different magnifications.

For each panel: top row=5x magnification, bottom row=20x magnification, I=Non-treated cells, II=40 nM of bortezomib, III=80 nM of bortezomib.

Results indicated a reduction of colonies area (§p<0.02), suggesting a cytostatic effect, and a reduction of the number of colonies (*p<0.05), supporting a cytotoxic effect, compared to NT (Fig. 14).

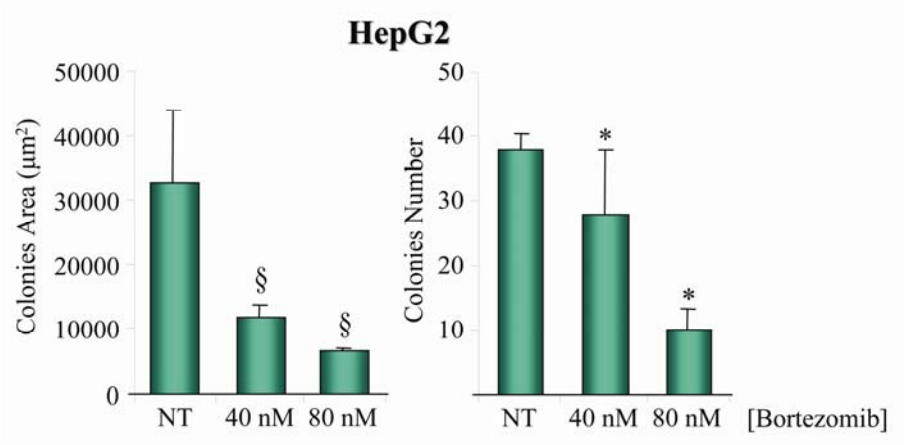

Figure 14. Evaluation of colonies area and number in HepG2 cell line.

On the left results about colonies area evaluation, while on the right colonies number detection. §p<0.02, *p<0.05, compared to NT. The results are expressed as means ±SEM, n=5.

In order to evaluate whether bortezomib exerts a cytostatic or a cytotoxic effect, a cell death or cytotoxicity test was evaluated by lactate dehydrogenase enzyme test.

2.2.3 Bortezomib exerts a cytotoxic effect

Lactate dehydrogenase (LDH) is a stable cytoplasmic enzyme which is present in cytosol of all cell types, and it is released into the cell culture supernatant upon damage of the cytoplasmic membrane. The test utilizes a coupled enzymatic reaction in which LDH oxidizes lactate to pyruvate, which then reacts with tetrazolium salt to form formazan. The increase in the amount of formazan produced in culture supernatant directly correlates to the increase in the number of lysed cells. The formazan-dye is water-soluble and can be detected spectrophotometrically at 500 nm.

For all HCC cell lines, we observed a dose-dependent increase in LDH enzyme in cell supernatant (Fig. 15). At concentration of 80 nM of bortezomib the rise in LDH amount

in HuH7 and JHH6 were more contained than in HepG2 (*p<0.014, #p<$8x10^{-5}$, §p<0.03, compared to NT).

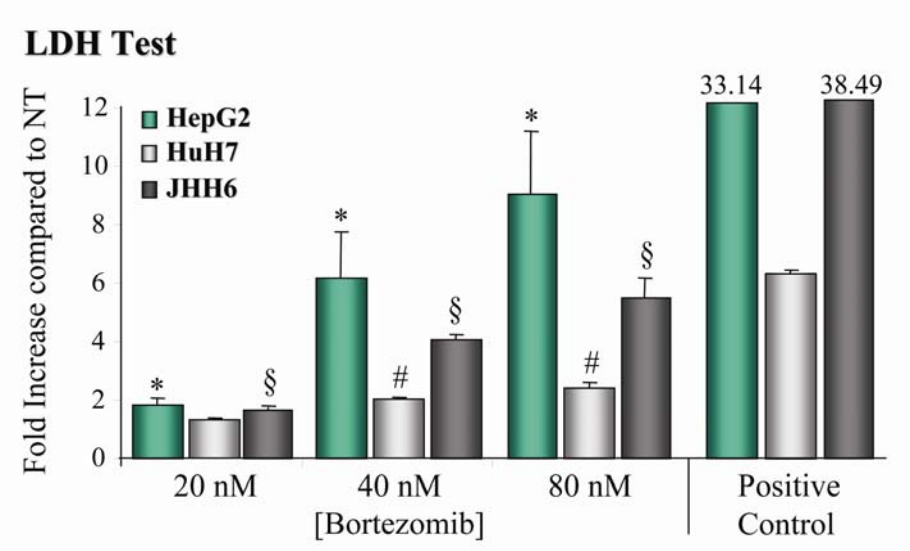

Figure 15. LDH cytotoxicity test.

For all HCC cell lines, we observed a dose-dependent increase in LDH enzyme in cell supernatant. At concentration of 80 nM of bortezomib the rise in LDH amount in HuH7 and JHH6 were more contained than in HepG2. The results are expressed as means ±SEM, n=6 (*p<0.014, #p<$8x10^{-5}$, §p<0.03, compared to NT).

We performed also the LDH test at 12 and 24 hours (Fig. 16) after bortezomib treatments in HepG2 and JHH6 cell lines (not for HuH7). Data indicated not only a dose-dependent cytotoxic effect of bortezomib (Fig. 15), but also a time-dependent increase of the enzyme amount in cells medium (Fig. 16). For HepG2, the cytotoxic effect was evident just at 12 hours (40 nM of bortezomib, §p<0.015), while at 24 hours the LDH enzyme amount approximately reached the level (§§p<$2.8x10^{-5}$) observed at 2 days of incubation (40 nM of bortezomib) and reported in Figure 15.

Regarding to JHH6, the undifferentiated HCC cell line, it confirmed to be less sensitive to bortezomib treatments compared to HepG2. At 12 hours JHH6 were affected few by treatments (40 nM of bortezomib, *p<0,02), while at 24 hours after bortezomib administration, the LDH enzyme amount observed (**p<0.007) was very similar with

HepG2 LDH enzyme amount detected at 12 hours (Fig. 16). At 20 nM of bortezomib JHH6 were not affected both at 12 and 24 hours after treatment.

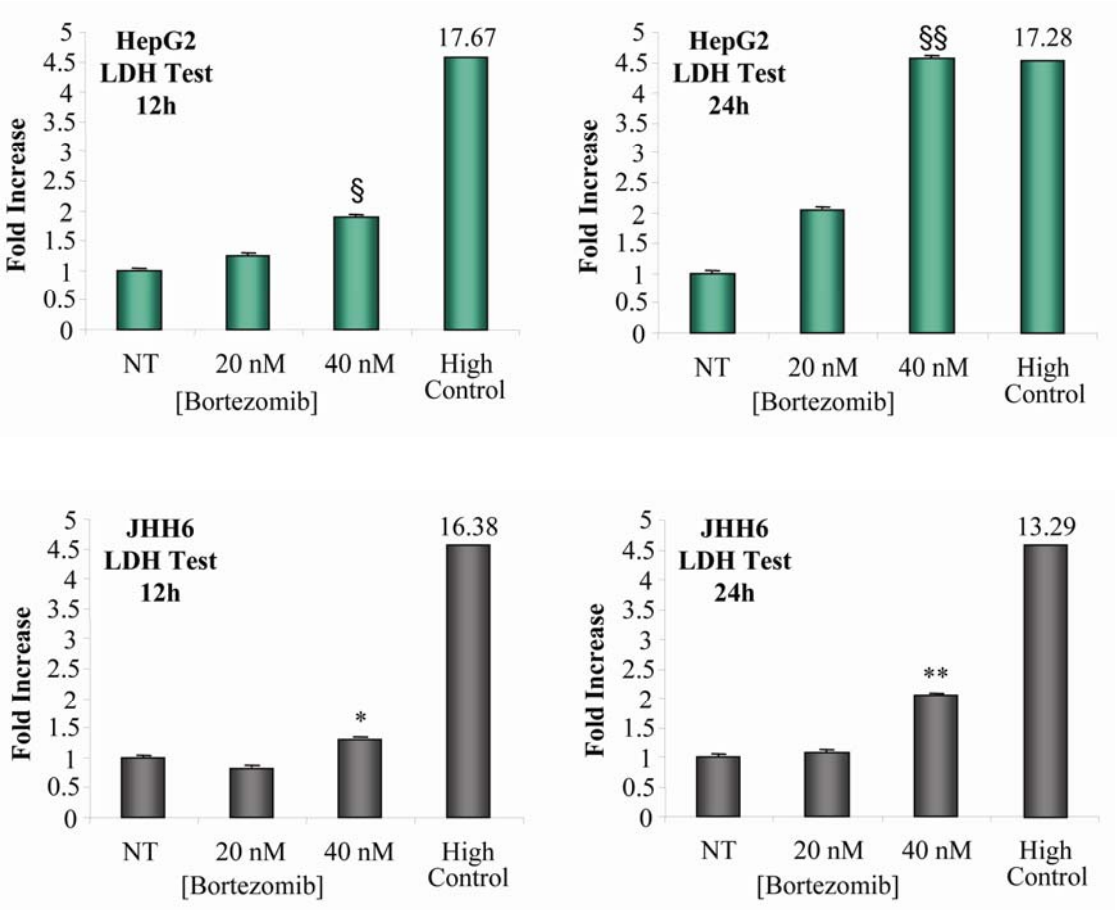

Figure 16. Time-dependent LDH cytotoxicity test.

For HepG2, the cytotoxic effect was evident just at 12 hours (40 nM of bortezomib, §$p<0.015$), while at 24 hours the LDH enzyme amount approximately reached the level (§§$p<2.8x10^{-5}$) observed at 2 days of incubation (40 nM of bortezomib) and reported in Figure 15. Regarding to JHH6, the undifferentiated HCC cell line, it confirmed to be less sensitive to bortezomib treatments compared to HepG2. At 12 hours JHH6 were affected few by treatments (40 nM of bortezomib, *$p<0,02$), while at 24 hours after bortezomib administration, the LDH enzyme amount observed (**$p<0.007$) was very similar with HepG2 LDH enzyme amount detected at 12 hours. At 20 nM of bortezomib JHH6 were not affected both at 12 and 24 hours after treatment. The results are expressed as means ±SEM, n=6.

Cytotoxicity LDH enzyme test was confirmed through cell debris evaluation by flow cytometry, after cell staining by propidium iodide. Propidium iodide (PI) binds to DNA by intercalating between the basis with little or no sequence preference and with a ratio

of one dye per 4/5 base pair of DNA. PI also binds RNA, so cell debris evaluation requires RNAse treatment in order to distinguish PI-DNA staining from PI-RNA (see Experimental Procedures). Once the dye is bound to nucleic acids, its fluorescence is enhanced 20- to 30-folds. PI is membrane impermeant and generally excluded from viable cells, so it could be used for identifying dead cells, which have pearced membranes. For this reason PI staining is an alternative cytotoxicity test and we used it to confirm LDH enzyme test.

We observed an increase of cell debris increasing bortezomib concentrations in all HCC cell lines (Fig. 17). Notably, at the concentrations of 40 and 80 nM of bortezomib, in JHH6 the rise in cell debris amounts were more contained than in HepG2 and HuH7 (#p<0.003, *p<0.033, §p<0.0001, compared to NT). At 80 nM of bortezomib it was not technically possible to evaluate HuH7 cell debris.

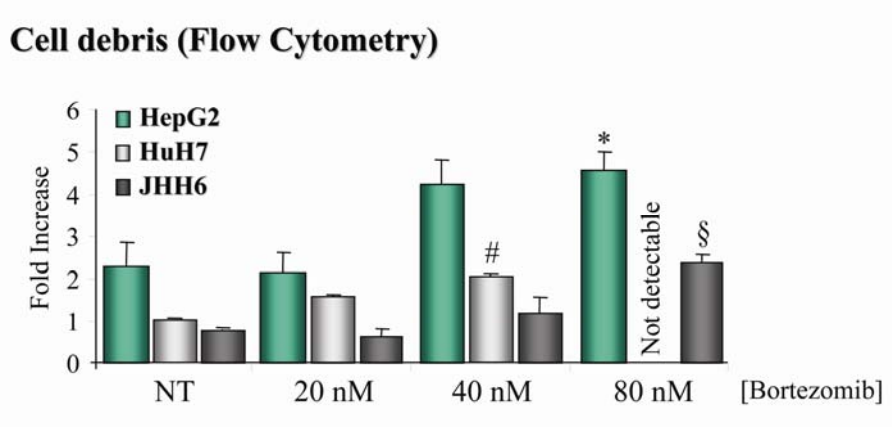

Figure 17. Cell debris evaluation in HCC cell lines.

An increase of cell debris increasing bortezomib concentrations was observed. At the concentrations of 40 and 80 nM of bortezomib, in JHH6 the rise in cell debris amounts were more contained than in HepG2 and HuH7. The results are expressed as means ±SEM, n=4 (#p<0.003, *p<0.033, §p<0.0001, compared to NT). At 80 nM of bortezomib it was not technically possible to evaluate HuH7 cell debris.

2.2.4 Bortezomib reduces cell viability

Cell viability was investigated in order to evaluate whether bortezomib exerts a dose-dependent effect as supposed above, using an MTT assay. The MTT assay is a test for measuring cell vitality by mithocondrial activity. Yellow (3-(4,5-dimethylthyazol-2-yl)-2,5-diphenyltetrazolium) bromide (MTT) is reduced to purple formazan by a mithocondrial reductase. The amount of purple formazan is indicative of the vitality of the cells. The formazan is dissolved in dimethylsulphoxide (DMSO) afterwards and then quantified by measuring the absorption at 590 nm (see Experimental Procedures). MTT test was performed two days after bortezomib administration (Fig. 18). A dose-dependent reduction in the amount of viable cells was observed (§$p<0.023$, #$p<2x10^{-9}$ and *$p<0.01$ for HepG2, HuH7 and JHH6 respectively, starting from 20 nM bortezomib, compared to NT).

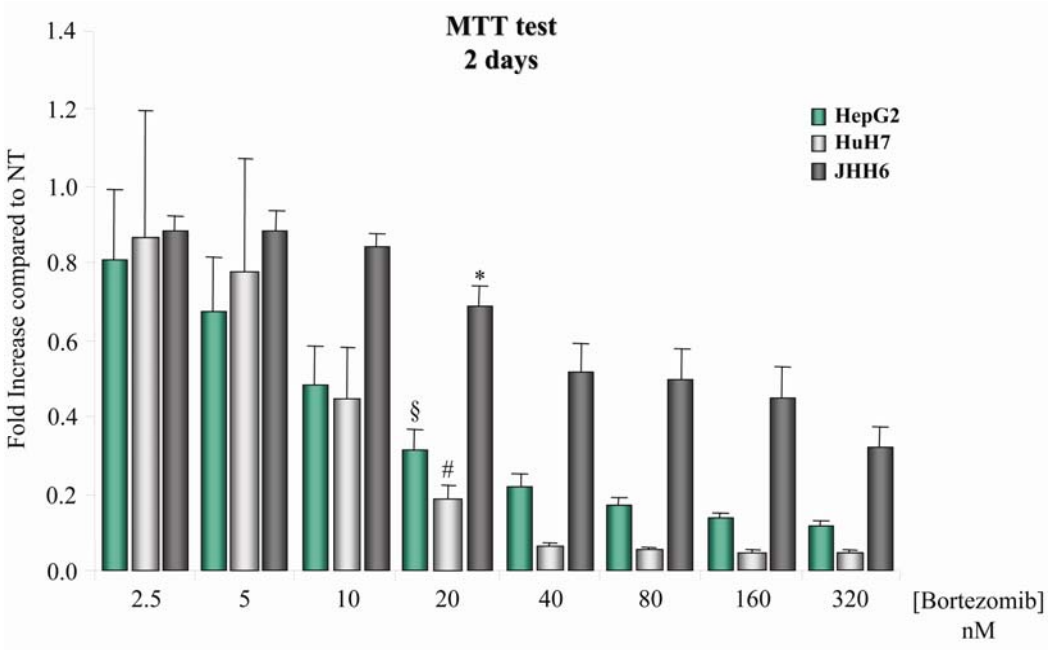

Figure 18. MTT test performed two days after bortezomib administration.

A dose-dependent reduction in the amount of viable cells was observed. The results are expressed as means ±SEM, n=7 (§$p< 0.023$, #$p<2x10^{-9}$ and *$p<0.01$ for HepG2, HuH7 and JHH6 respectively, starting from 20 nM bortezomib, compared to NT). JHH6 resulted to be less affected than HepG2 and HuH7 by bortezomib, particularly at concentration higher than 20 nM.

JHH6 resulted once again to be less affected than HepG2 and HuH7 by bortezomib, particularly at concentration higher than 20 nM. This experiment confirms the dose-dependent effect exerts by bortezomib.

Prolonging bortezomib incubation up to six days (Fig. 19), a similar behaviour was observed, but in the context of a more pronounced reduction in cell viability compared to the two days incubation. At six days, in HepG2 and HuH7 at 10 nM of bortezomib ($\S p<1.8x10^{-15}$, $\#p<1x10^{-15}$ respectively, compared to NT) we observed similar results found at 320 nM of bortezomib at two days of incubation (Fig. 18). At concentrations higher than 10 nM nor HepG2 nor HuH7 viable cells were detected. JHH6 vability decreased significantly at 20 nM of bortezomib ($*p<2.5x10^{-5}$, compared to NT). At 160 nM of bortezomib no viable cells were detected (Fig. 19).

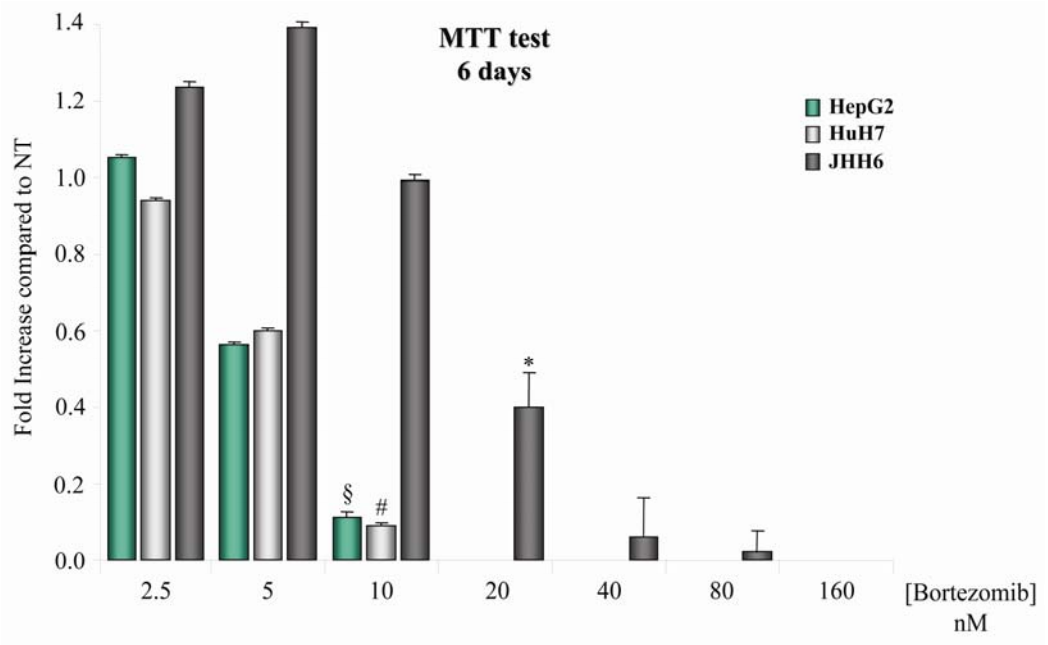

Figure 19. MTT test performed six days after bortezomib administration.

A similar behaviour was observed, but in the context of a more pronounced reduction in cell viability compared to the two days of incubation. Regarding to HepG2 and HuH7, at 10 nM of bortezomib ($\S p<1.8x10^{-15}$, $\#p<1x10^{-15}$ respectively, compared to NT) we observed similar results found at 320 nM of bortezomib at two days of incubation, while for JHH6 a significant reduction of viable cells were observed at 20 nM of bortezomib ($*p<2.5x10^{-5}$, compared to NT). The results are expressed as means ±SEM, n=7.

2.2.5 Effects of bortezomib on apoptosis activation

Apoptosis activation was evaluated by the Annexin V test as described above (see Experimental Procedures). Typical dot-plots related to apoptotic evaluation in HepG2, HuH7 and JHH6 cell lines are reported in Figure 20. Dot-plot is divided into four quadrants: Q3 (proliferating cells), Q4 (early apoptotic cells), Q2 (late apoptotic cells) and Q1 (cell debris). Apoptosis value is derived from Q2 + Q4 values sum.

In HepG2 a pro-apoptotic effect was detected at 20 nM of bortezomib, whereas at upper concentrations (40 nM shown only) the amount of cell debris were predominant. Regarding to JHH6 cell line, bortezomib exerts a major pro-apoptotic effect at 40 nM like in HepG2, but modest if compared with citotoxicity evidenced by increasing of cell debris (at 80 nM of bortezomib Q1=25,9%, Q1+Q4=4,8%, data not shown). In HuH7 we have not observed any pro-apoptotic effect mediated by bortezomib treatment at 20 nM, on the contrary at 40 nM a decreased of apoptotic cells compared to control, were observed.

Annexin V test was also performed monitoring the HepG2 and JHH6 cell lines 24 hours after bortezomib treatments, in order to exclude an earlier increase of apoptotic cells. Reported dot-plots (Fig. 21) evidenced no pro-apoptotic effect induced by bortezomib treatments. However, we cannot exclude that the reduction in the cell number and viability reported (Fig. 12 an 18) could also depend on the pro-apoptotic effect induced by bortezomib, observed at two days after treatments.

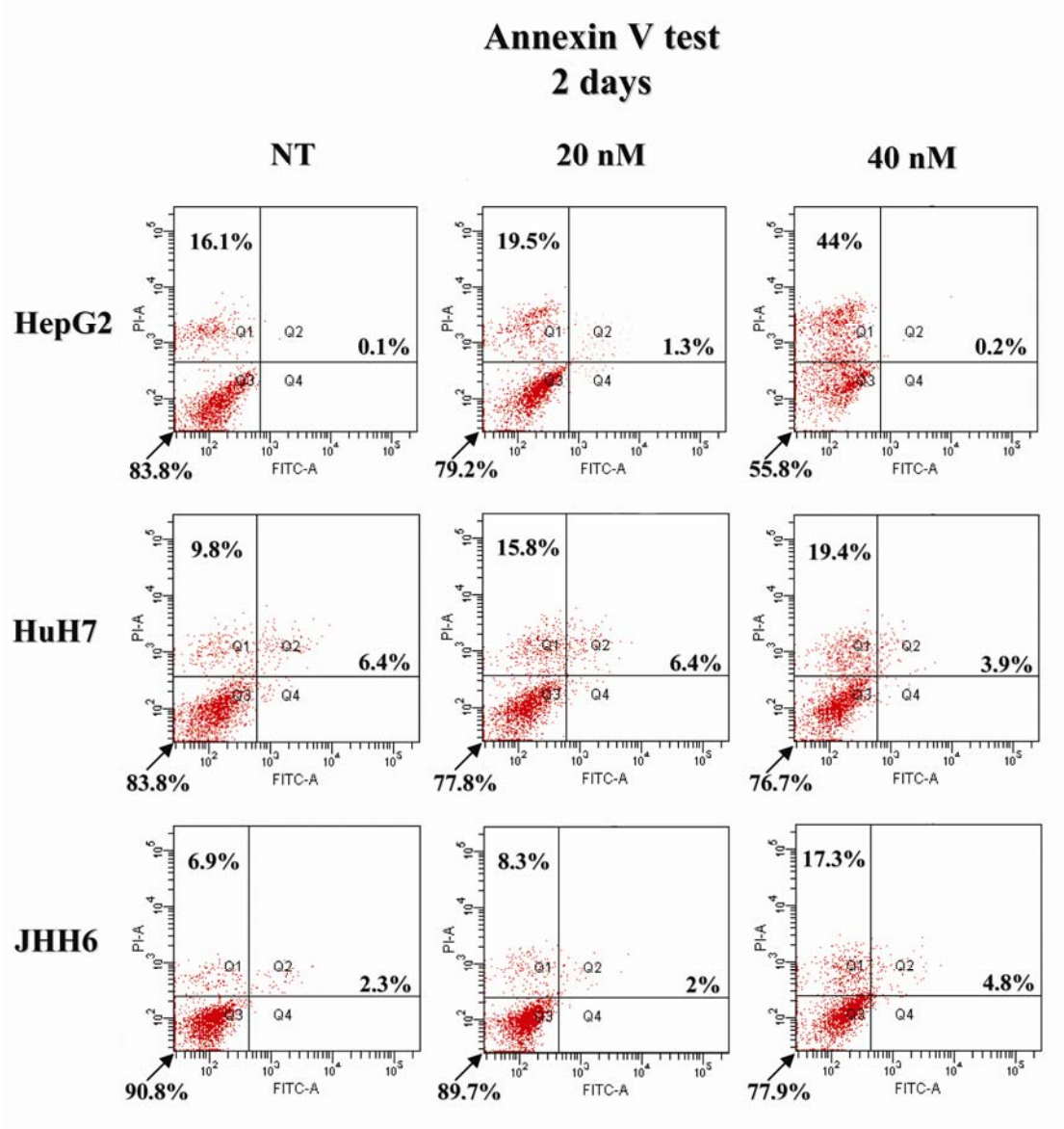

Figure 20. Dot-plots related to apoptotic evaluation at 2 days after treatments.

Q3=proliferating cells, Q4=early apoptotic cells, Q2=late apoptotic cells, Q1=cell debris, Q2+Q4=apoptotic cells

In HepG2 a pro-apoptotic effect was detected at 20 nM of bortezomib, whereas 40 nM the amount of cell debris were predominant. Regarding to JHH6 cell line, bortezomib exerts a major pro-apoptotic effect at 40 nM like in HepG2, but modest if compared with citotoxicity evidenced by increasing of cell debris (at 80 nM of bortezomib Q1=25,9%, Q1+Q4=4,8%, data not shown). In HuH7 we have not observed any pro-apoptotic effect mediated by bortezomib treatment at 20 nM, on the contrary at 40 nM a decreased of apoptotic cells compared to control, were observed. Dot-plots report fluorescent signal from Annexin V FITC on x-axis and PI detection on y-axis.

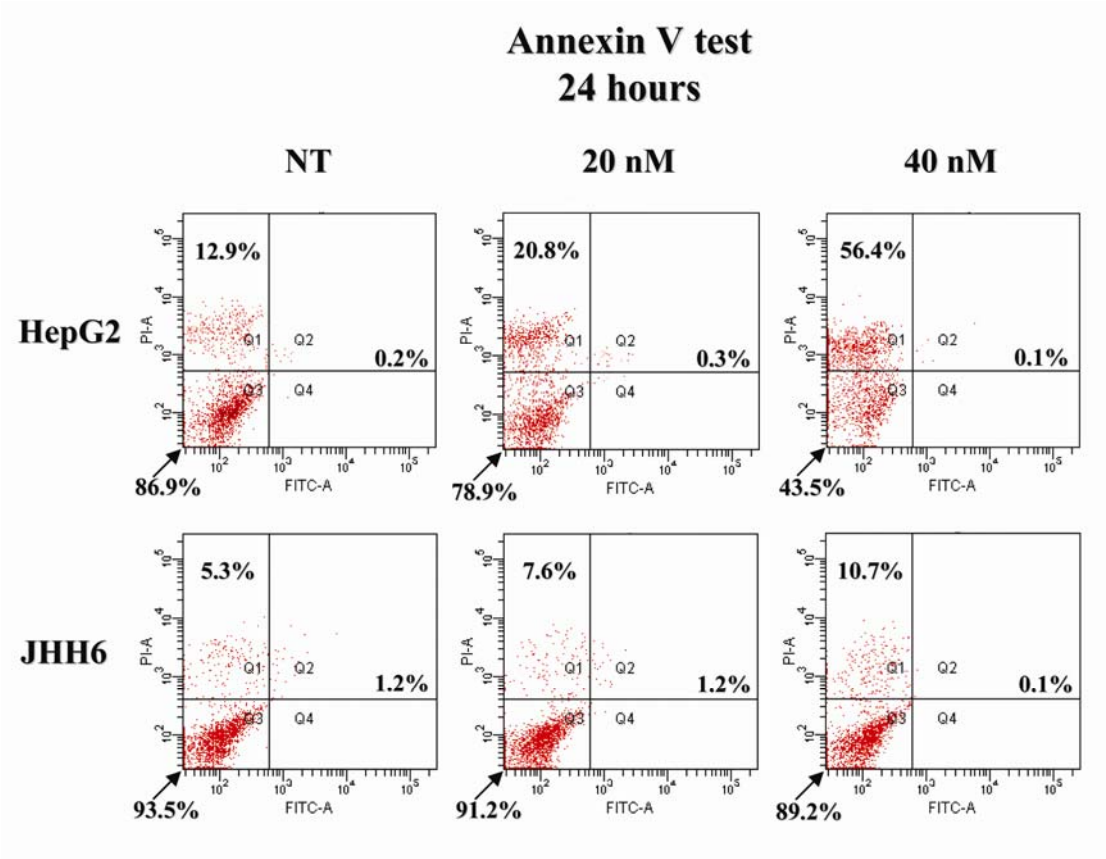

Figure 21. Dot-plots related to apoptotic evaluation at 24 hours after treatments.

Q3=proliferating cells, Q4=early apoptotic cells, Q2=late apoptotic cells, Q1=cell debris, Q2+Q4=apoptotic cells

Reported dot-plots evidenced no pro-apoptotic effect induced by bortezomib treatments for HepG2 and JHH6 cell lines. Dot-plots report fluorescent signal from Annexin V FITC on x-axis and PI detection on y-axis.

2.2.5.1 Western blot of Bax/Bcl-2 and PARP proteins

In order to evaluate apoptosis data observed by flow citometry, we considered some markers related to intrinsic apoptosis pathway. We investigated the protein levels of Bax/Bcl-2 and poly-(ADP)-ribose-polymerase (PARP) cleavage [18-20].

In a healty cell, the outer mitochondria membrane display the protein Bcl-2, that inhibits apoptosis. Internal damages to the cell causes the activation of protein Bax, which migrates to the surface of the mitochondria where it inhibits the protective effect of Bcl-2, inserts itself into the outer mitochondrial membrane punching holes in it and causing

the cytochrome c to leak out. The release of cytochrome c binds to the protein Apaf-1 (**A**poptosis **P**rotein **A**ctivating **F**actor-1), forming complexes called apoptosomes, that activate caspase-9 [21, 22].

The caspases are a family of proteins that are one of the main executors of the apoptotic process. They belong to a group of enzymes known as cysteine proteases and exist within the cell as inactive pro-forms or zymogens. These zymogens can be cleaved to form active enzymes following the induction of apoptosis. One of the hallmarks of apoptosis is the cleavage of chromosomal DNA into nucleosomal units. The caspases play an important role in this process by activating DNases, inhibiting DNA repair enzymes and breaking down structural proteins in the nucleus.

PARP is an highly conserved chromatin-associated protein which has the capacity to polymerize ADP-ribose (PAR) from nicotinamide adenine dinucleotide (NAD^+). In response to DNA damage caused by environmental genotoxic agents and endogenous cellular reactions, PARP binds rapidly to single-strand DNA nicks and catalyzes the transfer of ADP-ribose from its substrate NAD^+ to a number of nuclear acceptors, in order to assisting in the DNA repair. This ability of PARP to repair DNA damage is prevented following cleavage of PARP by caspase-3, leading cell to lysis and death [23, 24].

A representative western blot reported in Figure 22 confirmed the Annexin V test by flow cytometry (Fig. 20). In HepG2 at 20 nM of bortezomib we observed a decrease of anti-apoptotic protein Bcl-2 (not detectable in treatments) and pro-apoptotic protein Bax. The ratio Bax/Bcl-2 in treatments is in favour of the pro-apoptotic effect exerted by Bax itself, and this fact is supported by an increase of the cleaved PARP fragment (1.8 folds compared to control). In JHH6 cell line, bortezomib treatments increased Bax protein

levels (1.29 folds at 20 nM /1.36 folds at 40 nM, compared to control), while Bcl-2 levels were not affected like HepG2 cell line. The ratio Bax/Bcl-2 increase in treatments (1.32 folds at 20 nM and 1.65 folds at 40 nM of bortezomib, compared to control) Nevertheless, PARP cleavage was confirmed at 40 M of bortezomib only (4.15 folds compared to control), as observed through flow cytometry (Fig. 20).

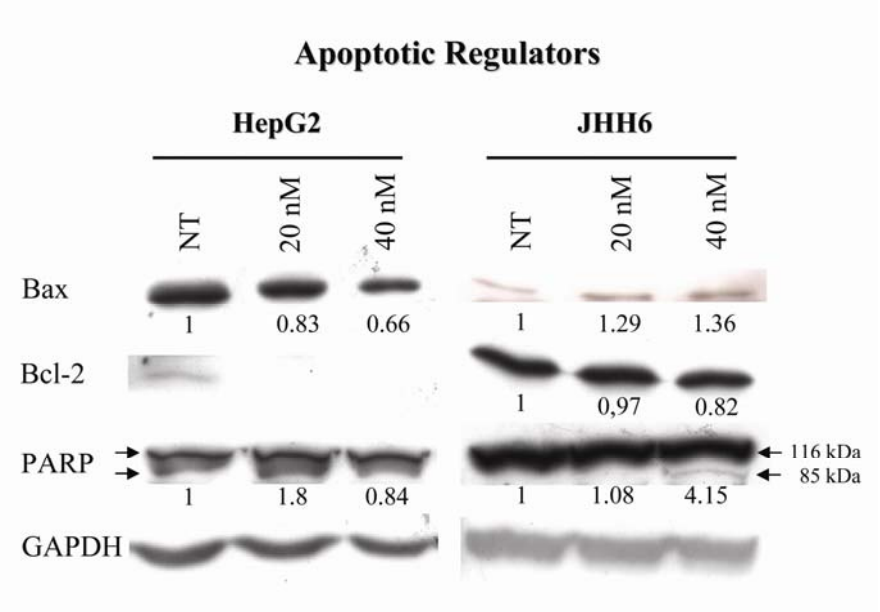

Figure 22. Western blot of apoptosis regulators

This is a representative western blot reporting Bax/Bcl-2 and PARP levels. In HepG2, at 20 nM of bortezomib we observed a decrease of anti-apoptotic protein Bcl-2 (not detectable in treatments) and pro-apoptotic protein Bax. The ratio Bax/Bcl-2 in treatments is in favour of the pro-apoptotic effect exerted by Bax itself, and this fact is supported by an increase of the cleaved PARP fragment (1.8 folds compared to control). In JHH6 cell line, bortezomib treatments increased Bax protein levels (1.29 folds at 20 nM /1.36 folds at 40 nM, compared to control), while Bcl-2 levels were not affected like HepG2 cell line. Nevertheless, PARP cleavage was confirmed at 40 M of bortezomib only (4.15 folds compared to control), as observed through flow cytometry (Fig. 20).

PARP protein is detected at 116 kDa, while the fragment cleavaged by caspase-3 at 85 kDa, as reported.

2.2.6 Effects of bortezomib on cell cycle phases distribution

We observed in HCC cell lines considered that bortezomib inhibits the chymotrypsin-like activity of 26S proteasome (Fig. 11), which resulted in a potent anti-proliferative effect, as evidenced by the decreased of cells number (Fig. 12) and cell viability (Fig.

18). This fact is reasonably related with the citotoxic effect induced by bortezomib (Fig. 15 and 17), and with a modest apoptosis induction observed (Fig. 20 and 22).

We investigated the effects of bortezomib to cell cycle, using a classical method for the analysis of cell cycle distribution by flow cytometric measurement of DNA content using bromodeoxyuridine (BrdU) and propidium iodide (PI) (see Experimental Procedures).

BrdU is an analog of the DNA precursor thymidine and it is incorporated into newly synthesized DNA by cells entering and progressing through the S phase of the cell cycle. The incorporated BrdU is stained with a specific anti-BrdU fluorescent antibody. The levels of cells-associated BrdU are then measured by flow cytometry. Staining with PI binds total DNA and with this combination, two-color flow cytometric analysis permits the enumeration and characterization of cells that are actively sinthesizing DNA (BrdU incorporation), in terms of their cell cycle position (G_1/G_0, S and G_2/M by PI staining intensities). Green fluorescence from the fluorescein-conjugated antibody is a measure of BrdU incorporation, while red fluorescence from the PI is a measure of DNA. A representative cell cycle dot-plots are reported in Figure 23.

Figures 24, 25 and 26 summarize the entire data about cell cycle phases evaluation in HepG2, HuH7 and JHH6 respectively.

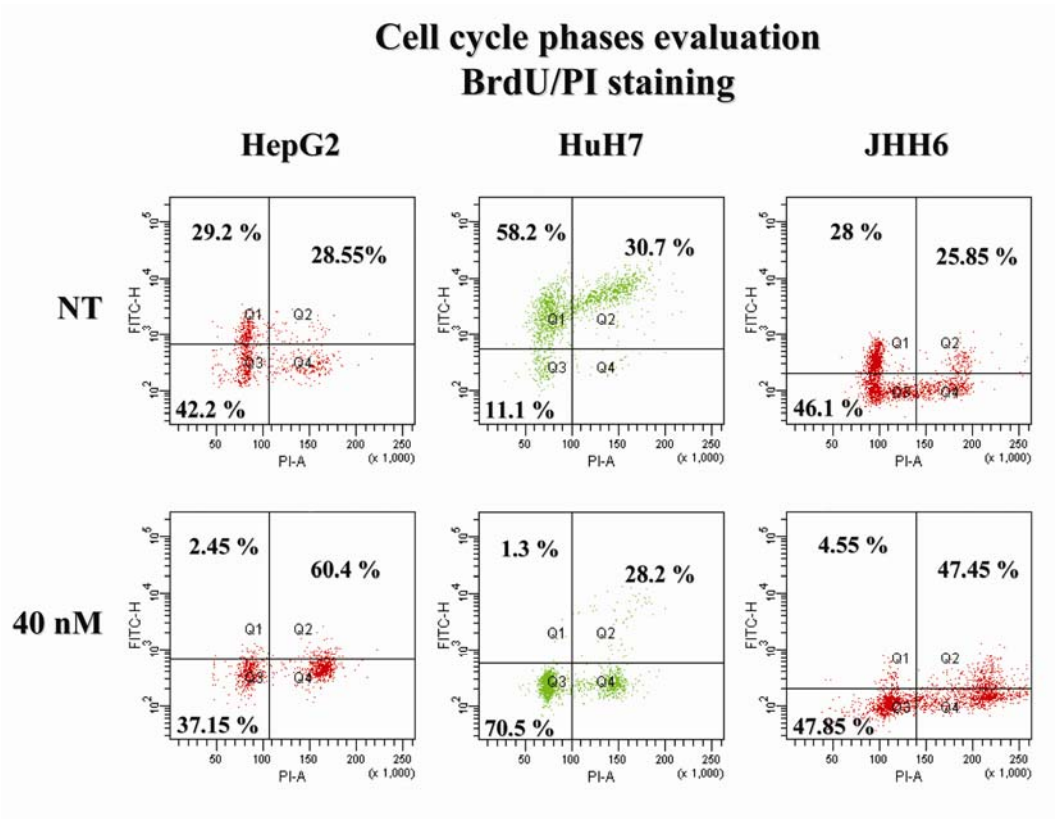

Figure 23. Representative dot-plot of bortezomib effects to cell cycle, limiting to NT and 40 nM of bortezomib.

Dot-plots report PI detection on x-axis and BrdU incorporation on y-axis (Q3=G_1/G_0 phase cells, Q1=S phase cells, Q2+Q4= G_2/M phase cells)

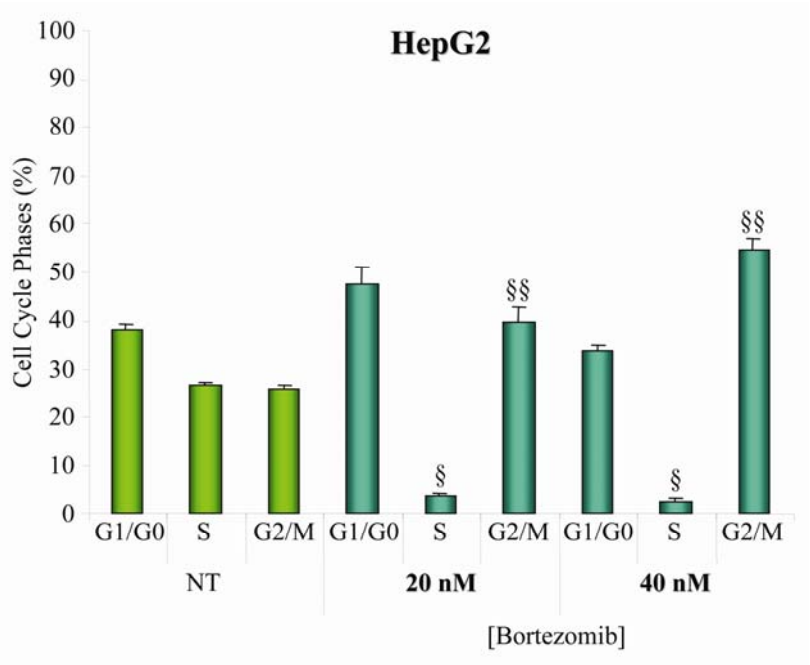

Figure 24. Summary of cell cycle phases evaluation in HepG2.

At 20 and 40 nM of bortezomib a marked reduction in the amount of S phase cells (§$p<6x10^{-8}$) and an increase of G_2/M (§§$p<6x10^{-4}$) phase cells were observed, compared to NT. The results are expressed as means ±SEM, n=6.

In HepG2 (Fig. 24), both at 20 and 40 nM of bortezomib a marked reduction in the amount of S phase cells (§p<$6x10^{-8}$) and an increase of G_2/M (§§p<$6x10^{-4}$) phase cells were observed, compared to NT. HuH7 (Fig. 25) evidenced a significant increase of G_1/G_0 (#p<0.01) at 20 nM of bortezomib. Regarding to S (##p<0.01) phase cells, in HuH7 was detected a similar reduction like in HepG2 at 20 and 40 nM of bortezomib, while the increase of G_2/M (###p<0.014) was evident only at 40 nM of bortezomib. In JHH6 (Fig. 26), a similar effect observed for HepG2 was plain only at 40 nM of bortezomib (*p<$7x10^{-4}$ and **p<$1x10^{-4}$ for S and G_2/M phase cells, respectively, compared to NT). No major variations in the amount of G_1 and G_0 phase cells were detected for HepG2 and JHH6. For all HCC cell lines, the decrease of S phase cells and increase of G_2/M phase cells trends were confirmed also at 80 nM bortezomib (data not shown). At higher bortezomib concentrations, the cytotoxic effect was preponderant over the anti-proliferative effect and no cell cycle analysis was technically possible.

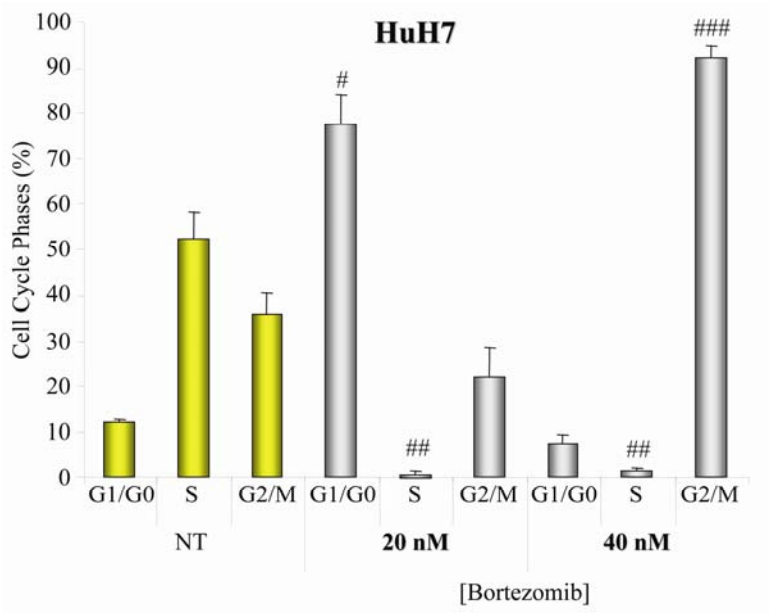

Figure 25. Summary of cell cycle phases evaluation in HuH7.

HuH7 evidenced a significant increase of G_1/G_0 (#p<0.01) at 20 nM of bortezomib, a marked reduction of S (##p<0.01) phase cells at 20 and 40 nM of bortezomib, while the increase of G_2/M (###p<0.014) was observed only at 40 nM of bortezomib, compared to NT. The results are expressed as means ±SEM, n=6.

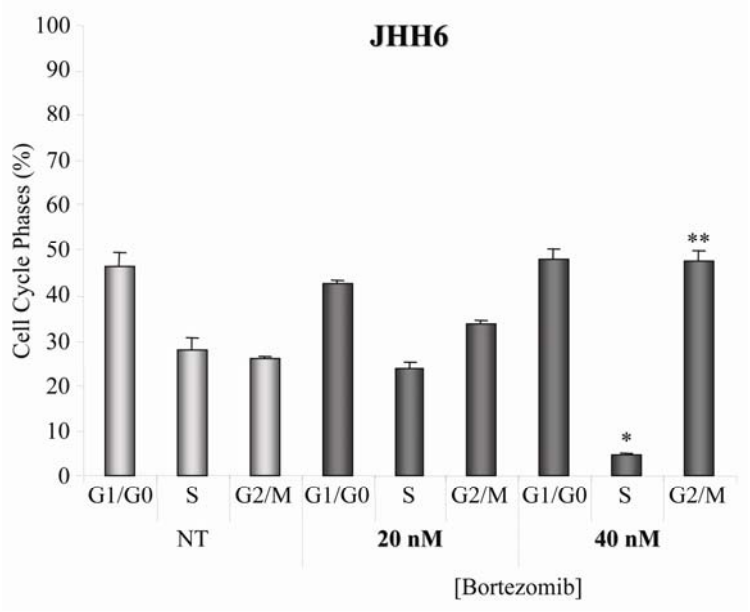

Figure 26. Summary of cell cycle phases evaluation in JHH6.

In JHH6 a similar effect observed for HepG2 was observed only at 40 nM of bortezomib (*$p<7x10^{-4}$ and **$p<1x10^{-4}$ for S and G_2/M phase cells, respectively, compared to NT). The results are expressed as means ±SEM, n=6.

2.2.6.1 Effects of bortezomib on the protein and mRNA levels of cell cycle regulators

In the three HCC cell lines considered, flow cytometry experiments revealed that bortezomib treatments cause an high decrease of S phase cells and an increase of G_2/M phase cells (Fig. 23, 24, 25 and 26). Regarding to HuH7 it was detected an increase of G_1/G_0 phase cells (only at 20 nM of bortezomib, Fig. 25). In order to understand these results, we evaluated the levels of the major cell cycle factors by western blot (Fig. 27A, 28A and 29A) and Real Time PCR (Fig. 27B, 28B and 29B). For each cell cycle protein considered, a representative blot, out of three independent experiments, is reported (Fig. 27A, 28A and 29A).

In HepG2, the protein levels of cyclin D1, cyclin A2, CdK2, of their transcription regulator E2F1 and of the hyper-phosphorylated form of pRB were considerably

decreased compared to control cells (Fig. 27A). The mRNA quantification revealed in HepG2 a significant decrease ($p<3x10^{-8}$) of cyclin D1 ($§p<3x10^{-8}$), E2F1 ($§§p<8x10^{-7}$), CdK2 and cyclin A2 ($p<8x10^{-5}$) mRNAs, consistent with the protein data (Fig. 27A) observed. No variation was observed for cyclin E1 mRNA (Fig. 27B). Moreover, a significant ($*p<3x10^{-9}$) and marked increase was observed for $p21^{waf1/cip1}$ together with a more contained ($**p<1x10^{-5}$) increase of $p27^{kip1}$ mRNA (Fig. 27B). A somewhat decrease in p53 levels were also observed ($**p<1x10^{-5}$).

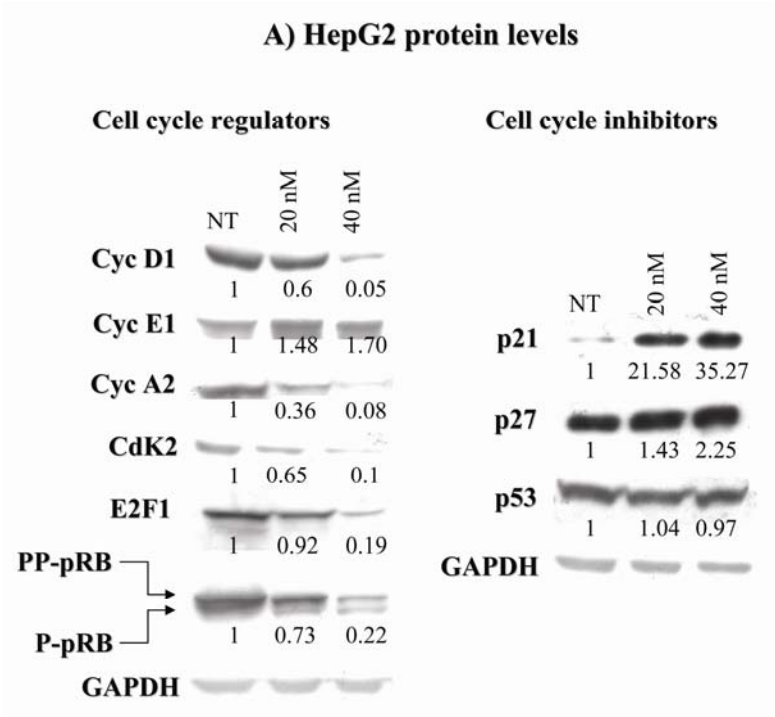

Figure 27A. A representative western blot of cell cycle regulators in HepG2 cell line.
PP-pRB=hyperphosphorylated pRB, P-pRB= hypophosphotylated pRB.

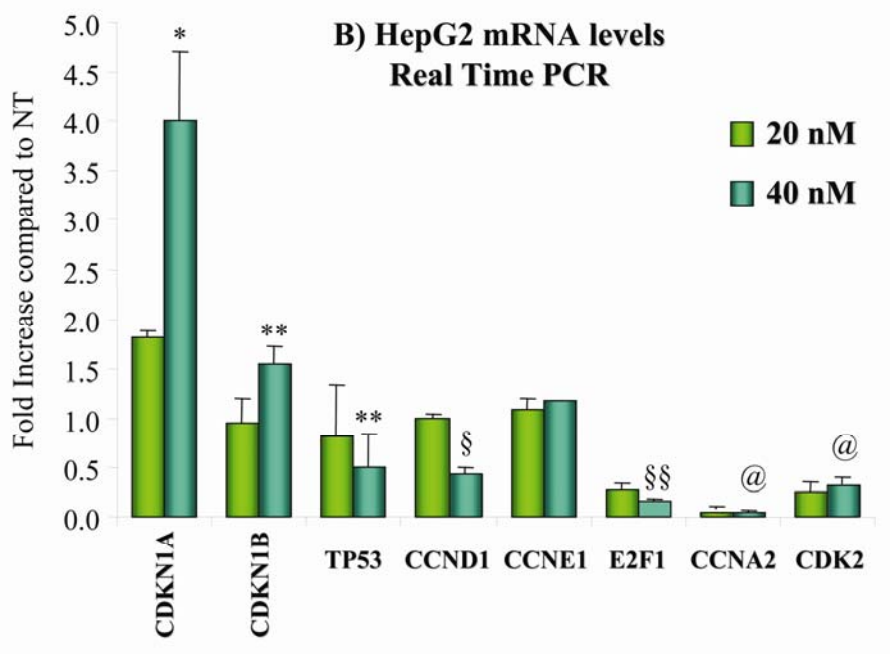

Figure 27B. mRNA levels of the cell cycle regulators in HepG2 cell line.

Bortezomib up-regulates the mRNA levels of CDKN1A (*$p<3x10^{-9}$) and CDKN1B (**$p<1x10^{-5}$). Up-regulation was observed for TP53 (**$p<1x10^{-5}$), CCND1 (§$p<3x10^{-8}$), E2F1 (§§$p<8x10^{-7}$), CCNA2 and CDK2 (@$p<7.4x10^{-5}$), compared to NT. No variation was observed for mRNA levels of CCNE1. Statistical analysis refers to 40 nM of bortezomib. CDKN1A=$p21^{waf1/cip1}$, CDKN1B=$p27^{kip1}$, TP53=p53, CCND1= cyclin D1, CCNE1= cyclin E1, CCNA2= cyclin A2. The results are expressed as means ±SEM, n=6.

In HuH7 a cosiderably decrease of the hyper-phosphorylated form of pRB, of E2F1 transcriptional factor and cyclin A2, together with a slight decrease of CdK2 was detected (Fig. 28A). As observed in HepG2, the levels of cyclin E1 were substantially not affected, as reported in western blot (1.29 folds for 40 nM of bortezomib, compared to control cells, Fig. 28A) and mRNA detection by Real Time PCR (Fig. 28B). Cyclin D1 protein levels were slightly decreased only at 40 nM of bortezomib. Regarding to cell cycle inhibitors it was found only a considerable increase of $p21^{waf1/cip1}$ (Fig. 28A).

Real Time PCR confirmed the data observed by western blot analysis: an increase of $p21^{waf1/cip1}$ (*$p<5x10^{-5}$), cyclin D1 (**$p<0.015$), and a decrease of E2F1 (§$p<0.001$), cyclin A2 (§§$p<8x10^{-8}$) and CdK2 (#$p<0.0001$) mRNAs, compared to NT (Fig. 28B).

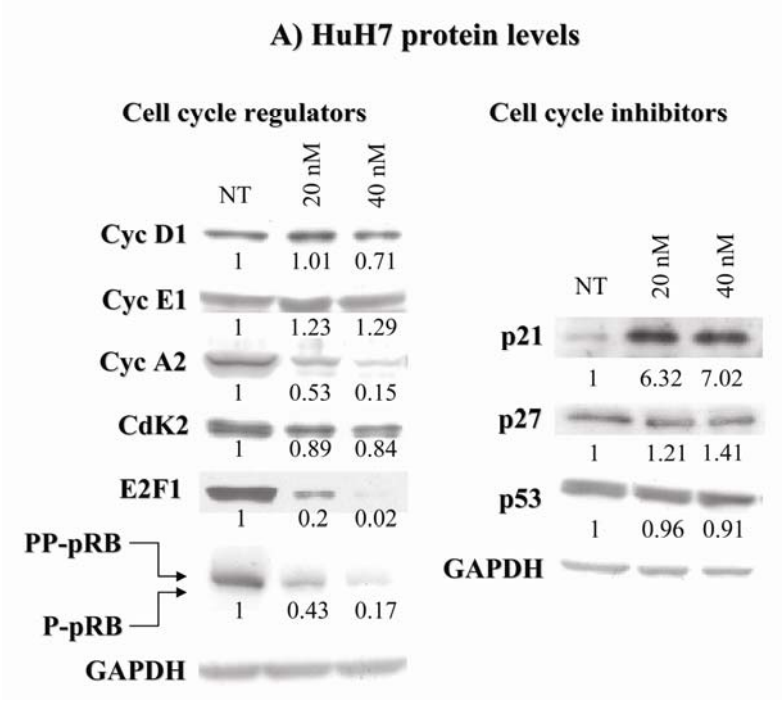

Figure 28A. A representative western blot of cell cycle regulators in HuH7 cell line.

PP-pRB=hyperphosphorylated pRB, P-pRB= hypophosphotylated pRB.

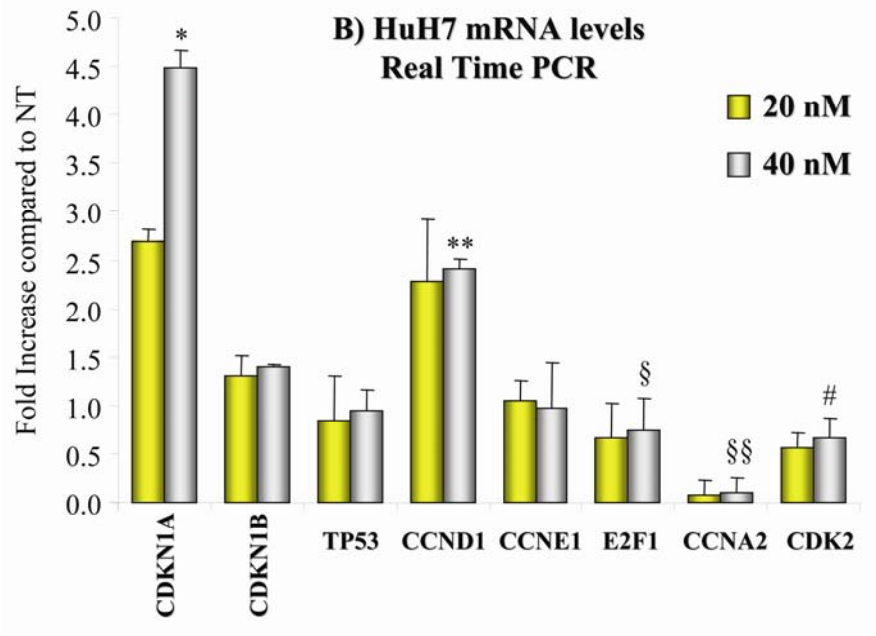

Figure 28B. mRNA levels of the cell cycle regulators in HuH7 cell line.

Bortezomib adminstration up-regulates the mRNA levels of CDKN1A (*$p<5x10^{-5}$) and cyclin D1 (**$p<0.015$). Down-regulation was observed for E2F1 (§$p<0.001$), CCNA2 (§§$p<8x10^{-8}$) and CDK2 (#$p<0.0001$), compared to NT. No variation was observed for mRNA levels of CCNE1. Statistical analysis refers to 40 nM of bortezomib. CDKN1A=$p21^{waf1/cip1}$, CDKN1B=$p27^{kip1}$, TP53=p53, CCND1= cyclin D1, CCNE1= cyclin E1, CCNA2= cyclin A2. The results are expressed as means ±SEM, n=6.

In JHH6, a reduction in the protein levels of cyclin A2, of the transcription factor E2F1 and of the hyper-phosphorylated form on pRB were observed compared to control cells (Fig. 28A). In JHH6, as observed in HepG2 and HuH7, the levels of cyclin E1 were substantially not affected, as reported in western blot (Fig. 29A) and mRNA detection by Real Time PCR (Fig. 29B). Additionally, protein levels of the other cell cycle regulators were substantially unaffected, except for $p21^{waf1/cip1}$, that evidenced a slight increase.

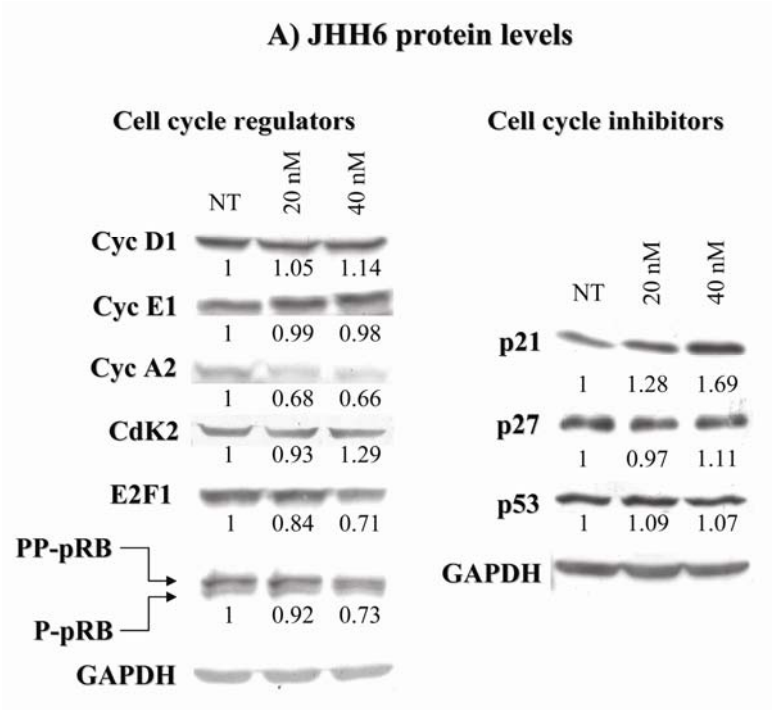

Figure 29A. A representative western blot of cell cycle regulators in JHH6 cell line.
PP-pRB=hyperphosphorylated pRB, P-pRB= hypophosphotylated pRB.

Regarding to mRNA levels, except for the increase of cyclin D1 (*$p<0.008$ at 40 nM of bortezomib, compared to NT), observed also in HuH7, and the tendency towards the decrease of cyclin A2, E2F1 and $p27^{kip1}$ mRNAs, no major variations were observed for the other mRNAs considered (Fig. 28B), confirming protein levels data.

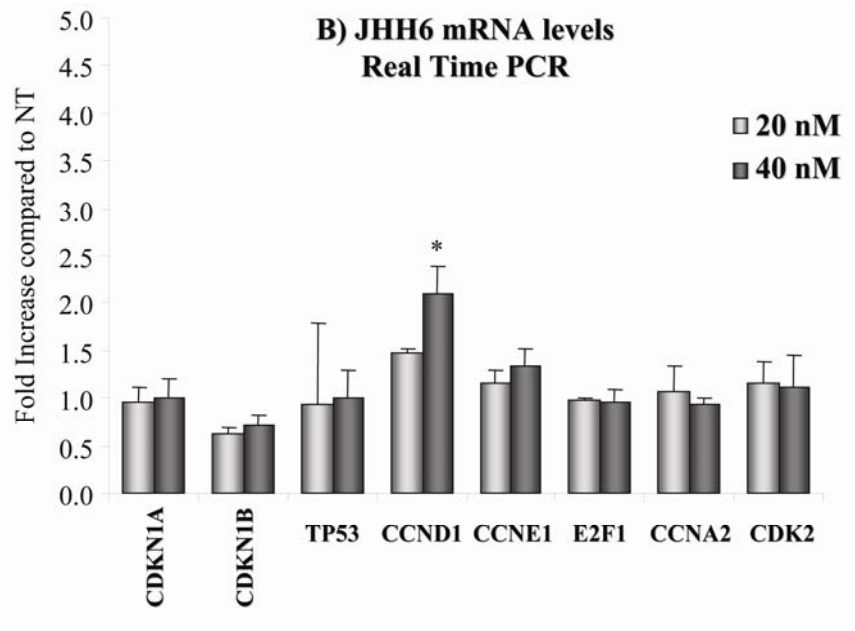

Figure 29B. mRNA levels of the cell cycle regulators in JHH6 cell line.

In JHH6, except for the increase of cyclin D1 (*p<0.008 at 40 nM of bortezomib, compared to NT) and the tendency towards the decrease of cyclin A2, E2F1 and $p27^{kip1}$ mRNAs, no major variations were observed for the other mRNAs considered, confirming protein levels data. CDKN1A=$p21^{waf1/cip1}$, CDKN1B=$p27^{kip1}$, TP53=p53, CCND1= cyclin D1, CCNE1= cyclin E1, CCNA2= cyclin A2. The results are expressed as means ±SEM, n=6.

Notably, both in HepG2 and JHH6, the depletion of E2F1 by an E2F1 directed siRNA (siE2F1), resulted in variation in the protein levels of the E2F1 regulated genes (cyclin D1, cyclin E1, cyclin A2, CdK2) and of the phosphorylation status of pRB not dissimilar to those observed following bortezomib treatment [Baiz et al]. This suggests that the variations in the expression levels of the E2F1 target genes observed following bortezomib treatment depends on E2F1 down-regulation.

2.2.6.2 Protein levels of P-cyclin E1 (T395)

The protein levels of cyclin E1, were slight increased in HepG2 and HuH7 (1.7 and 1.29 folds, compared to control cells, Fig. 27A and 27B). This fact neither depends on an increased mRNA amount detected by Real Time PCR (Fig. 27B and 28B) nor on a

reduced phosphorylation of cyclin E1 residue T395 (Fig. 30), a site whose phosphorylation is known to drive cyclin E1 degradation *via* proteasome [25].

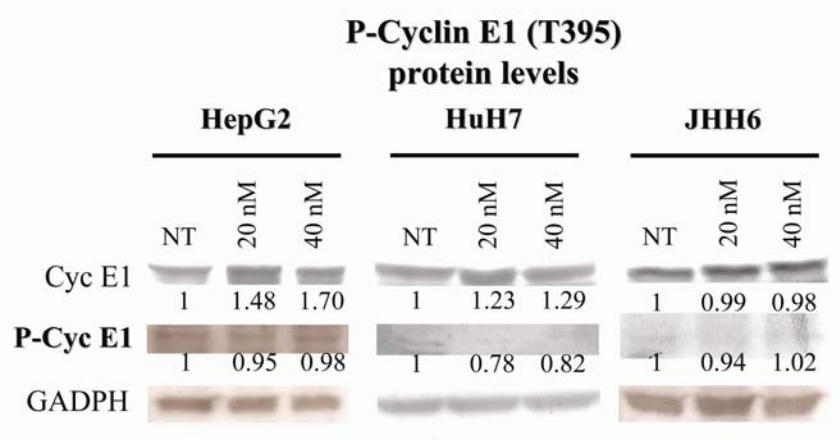

Figure 30. Western blot of Cyclin E1 phosphorylated at T395.

Cyclin E1 levels were sight increased in HepG2 and HuH7 (1.7 and 1.29 folds, compared to control cells). This fact neither depends on an increased mRNA amount detected by Real Time PCR (Fig. 27B and 28B) nor on a reduced phosphorylation of cyclin E1 residue T395, a site whose phosphorylation is known to drive cyclin E1 degradation *via* proteasome.

2.2.6.3 Relation between cyclin E1, E2F1 and LRH1

E2F1 is the pivotal transcription factor for cyclin E1 [26]. We therefore were surprised to observe a marked reduction in E2F1 expression (Fig. 27A and 28A) without a corresponding reduction in cyclin E1 mRNA levels (Fig. 27B and 28B). This prompted us to verify whether the expression levels of LRH1 (**L**iver **R**eceptor **H**omolog 1), a known alternative transcription factor for cyclin E1 in the hepatic lineage, was affected. LRH1 induces also cyclin D1 expression, acting as coactivator for β-catenin/Tcf4 complex. [27].

A marked decrease in E2F1 protein levels in HepG2 and HuH7 (Fig. 27A and 28A) were paralleled by a increase in the amount of LRH1 both at the protein (Fig. 32) and mRNA levels (*$p<0.001$, **$p<0.017$, compared to NT, Fig. 33). Accordingly, in JHH6, where the decrease of E2F1 protein level was modest compared to HepG2 and HuH7 (Fig. 27A

and 28A), no up-regulation, rather a down-regulation (Fig. 33, ***p<0.009 compared to NT) of LRH1 was observed.

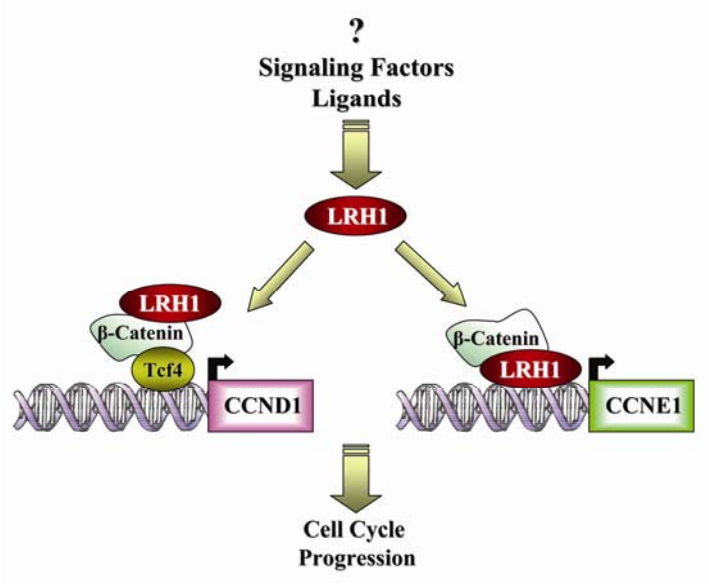

Figure 31. Liver Receptor Homolog 1.

LRH1 is an alternative transcriptional factor for cyclin D1 and cyclin E1 mRNAs in the hepatic lineage. (Bortrugno OA *et Al.* Synergy between LRH1 and β-catenin induces G_1 cyclin-mediated cell proliferation. *Molecular Cell,* 2004).

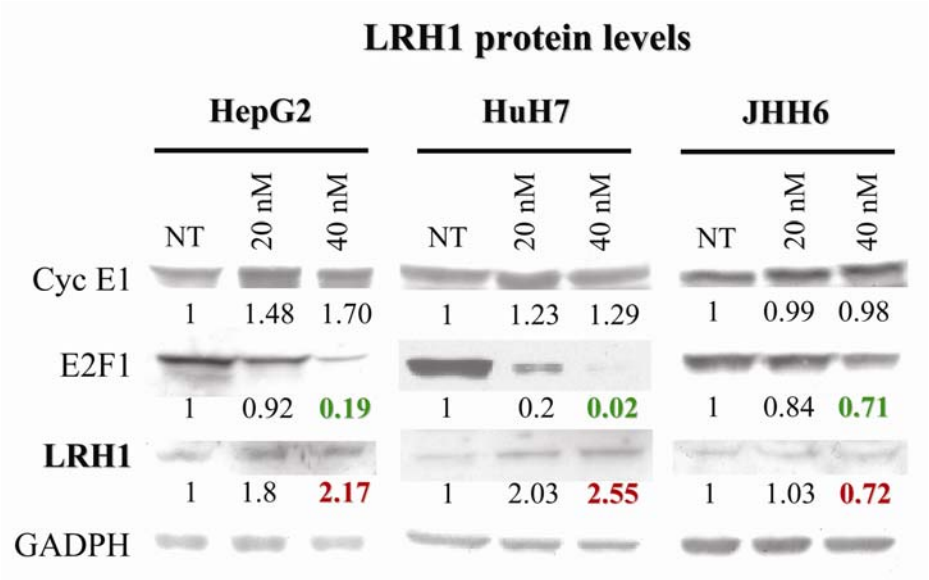

Figure 32. Representative western blot of transcriptional factor LRH1.

A marked decrease in E2F1 protein levels in HeG2 and HuH7 were paralleled by a increase in the amount of LRH1 protein, while in JHH6 the protein levels of both transcriptional factors were similar.

To verify whether in HepG2 the reduction of E2F1 level may promote LRH1 expression independently of bortezomib treatment, E2F1 was depleted in non-treated cell by a

specific siRNA and the expression levels of LRH1 and E2F1 monitored. The data reported indicate that despite the marked reduction of E2F1 mRNA level compared to controls ($p<0.0001$, compared to siGL2), no up-regulation of LRH1 mRNA was observed. Notably, this was true also in JHH6 cells. Thus, the E2F1/LRH1 inverse relation observed in HepG2 most likely represents a bortezomib-induced effect (see [28]).

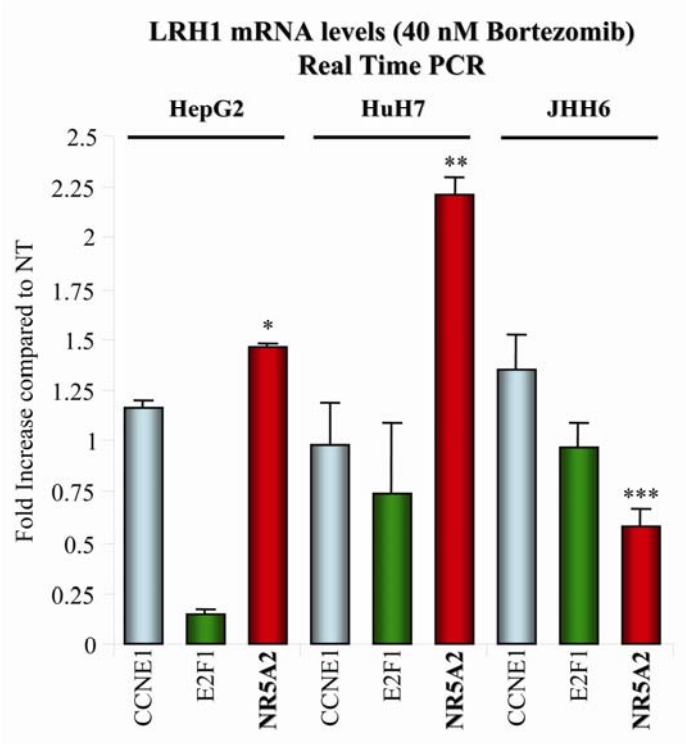

Figure 33. LRH1 mRNA levels in HCC cell lines.

A marked decrease in E2F1 protein levels in HepG2 and HuH7 were paralleled by a increase in the amount of LRH1 both at the protein (Fig. 32) and mRNA levels (*$p<0.001$, **$p<0.017$, compared to NT). Accordingly, in JHH6, where the decrease of E2F1 protein level was modest compared to HepG2 and HuH7 (Fig. 27A and 28A), no up-regulation, rather a down-regulation (***$p<0.009$, compared to NT) of LRH1 was observed. The results are expressed as means ±SEM, n=6.

2.2.7 Effect on cell viability of a combined administration of bortezomib and siE2F1

The reported data suggest that at least part of the bortezomib induced effects on HepG2, HuH7 and JHH6 occur *via* E2F1 down-modulation. We thus investigated whether siE2F1 could potentiate bortezomib effect. As reported in Figure 34, the combined bortezomib-siE2F1 treatment lead to an increased down-regulation of cell viability,

compared to the single administration of bortezomib (*p<0.004 for HepG2, **p<0.001 for HuH7, and ***p<0.003 for JHH6, compared to NT + 20nM of bortezomib).

This combined effect is more evident in HepG2 and in HuH7. However, in JHH6, the less bortezomib-affected HCC cell line, the specificity of the siE2F1 potentiates the bortezomib effect, decreasing the cell viability of about 30%, if compared with the single bortezomib treatment (Fig. 34).

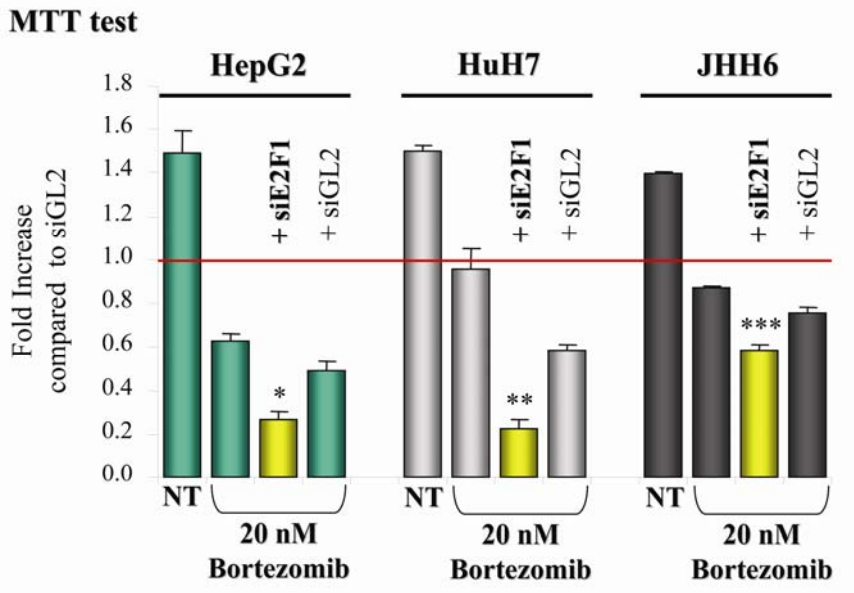

Figure 34. The combined effect of bortezomib-siE2F1 administration.

The combined bortezomib-siE2F1 treatment lead to an increased down-regulation of cell viability compared to the single administration of bortezomib. The results are expressed as means ±SEM, n=3 (*p<0.004 for HepG2, **p<0.001 for HuH7, and ***p<0.003 for JHH6, compared to NT+20 nM of bortezomib).

2.2.8 The peptidylproline cis-trans isomerase 1

In HepG2 (differentiated HCC cell line), 26S proteasome inhibition by bortezomib resulted in a marked decrease of protein and mRNA levels of the transcriptional factor E2F1 and of cyclin D1 (Fig. 27A and B), while in JHH6 (undifferentiated HCC cell line), no major variations were observed (Fig. 29A and B). Results in HuH7 (low

differentiated HCC cell line), were not so straightforward as in HepG2 and JHH6. In fact it was found a considerable decrease of E2F1 protein and mRNA levels, followed by the decrease of cyclin D1 protein levels, and increase of mRNA content (Fig. 28A and B). In order to understand these data, we investigated the protein and mRNA levels of the peptidylproline *cis-trans* isomerase 1 (Pin1), involved in cyclin D1 regulation.

Pin1 is a peptidylproline *cis-trans* isomerase (PPIase) that catalyzes the specific isomerization of Ser/Thr-Pro motifs only after phosphorylation, inducing conformational changes in order to regulate the function of Pin1 substrates [29]. Depending on the substrate protein, these conformational changes can affect enzymatic activity, phosphorylation status, protein-protein interactions, subcellular localization, or protein stability [30, 31]. Functionally, Pin1-catalyzed prolyl isomerization regulates such complex processes as cell cycle progression, transcription, and the response to DNA damage [32-34]. Furthermore, Pin1 has been shown to be involved in the pathogenesis of some human diseases, such as Alzheimer's disease [35].

Pin1 is a E2F downstream target gene essential for *Neu/Ras*-induced cyclin D1 activation ad cell transformation (Fig. 35 and 36).

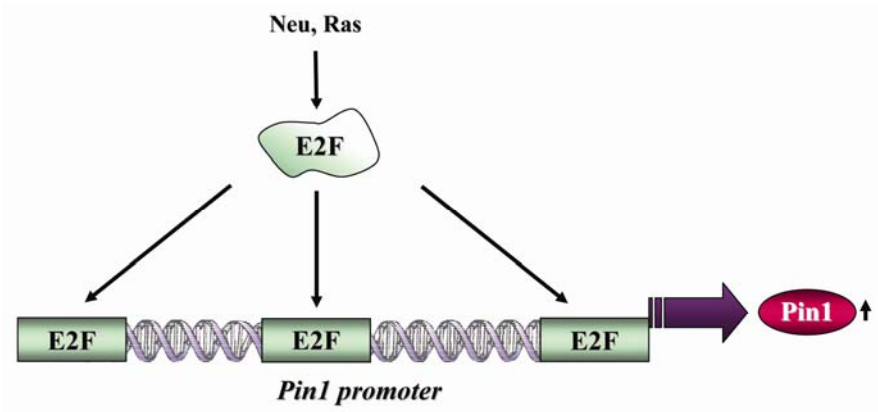

Figure 35. Regulation of Pin1 expression by E2F family.

Oncogenic *Neu/Ras* signalling transactivates the *PIN1* promoter through E2F activity.

PIN1, up-regulated by Neu/Ras signalling, enhances β-catenin and c-Jun signalling to transactivate the cyclin D1 gene. Furthermore, Pin1 binds to cyclin D1 and stabilizes it *via* a post-translational mechanism. It is possible that cyclin D1 also regulates Pin1 expression *via* E2F in a positive feedback loop (Fig. 36) [36].

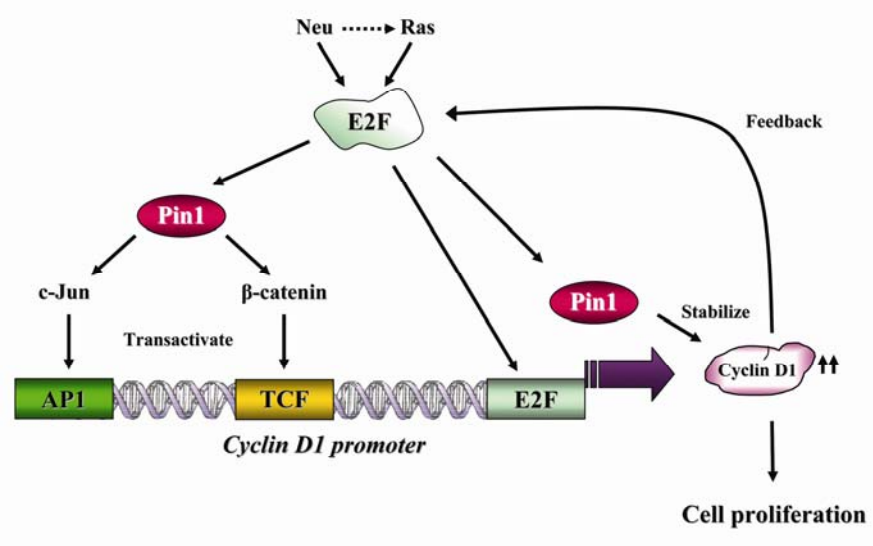

Figure 36. Regulation and functions of peptidylproline *cis-trans* isomerase 1.

PIN1, up-regulated by *Neu/Ras* signalling, enhances β-catenin and c-Jun signalling to transactivate the cyclin D1 gene. Furthermore, Pin1 binds to cyclin D1 and stabilizes it *via* a post-translational mechanism. It is possible that cyclin D1 also regulates Pin1 expression *via* E2F in a positive feedback loop.

2.2.8.1 Protein and mRNA levels of Pin1

Results indicated that in HepG2 and HuH7 a considerable decrease of E2F1 protein levels were parallel to Pin1 and cyclin D1 decrease, while in JHH6 no major variations were observed for Pin1 protein levels, as expected (Fig. 37).

Regarding to mRNA levels (Fig. 38), a down-regulation of PIN1 was detected in HepG2 and HuH7 (*$p<0.0003$ and **$p<7x10^{-7}$, respectively, compared to NT). Notably, in JHH6, no major variations were detected in E2F1 and PIN1 mRNA levels

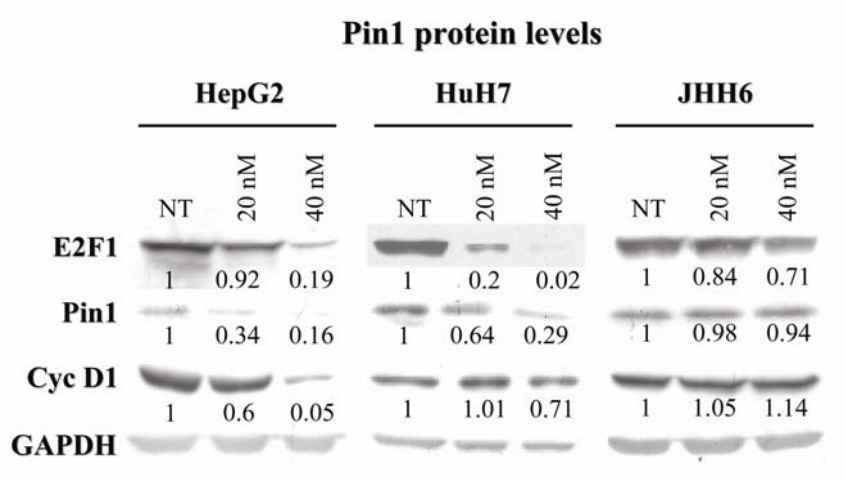

Figure 37. A representative western blot of Pin1.
Pin1 protein levels were decreased in HepG2 and HuH7, while in JHH6 no major variations were observed.

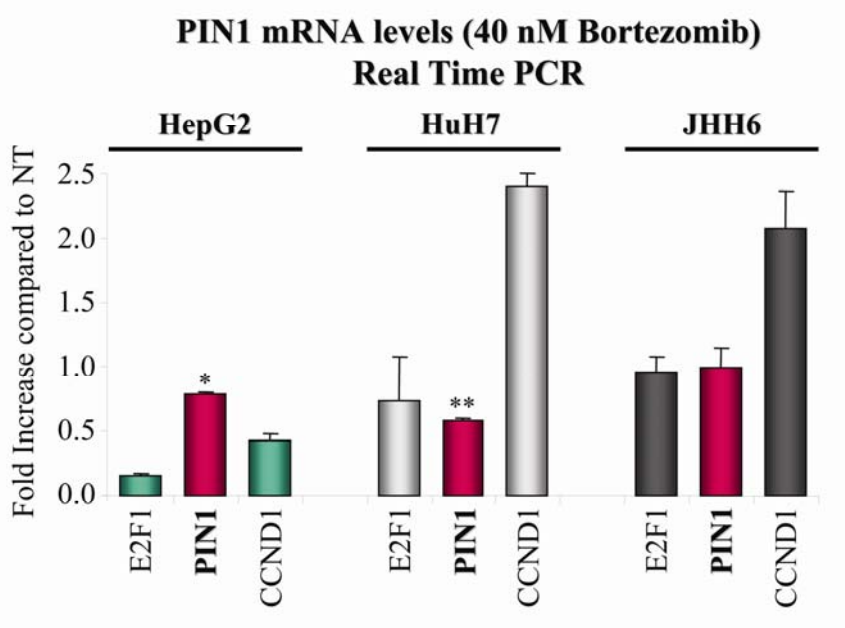

Figure 38. mRNA levels of PIN1 in HCC cell lines.

A down-regulation of PIN1 was detected in HepG2 and HuH7. The results are expressed as means ±SEM, n=6 (*$p<0.0003$ and **$p<7x10^{-7}$, respectively, compared to NT). CCND1= cyclin D1.

2.2.9 Two-color microarray-based gene expression analysis

Two-color microarray compares cRNAs prepared from two total RNAs samples (control cells versus 40 nM bortezomib-treated cells), which are labeled with two different fluorophores. Fluorescent dyes used for NT control cells cRNA labelling was cyanine 3-CTP, which has a fluorescence emission wavelength of 570 nm (corresponding to the green part of the light spectrum), while for 40 nM of bortezomib-treated cells was cyanine 5-CTP with a fluorescence emission wavelength of 670 nm (corresponding to the red part of the light spectrum). The two Cy-labelled cRNA samples were mixed and hybridized to a single microarray that was then scanned in a microarray scanner to visualize fluorescence of the two fluorophores after excitation with a laser beam of a defined wavelength. Relative intensities of each fluorophore were used in ratio-based analysis to identify up-regulated and down-regulated genes (Figure 39).

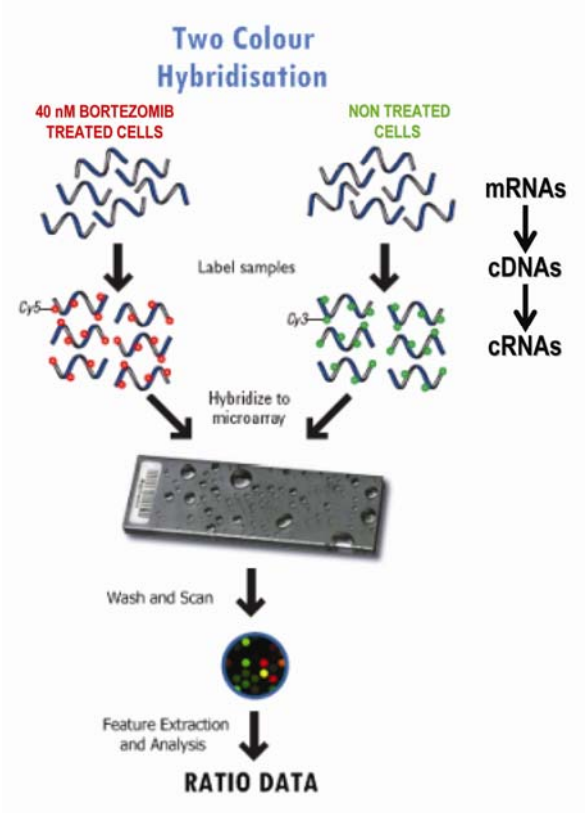

Figure 39. Two-color microarray-based gene expression analysis.

cRNAs prepared from two total RNA samples (control cells versus 40 nM bortezomib-treated cells), are labeled with cyanine 3-CTP, (NT cells), and cyanine 5-CTP (40 nM of bortezomib). The two Cy-labelled cRNA samples are mixed and hybridized to a single microarray that is then scanned in a microarray scanner to visualize fluorescence of the two fluorophores after excitation with a laser beam of a defined wavelength. Relative intensities of each fluorophore may then be used in ratio-based analysis to identify up-regulated and down-regulated genes.

Figure 40 reports the procedure for amplification of cRNAs. The method uses T7 RNA polymerase which simultaneously amplifies target material and incorporates cyanine 3- or cyanine 5-labeled CTP. T7 RNA polymerase is extremely promoter-specific, catalyzes the formation of RNA in the 5'→3' direction, and requires a DNA template.

Normalization of data was conducted with RNA-spike ins. An RNA spike-in is an RNA transcript used to calibrate measurements in a two-color microarray experiment. Oligonucleotide microarrays contain control probes designed to hybridize with RNA spike-ins. The degree of hybridization between the RNA spike-in and the control probes is used to normalize the hybridization measurements for the target probes. Each spike-in is designed to hybridize with a specific control probe on the target array. Known amounts of RNA spike-ins were mixed with samples during preparation. Subsequently the measured degree of hybridization between the spike-ins and the control probes was used to normalize the hybridization measurements of the sample RNAs.

Microarrays were performed in HepG2 and JHH6, in order to compare the differences in gene expression between a different phenotype and high affected by bortezomib HCC cell line and an undifferentiated and low affected by bortezomib HCC cell line. Comparisons between control versus 40 nM of bortezomib gene expression is reported in Figure 41.

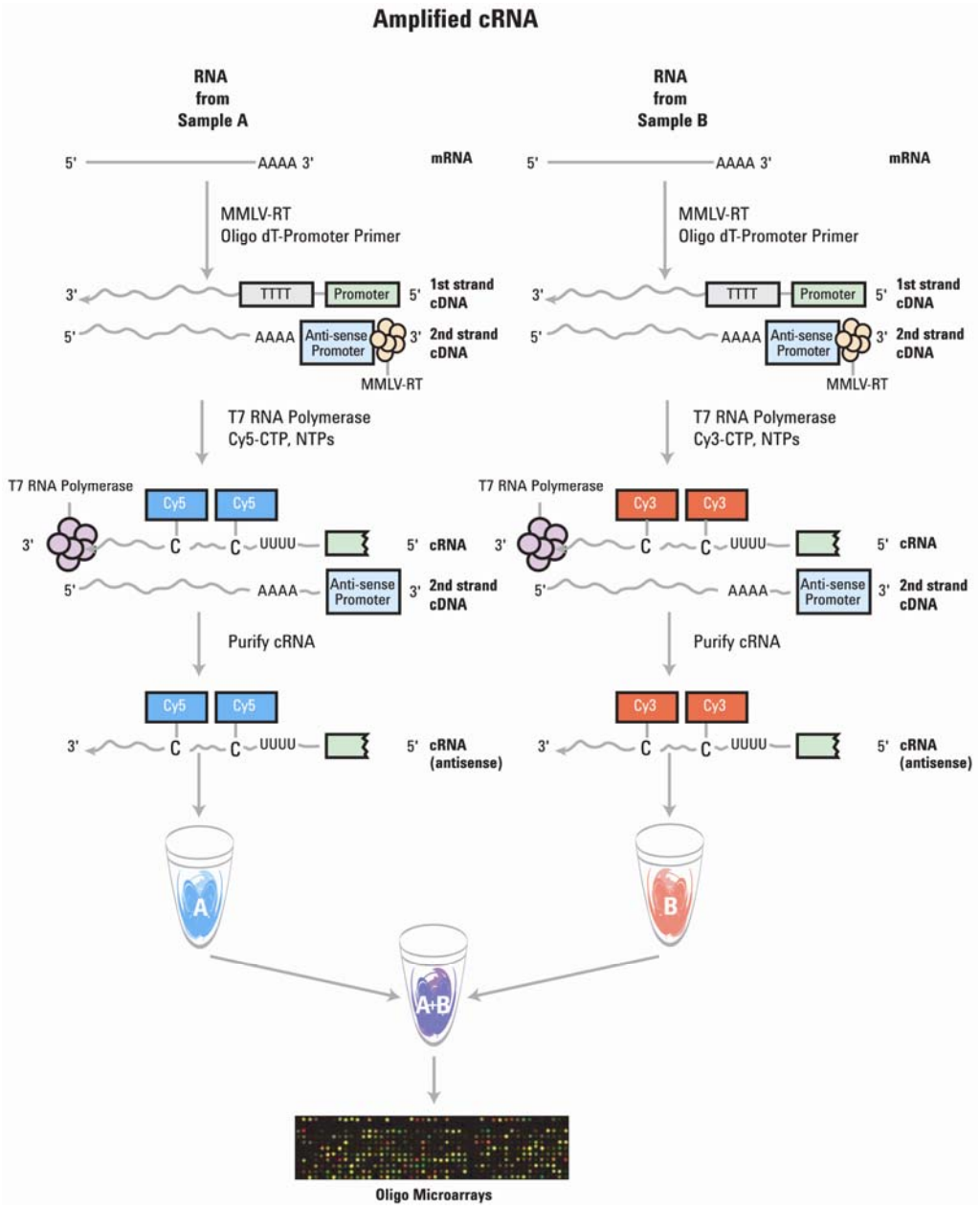

Figure 40. Amplification of cRNA using T7 RNA polymerase.

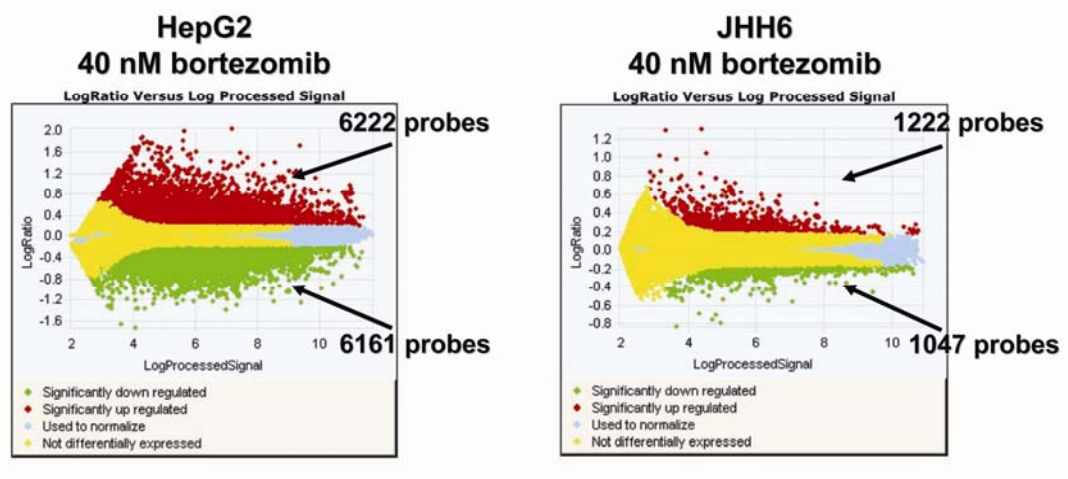

Figure 41. Comparison between HepG2 and JHH6 gene expression.

HepG2 are more affected than JHH6 by bortezomib treatment and this fact is evident in gene expression. Red spots refer to up-regulated genes, while green spots to down-regulated. Yellow spots are related to genes not differentially expressed (more evident in JHH6). Blue spots were used to normalize data by Agilent Scan B.

We were not surprised to find in HepG2 a more evident up- and down-regulation of genes than in JHH6, induced by bortezomib treatment. Although the up- and down-regulation genes ratio is comparable in the two cell lines, not affected genes group is marked increase in JHH6.

Analysis of cell cycle factors monitored confirm the trend evaluated by Real Time PCR detection (Fig. 27B and 29B). In HepG2, it was observed a marked increase of $p21^{waf1/cip1}$ (*$p<9x10^{-16}$), parallel with a decrease of p53 (**$p<4x10^{-10}$), E2F1 (§$p<8x10^{-36}$), cyclin D1 (§§$p<8x10^{-13}$), cyclin A2 (^$p<2x10^{-43}$), and CdK2 (^^$p<0.0002$) mRNAs, compared to control. No major variations were observed for cyclin E1 and LRH1 (NR5A2) mRNAs (Fig. 42).

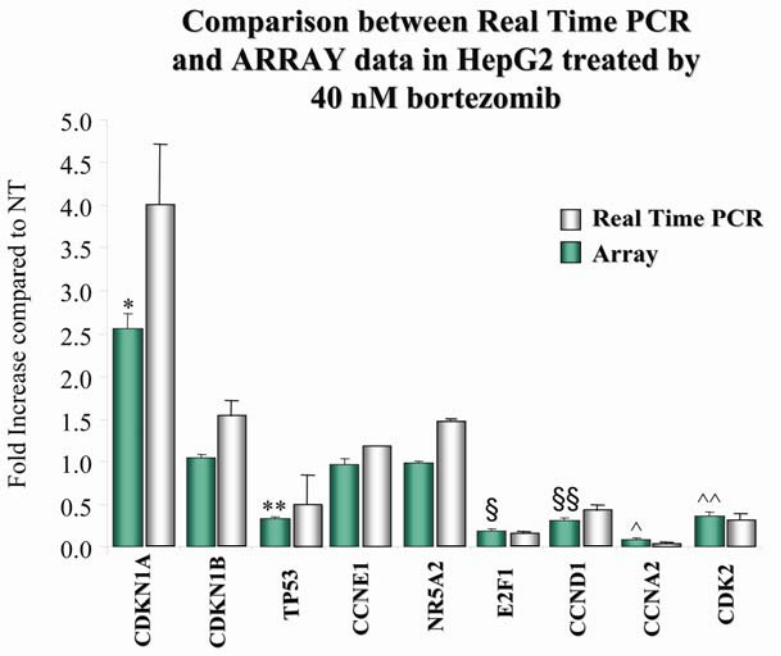

Figure 42. Comparison between Real Time PCR and Array data in HepG2.

It was observed a marked increase of $p21^{waf1/cip1}$ (*$p<9x10^{-16}$), a decrease of p53 (**$p<4x10^{-10}$), E2F1 (§$p<8x10^{-36}$), cyclin D1 (§§$p<8x10^{-13}$), cyclin A2 (^$p<2x10^{-43}$), and CdK2 (^^$p<0.0002$) mRNAs, compared to control. CDKN1A=$p21^{waf1/cip1}$, CDKN1B=$p27^{kip1}$, TP53=p53, CCND1= cyclin D1, CCNE1= cyclin E1, CCNA2= cyclin A2, NR5A2=LRH1. The results are expressed as means ±SEM, n=6.

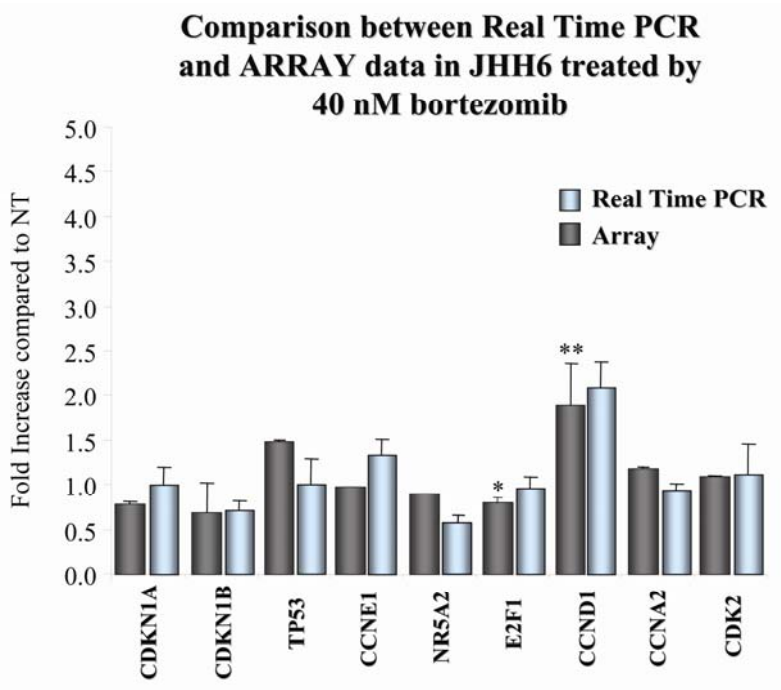

Figure 43. Comparison between Real Time PCR and Array data in JHH6.

Microarray analysis confirmed the slight decrease of E2F1 (*$p<2x10^{-10}$) and increase of cycln D1 (**$p<7x10^{-5}$) mRNAs. CDKN1A=$p21^{waf1/cip1}$, CDKN1B=$p27^{kip1}$, TP53=p53, CCND1= cyclin D1, CCNE1= cyclin E1, CCNA2= cyclin A2, NR5A2=LRH1. The results are expressed as means ±SEM, n=6.

Regarding to JHH6, the less sensitive cell line, it was confirmed the slight decrease of E2F1 (*$p<2x10^{-10}$) and increase of cycln D1 (**$p<7x10^{-5}$) mRNAs (Fig. 42).

2.2.9.1 $p16^{ink4a}$ levels

As mentioned above, $p16^{ink4a}$ is a cell cycle inhibitor that exerts its activity inhibiting the cyclin D-CdK4 complex, and in turn, G_1 phase. $p16^{ink4a}$ is not expressed in HuH7 and in JHH6 protein detection was not possible as in HepG2 with the same antibody. Analysing microarray data, we observed in HepG2 no major variations in $p16^{ink4a}$ mRNA levels, after bortezomib treatment (Fig. 44). This result was confirmed by western blot analysis.

In JHH6, nevertheless, microarray probes detect $p16^{ink4a}$ mRNA (Fig. 44), evidencing a significant decrease after bortezomib treatment (*p<0.007).

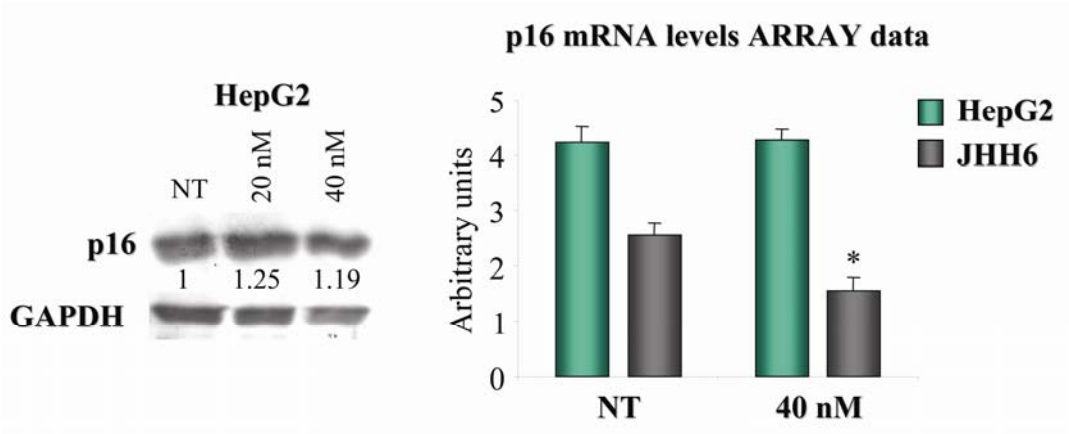

Figure 44. $p16^{ink4a}$ evaluation in HepG2 and JHH6.

No major variations were observed monitoring the $p16^{ink4a}$ protein levels (western blot, on the left) in HepG2. Regarding to mRNA levels, no major variations were detected in HepG2, while a significant decrease was observed in JHH6 (*p<0.007), on the right. The results are expressed as means ±SEM, n=6.

2.2.9.2 Pin1 levels

Microarray data were also used to compare mRNA analysis by Real Time PCR of Pin1 (Fig. 38). A considerable decrease of Pin1 mRNA was detected in HepG2 (*p<0.004), while no variations were observed in JHH6 (Fig. 45).

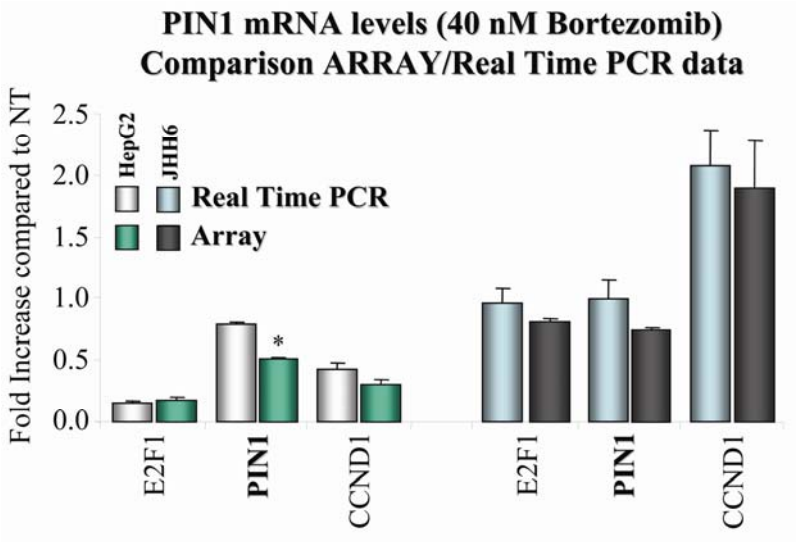

Figure 45. Comparison between Real Time PCR and Array data for PIN1.

A considerable decrease of Pin1 mRNA was detected in HepG2. The results are expressed as means ±SEM, n=6 (*p<0.004). CCND1= cyclin D1.

2.2.9.3 Effects of bortezomib on EEF1A levels

We discovered in HepG2 and JHH6 a significant increase of EEF1A1 mRNA levels compared to normal liver, while a marked increase of EEF1A2 mRNA was detected in JHH6 only (Fig. 2 and 3). Microarray data evidenced an increase of EEF1A2 mRNA (40 nM of bortezomib, *p<0.02). in JHH6 (Fig. 46).

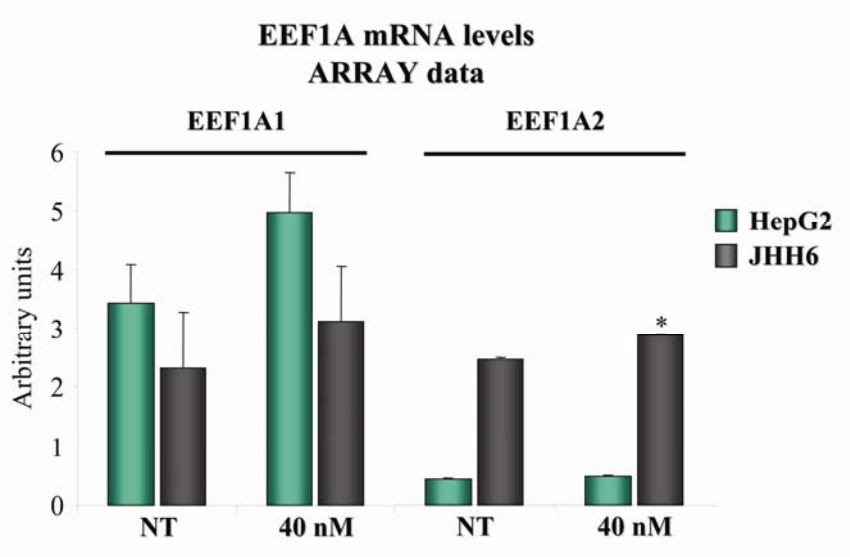

Figure 46. EEF1A mRNA levels in HepG2 and JHH6.

Microarray data revealed an increase of EEF1A1 mRNA levels in HepG2 and an increase of EEF1A2 mRNA levels in JHH6, comparing both NT cell lines, confirming our results (Fig. 2). Regarding to EEF1A2, a significant increase was observed in JHH6-treated cells (40 nM of bortezomib, *p<0.02). The results are expressed as means ±SEM, n=6.

Comparison between EEF1A1 and EEF1A2 mRNAs detected by Real Time PCR (only for HepG2), is reported in Figure 47. An increase of EEF1A1 (*p<0.004) compared to control, was observed in Real Time PCR and microarray data.

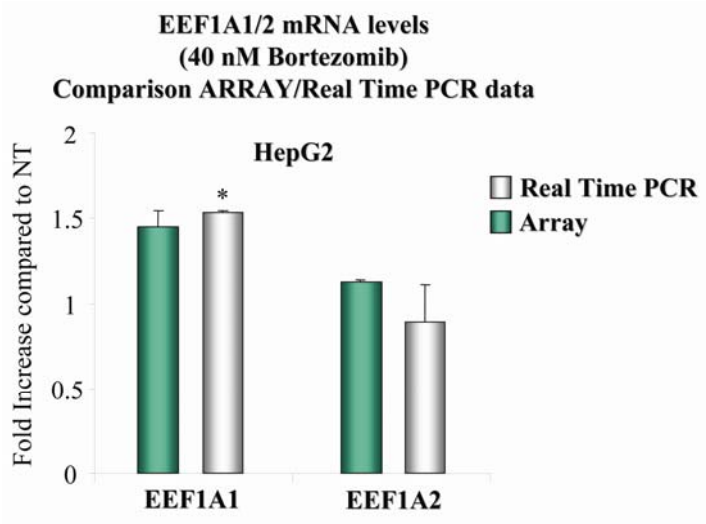

Figure 47. Comparison between Real Time PCR and Array data for EEF1A1/2 in HepG2.

Comparison between EEF1A1 and EEF1A2 mRNAs detected by Real Time PCR evidenced an increase of EEF1A1 (*p<0.004) compared to control, confirming microarray array data. The results are expressed as means ±SEM, n=6.

Regarding to protein levels, a marked decrease of eEF1A2 was found in HepG2, while a significant increase was observed in JHH6, compared to controls (Fig. 48), after bortezomib treatments. Detection of both eEF1A1 and eEF1A2 proteins (eEF1A) is reported.

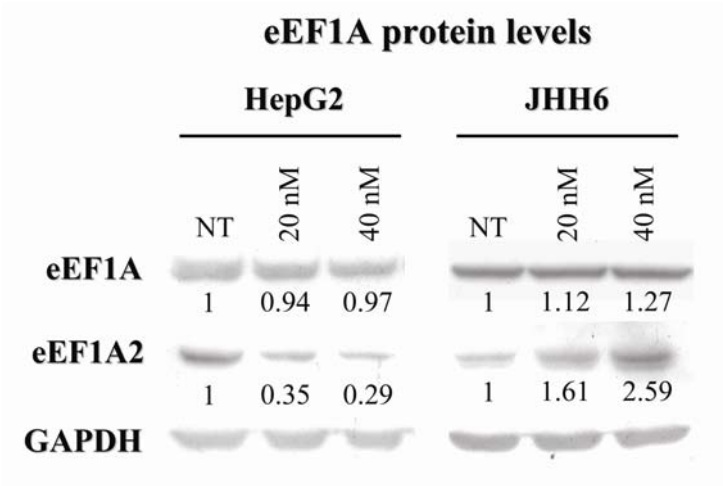

Figure 48. eEF1A2 protein levels in HepG2 and JHH6.
A marked decrease of eEF1A2 was found in HepG2, while a significant increase was observed in JHH6, compared to controls, after bortezomib treatments. Detection of both eEF1A1 and eEF1A2 proteins (eEF1A) is reported.

2.3 REFERENCES

1. Fujise, K., et al., *Integration of hepatitis B virus DNA into cells of six established human hepatocellular carcinoma cell lines.* Hepatogastroenterology, 1990. **37**(5): p. 457-60.
2. Nagamori, S., et al., *[Protein secretion of human cultured liver cells].* Hum Cell, 1988. **1**(4): p. 382-90.
3. Grassi, G., et al., *The expression levels of the translational factors eEF1A 1/2 correlate with cell growth but not apoptosis in hepatocellular carcinoma cell lines with different differentiation grade.* Biochimie, 2007. **89**(12): p. 1544-52.
4. Lee, J.M., *The role of protein elongation factor eEF1A2 in ovarian cancer.* Reprod Biol Endocrinol, 2003. **1**: p. 69.
5. Talapatra, S., J.D. Wagner, and C.B. Thompson, *Elongation factor-1 alpha is a selective regulator of growth factor withdrawal and ER stress-induced apoptosis.* Cell Death Differ, 2002. **9**(8): p. 856-61.
6. Duttaroy, A., et al., *Apoptosis rate can be accelerated or decelerated by overexpression or reduction of the level of elongation factor-1 alpha.* Exp Cell Res, 1998. **238**(1): p. 168-76.
7. Ruest, L.B., R. Marcotte, and E. Wang, *Peptide elongation factor eEF1A-2/S1 expression in cultured differentiated myotubes and its protective effect against caspase-3-mediated apoptosis.* J Biol Chem, 2002. **277**(7): p. 5418-25.
8. Liu, X.W., et al., *Tissue inhibitor of metalloproteinase-1 protects human breast epithelial cells against intrinsic apoptotic cell death via the focal adhesion kinase/phosphatidylinositol 3-kinase and MAPK signaling pathway.* J Biol Chem, 2003. **278**(41): p. 40364-72.
9. Quinn, C.M., et al., *Induction of fibroblast apolipoprotein E expression during apoptosis, starvation-induced growth arrest and mitosis.* Biochem J, 2004. **378**(Pt 3): p. 753-61.
10. Scaggiante, B., et al., *Interaction of G-rich GT oligonucleotides with nuclear-associated eEF1A is correlated with their antiproliferative effect in haematopoietic human cancer cell lines.* FEBS J, 2006. **273**(7): p. 1350-61.
11. Cavallius, J., S.I. Rattan, and B.F. Clark, *Changes in activity and amount of active elongation factor 1 alpha in aging and immortal human fibroblast cultures.* Exp Gerontol, 1986. **21**(3): p. 149-57.
12. Gangwani, L., et al., *Interaction of ZPR1 with translation elongation factor-1alpha in proliferating cells.* J Cell Biol, 1998. **143**(6): p. 1471-84.
13. Maeta, Y., et al., *Effect of promoter methylation of the p16 gene on phosphorylation of retinoblastoma gene product and growth of hepatocellular carcinoma cells.* Tumour Biol, 2005. **26**(6): p. 300-5.
14. Dimri, G.P., et al., *A biomarker that identifies senescent human cells in culture and in aging skin in vivo.* Proc Natl Acad Sci U S A, 1995. **92**(20): p. 9363-7.

15. Papandreou, C.N., et al., *Phase I trial of the proteasome inhibitor bortezomib in patients with advanced solid tumors with observations in androgen-independent prostate cancer.* J Clin Oncol, 2004. **22**(11): p. 2108-21.
16. Reinheckel, T., et al., *Comparative resistance of the 20S and 26S proteasome to oxidative stress.* Biochem J, 1998. **335 (Pt 3)**: p. 637-42.
17. Powell, S.R., K.J. Davies, and A. Divald, *Optimal determination of heart tissue 26S-proteasome activity requires maximal stimulating ATP concentrations.* J Mol Cell Cardiol, 2007. **42**(1): p. 265-9.
18. Skaper, S.D., *Poly(ADP-Ribose) polymerase-1 in acute neuronal death and inflammation: a strategy for neuroprotection.* Ann N Y Acad Sci, 2003. **993**: p. 217-28; discussion 287-8.
19. Frenzel, A., et al., *Bcl2 family proteins in carcinogenesis and the treatment of cancer.* Apoptosis, 2009.
20. Shabnam, M.S., et al., *Expression of p53 protein and the apoptotic regulatory molecules Bcl-2, Bcl-XL, and Bax in locally advanced squamous cell carcinoma of the lung.* Lung Cancer, 2004. **45**(2): p. 181-8.
21. Cohen, G.M., *Caspases: the executioners of apoptosis.* Biochem J, 1997. **326 (Pt 1)**: p. 1-16.
22. Campioni, M., et al., *Role of Apaf-1, a key regulator of apoptosis, in melanoma progression and chemoresistance.* Exp Dermatol, 2005. **14**(11): p. 811-8.
23. Li, P., D. Nijhawan, and X. Wang, *Mitochondrial activation of apoptosis.* Cell, 2004. **116**(2 Suppl): p. S57-9, 2 p following S59.
24. Danial, N.N. and S.J. Korsmeyer, *Cell death: critical control points.* Cell, 2004. **116**(2): p. 205-19.
25. Clurman, B.E., et al., *Turnover of cyclin E by the ubiquitin-proteasome pathway is regulated by cdk2 binding and cyclin phosphorylation.* Genes Dev, 1996. **10**(16): p. 1979-90.
26. Geng, Y., et al., *Regulation of cyclin E transcription by E2Fs and retinoblastoma protein.* Oncogene, 1996. **12**(6): p. 1173-80.
27. Botrugno, O.A., et al., *Synergy between LRH-1 and beta-catenin induces G1 cyclin-mediated cell proliferation.* Mol Cell, 2004. **15**(4): p. 499-509.
28. Baiz, D., et al., *Bortezomib arrests the proliferation of hepatocellular carcinoma cells HepG2 and JHH6 by differentially affecting E2F1, p21 and p27 levels.* Biochimie, 2008.
29. Lu, K.P., Y.C. Liou, and X.Z. Zhou, *Pinning down proline-directed phosphorylation signaling.* Trends Cell Biol, 2002. **12**(4): p. 164-72.
30. Shen, Z.J., et al., *The peptidyl-prolyl isomerase Pin1 facilitates cytokine-induced survival of eosinophils by suppressing Bax activation.* Nat Immunol, 2009.
31. Crenshaw, D.G., et al., *The mitotic peptidyl-prolyl isomerase, Pin1, interacts with Cdc25 and Plx1.* EMBO J, 1998. **17**(5): p. 1315-27.
32. Liu, W., et al., *Binding and regulation of the transcription factor NFAT by the peptidyl prolyl cis-trans isomerase Pin1.* FEBS Lett, 2001. **496**(2-3): p. 105-8.

33. Winkler, K.E., et al., *Requirement of the prolyl isomerase Pin1 for the replication checkpoint.* Science, 2000. **287**(5458): p. 1644-7.

34. Wulf, G.M., et al., *Role of Pin1 in the regulation of p53 stability and p21 transactivation, and cell cycle checkpoints in response to DNA damage.* J Biol Chem, 2002. **277**(50): p. 47976-9.

35. Nowotny, P., et al., *Association studies between common variants in prolyl isomerase Pin1 and the risk for late-onset Alzheimer's disease.* Neurosci Lett, 2007. **419**(1): p. 15-7.

36. Ryo, A., et al., *PIN1 is an E2F target gene essential for Neu/Ras-induced transformation of mammary epithelial cells.* Mol Cell Biol, 2002. **22**(15): p. 5281-95.

Discussion

There is a growing evidence of the involvement of components of the translation machinery in the development of cancer. In particular, the protein elongation factor eEF1A2 has been identified as an important player in many human tumors [1-3]. Despite these observations, no information are so far available on its possible contribution to the biology of hepatocellular carcinoma [4].

We show that the mRNA levels of both EEF1A1 and EEF1A2 are dramatically increased in the JHH6 cells compared either to the normal liver or HepG2 and HuH7 cells (Fig. 2). Since the differentiation grade decreases from HepG2 to HuH7 and JHH6 [5, 6], it is tempting to speculate that there might be a direct correlation between the mRNA levels of eEF1A1/2 and the neoplastic phenotype of hepatocellular carcinoma cells. It is possible that a more undifferentiated HCC cell needs higher amount of eEF1A mRNA to sustain a prompt protein synthesis, possibly required in cell proliferation and in the organization of cytoskeleton [7], both crucial aspects for an actively cycling/migrating cell.

Whereas only one of the two eEF1A forms is normally expressed in non transformed cells [8] in the HCC cell lines considered, we observed the contemporary elevation of the two EEF1A mRNAs, a phenomenon particularly marked in JHH6 cells (Fig. 2). This observation may in part depend on the parallel gene amplification detected for both EEF1A1 and EEF1A2 (Fig. 3). In fact, the modest extent of amplification can hardly account for the dramatic increase of the mRNA levels observed, especially in JHH6 cells. A better insight about this observation will come from the evaluation on the expression levels of eEF1A forms in an appropriate number of HCC biopsies from patients.

The increased mRNA expression of EEF1A genes in JHH6 with respect to HepG2, is paralleled by an increased of nuclear-enriched/cytoplasm protein ratio (Fig. 3A and 3B) in JHH6 (#p=0.038) compared to HepG2. The fact that by means of the nuclear protein extraction procedure the cytoskeleton sedimentation occurs, and with it sediments the eEF1A1 bound to actin [9, 10], may suggest that in JHH6, the higher levels of cytoskeleton-bound eEF1A1 are required for the non-canonical function of this protein in cytoskeletal organization [9]. The higher mRNA levels detected for eEF1A1 compared to normal tissue and HepG2 cells may thus represent a reservoir usable not only for a prompt protein synthesis but especially for cytoskeleton remodeling. As the antibody used to detect eEF1A does not discriminate between the two forms of the protein, we cannot exclude that part of the elevation of the nuclear-enriched amount of eEF1A may depend on eEF1A2 too (Fig. 4). Moreover, the dramatic elevation in eEF1A2 mRNA level favors the hypothesis that in JHH6, eEF1A2, at least indirectly, contributes to modulate cytoskeleton organization [11].

The different expression levels and/or the sub-cellular localization [11-14] of eEF1A have been related to cell proliferation in different cell types. In subconfluent HCC-derived cells, no significant differences were noted in cell growth rate (evaluated by DNA synthesis) and the expression of different cyclins and of the transcription factor E2F1 [12]. Thus, the different levels observed for $p16^{ink4a}$ and $p27^{kip1}$ in JHH6 compared to HepG2 (Fig. 6) may not have a functional meaning, at least within the experimental conditions used.

Since no detectable differences in the growing rate were evident in subconfluent cells, we speculated that differences might have arisen under not optimal growth conditions, such as those represented by prolonged culturing time where the marked increase in cell

number determines an increase of toxic metabolites and a decrease of nutrients per cell. A more pronounced attitude of HepG2 compared to JHH6 to exit cell cycle was observed between 2 and 4 days after reaching confluence as indicated by the staining for the senescence associated β-gal (Fig. 9). The fact that the exit from the cell cycle of HepG2 occurred some days after reaching confluence, suggests a minor contribution of cell contact inhibition to the escape from cell cycle.

The negligible number of JHH6 cells positive for the β-gal associated senescence staining suggests that these cells tend to be more resistant than HepG2 to aging/senescence and may have extended life capacity, a feature of aggressive cancer cells. Thus, in contrast to what reported in another cell type [13], in the hepatic cell line JHH6 the over-expression of EEF1A genes correlates with higher proliferation ability only under non optimal growing conditions either by activating cell survival mechanisms or by affecting cytoskeletal organization. Translated to the *in vivo* condition, this feature may confer to the cells a more aggressive tumor phenotype allowing the proliferation in areas of the tumor far from vessels were nutrients and oxygen concentration are reduced. It should be noted that, despite the relation observed between EEF1A gene expression and the proliferative features of JHH6 and HepG2, we cannot exclude that other biological factors can contribute to the different proliferation features observed.

The relation between eEF1A1/2 expression and apoptosis shown in other experimental models [14] prompted us to investigate this biological aspect in the HCC cells studied. In sub-confluent cells we did not detect any significant difference in apoptotic rate between JHH6 and HepG2 cells in the presence/absence of growth factors and when treated with a known pro-apoptotic agent such as staurosporin [12]. In some cases

increased eEF1A expression has been shown to favor apoptosis upon serum deprivation [15, 16], in other to protect [16, 17]. These observations together with our data seem to indicate a different cell specific relation between eEFA1/2 expression and apoptosis.

The data here reported indicate that in the hepatic cell lines used, HepG2, HuH7 and JHH6, bortezomib markedly reduces the amount of living cells (Fig. 11, 12, and 13) in a dose-dependent manner. Notably, this effect is less pronounced in JHH6 compared to HepG2 and HuH7 at low bortezomib concentration (20 nM). Moreover, it is evident an overall more contained increase of the necrotic marker LDH (Fig. 15) in JHH6 compared to HepG2 and HuH7. Finally, cell viability is constantly higher in JHH6 compared to other cell lines (Fig. 18). We can reasonably exclude a reduced bortezomib-mediated inhibition of the proteasome in JHH6 cells compared to HepG2 as similar decrease of proteasome activity was detected in the two cell lines (Fig. 11). These findings are in favour of a reduced sensitivity of JHH6 to bortezomib effects. Thus, HCC cell response to bortezomib is likely influenced by cell phenotype with possible clinical/therapeutic consequences.

In our experimental set up, beside inducing apoptosis (Fig. 20, and 22) in accordance to what detailed elsewhere [18-20], bortezomib promotes a potent anti-proliferative effect. Whereas in HepG2 and HuH7 this effect is detectable already at 20 nM, in JHH6 it is relievable at 40 nM, once again showing a reduced effect of bortezomib on JHH6 (Fig. 23, 24, 25 and 26). Notably, the effects on cell cycle distribution are similar in the three cell lines at 40 nM of bortezomib. A marked decrease of S phase cells, is paralleled by an increase of G_2/M phase cells with no major variation in G_1 and G_0 phase cells. These effects seem to be cell type specific as, for example, in prostate tumor cell PC-3 [21], in squamous cell carcinoma cell lines SCC [22] and in Ewing's sarcoma derived cells [23],

bortezomib induced an increase of both S and G_2/M phase cells. Regarding to HuH7, it was shown a marked increase of G_1/G_0 phase cells at 20 nM of bortezomib (Fig. 25). This fact could be related to the absence of G_1 cell cycle inhibitor $p16^{ik4a}$, as reported in Figure 7 and previously evidenced [24].

The decrease of S phase and the accumulation of G_2/M phase cells observed is consistent with the expression levels of the cell cycle regulators considered. In HepG2, a marked reduction of the major G_1 and G_1/S regulators such as cyclin D1, the transcription factor E2F1, the hyper-phosphorylated form of the retinoblastoma protein and the increase of the cyclin-dependent kinase inhibitors $p21^{waf1/cip1}$ and $p27^{kip1}$ (Figure 27A and 27B), prevent the cells to go through the G_1 phase thus determining a drastic reduction in the amount of S phase cells. The reduction of cyclin A2 and the increase of $p21^{waf1/cip1}$ [25], positive and negative regulators of G_2/M progression, respectively, can justify the G_2/M accumulation. Thus, in HepG2, a pathway through which bortezomib induces cell cycle arrest involves the increase of the levels of $p21^{waf1/cip1}$ and $p27^{kip1}$ which, in turn, inhibit the biological functions of the various cyclin/CdK complexes (see Fig. A for a scheme). Notably, as $p21^{waf1/cip1}$ transcriptional activation does not go in parallel with an increase of p53 protein levels (Fig. 27A), a p53-independent up-regulation of $p21^{waf1/cip1}$ seems to occur. Finally, we cannot exclude the contribution of $p16^{ink4a}$ to cyclin D1-CdK4 complex inhibition, as evidenced in Figure 44.

In addition to promote $p21^{waf1/cip1}$ and $p27^{kip1}$ up-regulation, bortezomib-induced cell cycle arrest is reinforced by the down-regulation of the transcription factor E2F1. This, in turn, leads to the transcriptional down-regulation of the E2F1 target genes cyclin D1, cyclin A2, CdK2 and to the reduction in the amount of the phosphorylated form of the retinoblastoma protein (Fig. 27B).

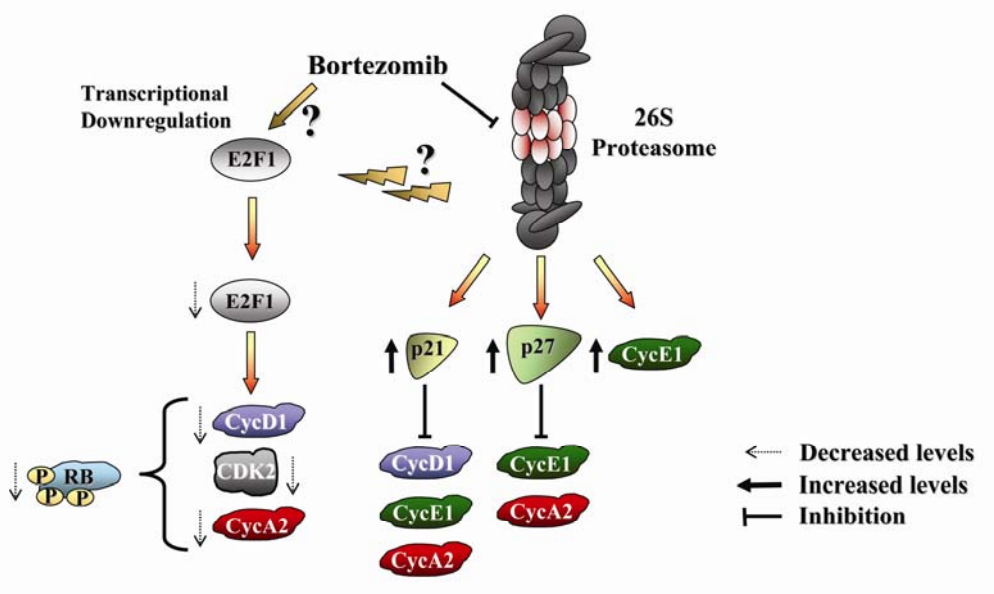

Figure A. A molecular model suggested on HepG2 cell line.

Cell cycle arrest is induced by increasing the levels of $p21^{waf1/cip1}$ and $p27^{kip1}$ which in turn inhibit the biological functions of the various cyclin/CdK complexes. Moreover, E2F1 transcript and protein amounts are reduced thus resulting in the transcriptional down-regulation of the E2F1target genes cyclin D1, cyclin A2 and CdK2 and E2F1 itself.

Notably, an siRNA-mediated depletion of E2F1 induces similar variations in the levels of E2F1-target genes [26] and in the amount of the phosphorylated form of pRB. This observation favors the idea that bortezomib-induced variation of E2F1 related genes is indeed dependent of E2F1 down-regulation.

HuH7 has a low differentiated HCC phenotype and this feature was clear evident after bortezomib treatments. A decrease of E2F1, of the hyper-phosphorylated form of pRB, of cyclin A2, and in minor part of CdK2, while an increase of $p21^{waf1/cip1}$ were detected (Fig. 28A and 28B), as observed in HepG2. Regarding to cyclin D1 and $p27^{kip1}$, a similar behaviour as in JHH6 (see below), was observed.

In JHH6, an overall less pronounced modification of the expression of the cell cycle regulators considered was observed (Fig. 29A and 29B). In particular, no major

variations in the protein levels of cyclin D1, CdK2 and $p27^{kip1}$, a more contained reduction of cyclin A2 and E2F1, the hyper-phosphorylated form of pRB and a more modest $p21^{waf1/cip1}$ elevation were observed. Despite these differences, a clear block of cell proliferation was evident. Whereas this may be due to an increased sensibility of JHH6 to the level variations of these cell cycle regulators, other mechanisms cannot be excluded.

In this regards, the reduction of LRH1 levels (Fig. 32 and 33), a gene product implicated in cell proliferation and tumorigenesis [27, 28] may contribute to explain JHH6 growth arrest. In HepG2, despite the marked reduction of the amounts of E2F1-pRB, a cellular circuit known to promote cyclin E1, and indirectly cyclin D1 expression [29, 30], no decrease of cyclin E1 mRNA levels were observed (Fig. 27B and 33). Our data indicate that cyclin E1 mRNA amounts may be maintained similar to that of non-treated cells by the increased expression of LRH1 (Fig 32 and 33), a protein shown to act as a cyclin E1 transcription factor in the hepatic lineage [30]. Interestingly, in HuH7, where the down-regulation of the E2F1-pRB circuit was similar, a major increase of LRH1 protein and mRNA was observed (Fig. 32 and 33) compared to HepG2. This fact could explain not only the cyclin E1 mRNA amounts observed, but also the increase of cyclin D1 mRNA detected (Fig. 28B).

In JHH6, where the down-regulation of the E2F1-pRB circuit was less pronounced than in HepG2 and HuH7, LRH1 expression was not increased but reduced. Thus, upon bortezomib-induced de-regulation of cell cycle mediators, the hepatic cell HepG2 and HuH7 seem to react by trying to maintain cyclin E1 synthesis *via* an inverse expression of E2F1 and LRH1. The reasons for the cellular necessity to keep cyclin E1 mRNA levels constant upon bortezomib treatment remain to be clarified. A possibility is that

proper cyclin E1 is required to minimize hepatic cell apoptosis. In this regard, cyclin E1 depletion by siRNAs induced a marked apoptosis in HepG2 [31].

Rather then being a general phenomenon, the up-regulation of LRH1 following E2F1 protein decrease in HepG2 and HuH7 seems to be a bortezomib-dependent effect. Indeed, upon siRNA-mediated depletion of E2F1 (siE2F1) no up-regulation of LRH1 was observed in HepG2 and also confirmed in JHH6 [26]. It is thus possible that, in HepG2 (but probably also in HuH7), the E2F1/LRH1 circuit might represent a pro-survival mechanism triggered by un-favorable survival conditions, i.e. bortezomib treatment.

Beside being useful to better characterize the cyclin E1-LRH1-E2F1 circuit, the siE2F1 allowed us to prove that it can be used to potentiate bortezomib effects on cell viability (Fig. 34). This observation may potentially open the way to an HCC therapeutic approach based on the combined administration of the siE2F1 and bortezomib, a strategy which could reduce bortezomib dosage and thus side effects. This observation may be particularly helpful for HCC cell types which show reduced bortezomib sensitivity such as JHH6.

One mechanism involved in JHH6 survival could be represented by the relation between E2F1-Pin1-cyclin D1. Maintenance of Pin1 and cyclin D1 levels are related to E2F1 activity. In addition, Pin1 contributes to cyclin D1 stabilization that in turn, creates a positive loop that stimulates E2F1 activity again, increasing survival (Figure 37, 38 and 45) [32].

The second mechanism could be related to the increase of eEF1A2 expression. We have reported that this factor is dramatically over-expressed in JHH6, the more tumorigenic cell line, compared with normal liver, HepG2 and HuH7 (Fig. 2). eEF1A2 mRNA and

protein levels are increased in JHH6 after bortezomib treatments (Fig. 46 and 48 respectively). It is tempting to speculate that eEF1A2 expression could lead to an overall increase in protein translation and an increase in bulk protein synthesis, enhancing JHH6 replication. Since cell division requires sufficient protein production to fulfill the metabolic and size requirements of two new daughter cells, it is hard to understand, however, how eEF1A2 could up-regulate the production of specific proteins related to cell survival, and further investigations occur [33]. It is a fact, nevertheless, that EEF1A2 gene silencing reduced cell viability as well as proliferation and increased apoptosis rates in HCC cell lines [34].

In conclusion, we have shown that in the HCC cell lines HepG2, HuH7 and JHH6, EEF1A1 and, in JHH6 only, EEF1A2 are over-expressed when compared to normal liver tissue and that this only in part depends on gene amplification. Moreover, the increased nuclear-enriched/cytoplasmic protein ratio of eEF1A and the marked raise of both gene expression detected in JHH6 do not relate with apoptosis resistance. Finally, the increased eEF1A expression is associated with an higher proliferation capacity in the undifferentiated JHH6 under sub-optimal growth conditions only. Future studies in HCC biopsies will contribute to further clarify the significance of eEF1A in the biology of hepatocellular carcinoma and will indicate its possible role in tumour aggressiveness.

Our data show the mechanisms regulating cell toxicity and proliferation inhibition effects of bortezomib on the HCC cell lines JHH6 and HuH7, expanding the knowledge on HepG2. The different phenotypes, hepatocyte-like for HepG2, low differentiated for HuH7 and undifferentiated for JHH6, together with the less overall effect of bortezomib on JHH6, suggests that *in vivo* not all HCC forms may respond similarly to bortezomib treatment. Despite this fact, the potent pro apoptotic effect reported [19], the cytotoxic

and anti-proliferative actions here described together with the *in vitro* observed negligible toxicity on normal human hepatocytes [34], make of bortezomib an attractive candidate for future experimentation in animal models, alone or in combination with specific molecular-targeted drugs, such as siRNA, possibly leading to a novel treatment for HCC.

3.1 REFERENCES

1. Tanner, M.M., et al., *Frequent amplification of chromosomal region 20q12-q13 in ovarian cancer.* Clin Cancer Res, 2000. **6**(5): p. 1833-9.
2. Hodgson, J.G., et al., *Genome amplification of chromosome 20 in breast cancer.* Breast Cancer Res Treat, 2003. **78**(3): p. 337-45.
3. Schlegel, J., et al., *Comparative genomic in situ hybridization of colon carcinomas with replication error.* Cancer Res, 1995. **55**(24): p. 6002-5.
4. Thorgeirsson, S.S. and J.W. Grisham, *Molecular pathogenesis of human hepatocellular carcinoma.* Nat Genet, 2002. **31**(4): p. 339-46.
5. Nagamori, S., et al., *[Protein secretion of human cultured liver cells].* Hum Cell, 1988. **1**(4): p. 382-90.
6. Fujise, K., et al., *Integration of hepatitis B virus DNA into cells of six established human hepatocellular carcinoma cell lines.* Hepatogastroenterology, 1990. **37**(5): p. 457-60.
7. Lichter, P., *Multicolor FISHing: what's the catch?* Trends Genet, 1997. **13**(12): p. 475-9.
8. Abbott, C.M. and C.G. Proud, *Translation factors: in sickness and in health.* Trends Biochem Sci, 2004. **29**(1): p. 25-31.
9. Gross, S.R. and T.G. Kinzy, *Translation elongation factor 1A is essential for regulation of the actin cytoskeleton and cell morphology.* Nat Struct Mol Biol, 2005. **12**(9): p. 772-8.
10. Munshi, R., et al., *Overexpression of translation elongation factor 1A affects the organization and function of the actin cytoskeleton in yeast.* Genetics, 2001. **157**(4): p. 1425-36.
11. Amiri, A., et al., *eEF1A2 activates Akt and stimulates Akt-dependent actin remodeling, invasion and migration.* Oncogene, 2007. **26**(21): p. 3027-40.
12. Grassi, G., et al., *The expression levels of the translational factors eEF1A 1/2 correlate with cell growth but not apoptosis in hepatocellular carcinoma cell lines with different differentiation grade.* Biochimie, 2007. **89**(12): p. 1544-52.
13. Gangwani, L., et al., *Interaction of ZPR1 with translation elongation factor-1alpha in proliferating cells.* J Cell Biol, 1998. **143**(6): p. 1471-84.
14. Lee, J.M., *The role of protein elongation factor eEF1A2 in ovarian cancer.* Reprod Biol Endocrinol, 2003. **1**: p. 69.
15. Duttaroy, A., et al., *Apoptosis rate can be accelerated or decelerated by overexpression or reduction of the level of elongation factor-1 alpha.* Exp Cell Res, 1998. **238**(1): p. 168-76.
16. Ruest, L.B., R. Marcotte, and E. Wang, *Peptide elongation factor eEF1A-2/S1 expression in cultured differentiated myotubes and its protective effect against caspase-3-mediated apoptosis.* J Biol Chem, 2002. **277**(7): p. 5418-25.
17. Talapatra, S., J.D. Wagner, and C.B. Thompson, *Elongation factor-1 alpha is a selective regulator of growth factor withdrawal and ER stress-induced apoptosis.* Cell Death Differ, 2002. **9**(8): p. 856-61.

18. Calvaruso, G., et al., *Bortezomib induces in HepG2 cells IkappaBalpha degradation mediated by caspase-8.* Mol Cell Biochem, 2006. **287**(1-2): p. 13-9.
19. Lauricella, M., et al., *JNK and AP-1 mediate apoptosis induced by bortezomib in HepG2 cells via FasL/caspase-8 and mitochondria-dependent pathways.* Apoptosis, 2006. **11**(4): p. 607-25.
20. Calvaruso, G., et al., *Hsp72 controls bortezomib-induced HepG2 cell death via interaction with pro-apoptotic factors.* Oncol Rep, 2007. **18**(2): p. 447-50.
21. Adams, J., et al., *Proteasome inhibitors: a novel class of potent and effective antitumor agents.* Cancer Res, 1999. **59**(11): p. 2615-22.
22. Sunwoo, J.B., et al., *Novel proteasome inhibitor PS-341 inhibits activation of nuclear factor-kappa B, cell survival, tumor growth, and angiogenesis in squamous cell carcinoma.* Clin Cancer Res, 2001. **7**(5): p. 1419-28.
23. Lu, G., V. Punj, and P.M. Chaudhary, *Proteasome inhibitor Bortezomib induces cell cycle arrest and apoptosis in cell lines derived from Ewing's sarcoma family of tumors and synergizes with TRAIL.* Cancer Biol Ther, 2008. **7**(4): p. 603-8.
24. Maeta, Y., et al., *Effect of promoter methylation of the p16 gene on phosphorylation of retinoblastoma gene product and growth of hepatocellular carcinoma cells.* Tumour Biol, 2005. **26**(6): p. 300-5.
25. Dulic, V., et al., *Nuclear accumulation of p21Cip1 at the onset of mitosis: a role at the G2/M-phase transition.* Mol Cell Biol, 1998. **18**(1): p. 546-57.
26. Baiz, D., et al., *Bortezomib arrests the proliferation of hepatocellular carcinoma cells HepG2 and JHH6 by differentially affecting E2F1, p21 and p27 levels.* Biochimie, 2008.
27. Schoonjans, K., et al., *Liver receptor homolog 1 contributes to intestinal tumor formation through effects on cell cycle and inflammation.* Proc Natl Acad Sci U S A, 2005. **102**(6): p. 2058-62.
28. Annicotte, J.S., et al., *The nuclear receptor liver receptor homolog-1 is an estrogen receptor target gene.* Oncogene, 2005. **24**(55): p. 8167-75.
29. Geng, Y., et al., *Regulation of cyclin E transcription by E2Fs and retinoblastoma protein.* Oncogene, 1996. **12**(6): p. 1173-80.
30. Botrugno, O.A., et al., *Synergy between LRH-1 and beta-catenin induces G1 cyclin-mediated cell proliferation.* Mol Cell, 2004. **15**(4): p. 499-509.
31. Li, K., et al., *Use of RNA interference to target cyclin E-overexpressing hepatocellular carcinoma.* Cancer Res, 2003. **63**(13): p. 3593-7.
32. Ryo, A., et al., *PIN1 is an E2F target gene essential for Neu/Ras-induced transformation of mammary epithelial cells.* Mol Cell Biol, 2002. **22**(15): p. 5281-95.
33. Johnston, G.C., J.R. Pringle, and L.H. Hartwell, *Coordination of growth with cell division in the yeast Saccharomyces cerevisiae.* Exp Cell Res, 1977. **105**(1): p. 79-98.
34. Ganten, T.M., et al., *Proteasome inhibition sensitizes hepatocellular carcinoma cells, but not human hepatocytes, to TRAIL.* Hepatology, 2005. **42**(3): p. 588-97.

Experimental procedures

4.1 Cell cultures

HepG2 and Hela cell lines were cultured in Dulbecco's modified Eagle's medium (DMEM) (Euroclone, Celbio, Devon, UK); JHH6 and HuH7 [1], derived from Japan Health Science Research Resources Bank (HSRRB, JCRB1030 depositor Dr. Nagamori, S). JHH6 and HuH7 were cultured in William's medium E (Sigma-Aldrich, St Louis, Mo, USA) and Dulbecco's modified Eagle's high glucose medium DMEM (Euroclone, Celbio, Devon, UK), respectively. All media contained 10% fetal bovine serum (FBS), 2 mM L-glutamine, 100 U/ml penicillin and 100 μg/ml streptomycin (Euroclone, Celbio, Devon, UK).

HepG2, HuH7 and JHH6 were assigned to high, medium and low hepatocyte differentiation grade on the basis of their capacity to synthesize albumin, a known marker of hepatic differentiation [2]. HepG2 and HuH7 displayed 3.6±1.6 and 1±0.1 albumin mRNA content, respectively, whereas no albumin mRNA was detected in JHH6 (data not shown). However, JHH6 were able to synthesize ferritin, thus showing a residual hepatic phenotype (data not shown).

4.2 RNA and DNA extraction (EEF1A1/2 genes)

Total RNA and DNA were extracted from 2 x 10^6 cells cultured near confluence by using Tri-reagent procedure (Sigma Chem. Co. St.Louis, MO, USA) and suspended in 50 μl of DEPC water or in an adequate volume of 8 mM NaOH, respectively. The quality and integrity of total RNA and DNA were evaluated by both gel electrophoresis and spectrophotometric determination (Spectra Max plus 384, Molecular Devices).

4.3 cDNA synthesis (EEF1A1/2 genes)

The samples were treated with amplification grade DNase I (Sigma Chem.Co, St.Louis) following the producer's protocol and directly used for reverse transcription. 2 μg of total RNA solution were incubated at 80°C for 10 min and then at 25°C with 0.01 mg/ml random hexamers (Pharmacia, Biotech, Uppsala, Sweden) for 10 min. Subsequently, reverse transcription was performed as described above.

4.4 Quantification of the mRNA levels and gene amplification for EEF1A1/2

Real Time PCR was performed in single-plex reactions (7900/HT Sequence Detection System - Applied Biosystems). The primers used are reported in Table 2, while Table 3 reports primers used for gene amplification. All amplifications were conducted in a final volume of 25 μl of SYBR/Master Mix buffer (Applied Biosystems-Applera Corporation,USA), containing primers (300 nM each), SYBR green, dNTPs (200 mM each), Taq DNA polymerase and 1 μl of cDNA reverse transcription solution. 28S rRNA, EEF1A1 and EEF1A2 were submitted to 40 cycles of amplification with enzyme activation at 50°C for 2 min, pre-denaturation at 95°C for 10 min, denaturation at 95°C for 15 sec, annealing and extension at 62° for 60 sec. EEF1A1, EEF1A2, and 28S rRNA, were analyzed for each samples in a unique plate to assure the same amplification efficiency. The samples were treated by DNase prior to perform reverse transcription in order to completely exclude the possibility that amplicons of EEF1A could derived from non-actively transcribed retropseudogenes [3].

The relative amounts of the mRNA of target genes were normalized by 28S rRNA content.

Table 2. EEF1A1/2 Real Time PCR primers pair.

GenBank Number	mRNA	Primer pair	Amplification Region	Length (bp)
NM_001402	EEF1A1	(FwEF1A) 5'-AACATTGTCGTCATTGGACA-3' (RvBL5) 5'-ACTTGCTGGTCTCAAATTTC-3'	88-316	228
NM_001958	EEF1A2	(FwEEF1A2) 5'-GCCACCGTCAATAGGTGGAC-3' (Rv3) 5'-TGATGTGGGTCTTCTCCTTG-3'	9-191	182
M11167	28S rRNA	(Fw28S) 5'-TGGGAATGCAGCCCAAAG-3' (Rv28S) 5'-CCTTACGGTACTTGTTGACTATCG-3'	282-365	83

Table 3. EEF1A1/2 gene amplification primers pair.

GenBank Number	DNA	Primer pair	Restriction digestion	Length (bp)
J04617	EEF1A1	(FwEF1A) 5'-ACATTGTCGTCATTATCGAC -3' RvEEF1A1 DNA-I 5'-TTGATCTTTCCCTTTCTGGT-3'	MnII + 102 + 49+ 39 + 9	151
AF163763	EEF1A2	FwEEF1A2 DNA 5'-ACCAAACATGGGGGCTTGGT-3' RvEEF1A2 I-E 5'-TGATGTGGGTCTTCTCCTTG-3'	PstI 134 + 71	206

4.5 Bortezomib experimental set up

Unless otherwise indicated, in all the experiments the cells were seeded at $3.8x10^3$ cells/cm^2 in 6-wells plate, allowed to adhere 24 hr, cultured for two days in the presence of complete medium and bortezomib (once administered). The bortezomib was in the commercial form Velcade (Janssen-Cilag International N.V. – 0.09 mg Bortezomib/1 mg Velcade), resuspended in phosphate buffer saline solution (PBS).

4.6 Assay for proteasome activity

Cells were collected, disrupted (by three freezing/thawing steps using liquid nitrogen) in 10 volumes of HEPES buffer (25 mM, pH 7.5) containing: 2.5 mM $MgCl_2$, 0.5 mM DTT and then centrifuged at 10000xg for 30 min, all at 4°C [4]. Sixty μg of proteins were resuspended in 250 μl of HEPES buffer containing ATP (GE Healthcare, 5 μM) and Suc-LLVY-AMC proteasome 26S substrate (BostonBiochem, 1 mM). The reaction was run for 45 min at 37°C, quenched by adding 250 μl ice-cold ethanol and filled up to 1.5 mL with H_2O. Each sample was read in triplicate using a 96-black wells microtiter plate (Plate Chamaleon - Hidex). Inhibition of 26S proteasome activity by bortezomib was calculated comparing the fluorescence value of the maximal proteosome activity (non-treated cells control) with the fluorescent values of bortezomib-treated cells using the Mikro Win 2000 software.

4.7 Cell morphology and count

The evaluations of cell morphology and number were made by direct microscopic observation (Nikon Eclipse TS100) and with Thoma's haemocytometer chamber, respectively. Cell viability was evaluated by 0.05% trypan blue dye staining (w/v in PBS) (1:1, v/v). Total viable cell number was calculated by the formula:

$$X_n = N° \times 2 \times 10^4$$

where X_n is the cell number in 1 ml of sample, N° is the viable cells number, 2 is the dilution factor with trypan blue dye and 10^4 is the Thoma's haemocytometer conversion factor.

4.8 Measurement of HepG2 colony number and area

Cells were washed gently by PBS, then fresh medium was added before analysis by an inverted microscope (Leica Mycrosystem, Wetzlar, Germany). Colony morphometrical analysis and number were calculated using the Sigma Scan Pro program, considering five fields for each treatment, each containing at least 20 events (magnification = 5x).

4.9 Cytotoxicity assays

Extracellular lactate dehydrogenase (LDH) was evaluated by a kit (BioVision Prod., Mountain View CA) according to manufacturer instructions. 100 µl of cells supernatant were transferred into an optically clear 96-well plate in triplex and added with 100 µl of reaction solution (containing Catalyst/Dye solutions at 1/45 proportions). Samples were incubated for 30 min at room temperature protecting plate from light exposure. Detection of LDH enzyme amount was performed at 500 nm using a spectrophotometer (Spectra Max plus 384, Molecular Devices). As positive control, triton X-100-treated cells (at 1% final concentration) was used; free medium represented the negative control.

The percentage of cytotoxicity was calculated applying the formula:

$$\text{Cytotoxicity (\%)} = \frac{(\text{test sample} - \text{negative control})}{(\text{positive control} - \text{negative control})} \text{ x100}$$

4.10 Cell viability assays

MTT assay was performed in 96-wells microtiter plates, where cells were seeded at $1.25x10^3$/well and $0.6x10^3$/well for the 2 and 6 days assay, respectively, in 200 µl of complete medium. After 24 hr of incubation, bortezomib was added directly to the medium. Each sample was analysed in triplicate. 3-(4,5-dimethylthiazol-2-yl)-2,5-diphenyl-tetrazolium bromide (MTT, Sigma-Aldrich, St Louis, Mo, USA) test was conducted according to standard procedures, adding 25 µl (4 mg/ml) of MTT solution for each well directly. After 4 hr cell viability was monitored at 590 nm spectrophotometrically (Spectra Max plus 384, Molecular Devices).

4.11 Apoptosis evaluation

Apoptosis was evaluated by the Annexin V test (Bender – Med System, Burlingame, CA) and propidium iodide (PI) staining (BD Pharmingen) according to manufacturer's instructions. Briefly, cells were seeded at 3.8 $x10^3$ cells/cm^2 in 6 wells plates and kept in complete medium for 2.5 days (70% confluent cells) or in complete medium overnight and then in serum-free medium (starved cells) for two days. The cells were then collected, resuspended in binding buffer at the concentration of 2-5$x10^5$ cell/ml and incubated with annexin V antibody for 15 min. Cells were then sedimented, resuspended in the binding buffer and incubated with propidium iodide for 20 min at room temperature. After a final washing step, cells were resuspended in 0.5 ml of PBS/0.5% BSA (bovin serum albumin) and analyzed by flow cytometry (FACSCanto, BD) using the DIVA software.

Annexin V positive cells were considered apoptotic, events positive for propidium-iodide only were considered cellular debris. As positive control, an aliquot of cells kept

in complete medium was treated with 1 μM staurosporin (Sigma Chem.Co, St.Louis) for 3 hr prior to harvesting.

4.12 Cell cycle phases evaluation

Cell cycle phases can be evaluated by the measurement of bromodeoxyuridine (BrdU) incorporation into newly synthesized DNA and propidium iodide staining. Moreover, to distinguish between G_0 and G_1 phase cells, Ki-67 test was performed. Ki-67 is a nuclear cell proliferation-associated antigen expressed in all cell cycle phases except G_0 stage [5]. The cells were seeded at 3.8 $x10^3$ cells/cm^2 in 6 wells plates and 20 hr before harvesting (70% confluent cells), they were pulsed with bromodeoxyuridine (BrdU) at a final concentration of 10 μM. Cells were prepared for BrdU staining by resuspension in 70% ice cold Et-OH over night. After a washing step with PBS/0.5% BSA, the cells were treated with 1M HCl/0.5% BSA for 1 hr. After another washing step, the cells were resuspended in 0.1 M $Na_2B_4O_7$ pH 8.5 for 2 min and then washed again with PBS/0.5% BSA. Each sample was incubated with fluorescein-isothiocyanate (FITC) – conjugated mouse monoclonal antibody (BD PharMigen) anti-BrdU for 1 hr. As background control, one sample was incubated with fluorescein-isothiocyanate (FITC) – conjugated mouse IgG_1 Isotype Control. After a washing step, the samples were incubated with 4 μl PI Staining Solution (BD Pharmingen) and 100 μl Ribonuclease A 100 μg/ml (Sigma) for 1 hr. Cells, resuspended in PBS containing 0.5% BSA, were analyzed by flow cytometry (FACScanto, BD) using the DIVA software. Ki-67 staining (BD PharMigen) was performed according to manufacturer instructions.

4.13 Proliferation assay

Senescence associated test [6] was performed between one and four days after cells reached confluence. At seeding a sterile cover glass for microscopy was placed on the bottom of a 3 cm diameter well dish. At different time points, the cells on the cover glass were rapidly washed with PBS and fixed with 2 ml of Fixation Solution (2% w/v Formaldehyde, 0.2% w/v Glutaraldehyde in PBS) for 20 min. Subsequently, cells were quickly washed twice with PBS and covered with 2 ml of Staining Mixture. The staining mixture was obtained adding to a previously prepared Staining Solution (40mM Sodium Citrate/Orthophosphoric acid, pH 6; 150 mM NaCl; 2 mM $MgCl_2$) Potassium Exacianoferrate (II) and Potassium Exacianoferrate (III), to reach a final concentration of 5 mM, and X-Gal (Sigma) at a final concentration of 1g/l. Staining was performed over night in the dark at 37°C. Subsequently, the supernatant was removed, cells rapidly washed twice in PBS, then in H_2O and finally over-layered by a drop of glycerol. The cover glass was fixed on a microscopy slide with cells turned over the glycerol drop (to avoid air bubble formation). After 30 minutes of gentle heating at 37°C to dry any excess of water, cover glasses were sealed and analysed by microscope.

4.14 Protein extraction procedures

Protein extracts were prepared from aliquots of $6x10^6$ subconfluent (70% confluent) cells that were washed with phosphate buffer saline solution (PBS) and lysed as described by Mansilla *et al.* [7].

Cytoplasmic and nuclear-enriched extracts were prepared as described by Scaggiante *et al.* [8]. Cells were resuspended in 400 μl/10^6 cells ice-cold 10 mM Hepes pH 7.9, 1.5 mM $MgCl_2$, 10 mM KCl (solution A) containing 1 mM dithiotreitol, 1 mM

phenylmethylsulphonyl fluoride, and 0.05% Nonidet P-40. After 10 minutes of incubation on ice, the cells were controlled by trypan blue dye incorporation to monitor membrane cell disruption and, if necessary, the incubation time was increased up to reach 90% cell dye inclusion. The cells were then centrifuged at 800xg for 5 minutes at 4°C, the supernatant containing the cytoplasm was collected and the pellet was rinsed once with solution A without Nonidet P-40. The cytoplasmic extract was complemented with 0.5 M NaCl, 25% glycerol and 0.2 mM EDTA (final concentrations) and stored in small aliquots at -80°C. The pellet containing nuclei was resuspended in 80 µl/10^6 cells ice-cooled solution B (20 mM Hepes, pH 7.9, 420 mM NaCl, 1.5 mM $MgCl_2$, 0.2 mM EDTA, 25% glycerol) containing 1 mM dithiotreitol and 1 mM phenylmethylsulphonyl fluoride. After 20 min incubation on ice with constant stirring, the suspension was vortexed for 60 seconds, then centrifuged at 10000xg for 10 minutes at 4°C. The supernatant containing nuclear-enriched extract was recovered and stored in small aliquots at -80°C.The protein concentration was evaluated by BCA protein assay reagent (Pierce, Rockford, IL).

4.15 Western blotting

Western blotting was performed with 20-40 µg of proteins separated by 12% SDS-PAGE, and transferred onto a 0.22 µm nitrocellulose membrane (Schleicher & Schuell, Keene, NH). The antibodies used were: mouse anti-eEF1A (0.5 µg/ml) (Upstate Biotechnology, Lake Placid, NY); mouse anti-EF1A2 (Abnova); mouse anti-$p21^{waf1/cip1}$ (0.7 µg/ml), mouse anti-$p27^{kip1}$ (1 µg/ml), mouse anti-p53 DO-1 (0.4 µg/ml), mouse anti-CdK 2 (1 µg/ml), rabbit anti-cyclin D1 (0.4 µg/ml), rabbit anti-cyclin A (0.4 µg/ml), rabbit anti-SRF (0.7 µg/ml) and rabbit anti-GAPDH (0.2 µg/ml) (Santa Cruz

Biotechnology, California, USA); mouse anti-$p16^{ink4a}$ (2 μg/ml), mouse anti-cyclin E1 (0.5 μg/ml), mouse anti-E2F1 (5 μg/ml), mouse anti-RB (1.25 μg/ml), mouse anti-PARP (0.5 μg/ml) (BD Bioscience Pharmingen San Jose, California, USA). Antibody rabbit anti-pin1 was gently gifted by prof. G. Del Sal (Dept. of Life Sciences, University of Trieste, Italy).

After incubation, the corresponding secondary horseradish peroxidase antibodies was used (Santa Cruz Biotechnology). The blots were developed by using an enhanced chemiluminescent substrate (Supersignal West Pico, Pierce, Rockford, IL).

For each protein considered, al least three independent western blottings were performed.

4.16 Quantification of mRNA levels, RT-PCR and Real Time PCR

Total RNA was extracted using RNeasy Mini kit (Qiagen S.p.A., Italy). The quality, integrity and quantification of total RNA was evaluated by spectrophotometric determination using a Lab-on-Chip-System Bioanalyzer 2100 (Applera Corporation, USA) and a NanoDrop ND-1000 (CelBio, Euroclone, Italy). Reverse transcription was performed with 1 μg of total RNA by oligo-dT_{16} and murine myeloblastosis virus reverse transcriptase (Applera Corporation, USA), using the master mix solution reported on Table 4. Real Time PCR was performed in triplicate in a final volume of 10 μL of SYBR/Master Mix buffer (Applied Biosystems-Applera Corporation,USA), containing primers (300 nM each), SYBR green, dNTPs (200 mM each), Taq DNA polymerase and 1 μl of cDNA reverse transcription solution. (7900/HT Sequence Detection System - Applied Biosystems). The primers (300 nM, MWG Biotech, GA) used to detect cell cycle regulators by Real Time PCR are reported in Table 5. Primers

annealing temperature and specific amplification products were first evaluated by step-gradient PCR and gel electrophoresis.

Table 4. Reverse transcription Master Mix

Component	Final concentration
25 mM $MgCl_2$ solution	5 mM
10X PCR Buffer II	1X
Oligo dT_{16}	2.5 µM
dATP	1 mM
dCTP	1 mM
dGTP	1 mM
dTTP	1 mM
RNase inhibitor	1 U/µL
MuLV Reverse Transcriptase	2.5 U/µL

Real time PCR amplification steps were: pre-denaturation at 95°C for 10-min, 40 cycles of amplification with denaturation at 95°C for 15-sec, annealing at proper temperature for 60-sec and extension at 72°C for 30-sec. A final extension at 72°C for 10-min and a dissociation stage (95°C/60°C/95°C for 15-sec. each) was then added. GAPDH house-keeping gene was used to normalize the relative mRNA amounts.

Table 5. Real Time PCR primers pair (cell cycle regulators).

GenBank Number	mRNA	Primer pair	T_A (°C)	Amplif. Region	Length (bp)
NM_001237	CCNA2	(F) 5'-GAAGACGAGACGGGTTGCA-3' (R) 5'-GAGATTCAGCTGGCTTCTTCTG-3'	62	308-459	151
NM_053056	CCND1	(F) 5'-CCGTCCATGCGGAAGATC-3' (R) 5'-CCTCCTCCTCGCACTTCTGT-3'	62	369-438	70
NM_001238	CCNE1	(F) 5'-TGCCTGTACTGAGCTGGGCA-3' (R) 5'-GGCTGCAGAAGAGGGTGTTG-3'	60	497-608	112
NM_001798	CDK2	(F) 5'-CAAGCTGCTGGATGTCATTC-3' (R) 5'-AGCAGCTGGAACAGATAGCTCT-3'	62	429-572	144
NM_000389	CDKN1A	(F) 5'-AGTGGACAGCGAGCAGCTGA-3' (R) 5'-CGAAGTTCCATCGCTCACGG-3'	62	166-248	83
NM_004064	CDKN1B	(F) 5'-CGGTGGACCACGAAGAGTTAA-3' (R) 5'-GGCTCGCCTCTTCCATGTC-3'	60	569-634	65
NM_005225	E2F1	(F) 5'-CCAGGAAAAGGTGTGAAATC-3' (R) 5'-AAGCGCTTGGTGGTCAGATT-3'	62	466-539	74
NM_002046	GAPDH	(F) 5'-CCCATCACCATCTTCCAGGAG-3' (R) 5'-CTTCTCCATGGTGGTGAAGACG-3'	60/62	319-423	105
NM_205860	NR5A2	(F) 5'-CCGACAAGTGGTACATGGAA-3' (R) 5'-ACTCATGAGGTTGTTGAGGG-3'	60	1382-1474	92
NM_006221	PIN1	(F) 5'-TTGAGTCTCTGGCCTCACAGTTCA-3' (R) 5'-CAAACGAGGCGTCTTCAAATGGCT-3'	60	308-418	110
NM_000546	TP53	(F) 5'-TACAAGCAGTCACAGCACATGACG-3' (R) 5'-ACACGCAAATTTCCTTCCACTCGG-3'	60	684-805	122

4.17 Anti-E2F1 siRNA

A preliminary selection of siRNAs was conducted according to previously reported guide lines [9, 10].

Anti-E2F1 siRNA (siE2F1)

Sense strand: 5'-GAGGAGUUCAUCAGCCUUU-3'

Antisense strand: 5'-AAAGGCUGAUGAACUCCUC-3'

As control a siRNA directed against the luciferase gene (siGL2) was analysed in parallel:

Sense strand: 5'-CGUACGCGGAAUACUUCGA-3'

Antisense strand: 5'-UCGAAGUAUUCCGCGUACG-3'

For each cell line considered, uptake studies were previously performed using variable amounts of transfection reagent and siRNA conjugated with a fluorescent-isothiocyanate (FITC) molecule, in order to optimize the weight ratio of siRNA/transfection reagent. Transfection time was also optimized (1-6 hours), evaluating the amount of FITC positive cells using a fluorescence microscopic inspection (Leica Mycrosystem, Wetzlar, Germany). A quantitative evaluation of FITC positive transfected cells was carried out by flow cytometry (FACScanto, Becton Dickson, DIVA software) after cell trypsinization.

The optimized transfection condition for HCC cells was 7.65 μg of liposome (Lipofectamin2000 – 1mg/mL, Invitrogen) for HepG2 and 2.55 μg of liposome for HuH7 and JHH6 cells, mixed with 125 μl of medium (Optimem, Invitrogen) containing 2.55 μg of the selected siRNAs and incubated for 15 minutes at room temperature. After 20 min, necessary to allow liposome/siRNA complexes formation, the solution was added to 800 μl of DMEM High Glucose medium to reach a final siRNA concentration of 220 nM and then administered to HCC cells seeded in 96-wells plate at $4x10^3$/well. After three hours of incubation the tranfection medium was replaced by a proper volume of complete medium and the cells maintained in culture for the indicated times.

For the evaluation of the combined effects of siE2F1 and bortezomib, the cells were seeded in a 96-wells microtiter plate at $4x10^3$/well. Following siE2F1 transfection, the

cells were incubated for one day with complete medium and then treated by 20 nM bortezomib and cultured for two days before performing the MTT viability assay. Each sample was analysed in triplicate.

4.18 Two-color microarray-based gene expression analysis

Two-color microarray-based gene expression analysis was performed according to Agilent Technologies protocol, using Agilent Scan B (supported with GenePix 4000B scanner and Feature Extraction software, version 9.5.3. – Agilent Technologies, USA).

In particular, total RNA was extracted from cell cultures using RNeasy Mini kit (Qiagen S.p.A., Italy). The quality, integrity and quantification of total RNA were evaluated by spectrophotometric determination using a Lab-on-Chip-System Bioanalyzer 2100 (Applera Corporation, USA) and a NanoDrop ND-1000 (CelBio, Euroclone, Italy). Fluorescent cRNA (complementary RNA) was created using Agilent's Quick Amp Labeling Kit (Agilent Technologies, USA) with a sample input of total RNA of 200 ng. Complementary RNAs were purified using RNeasy Mini kit (Qiagen S.p.A., Italy) and quantification was performed using a NanoDrop ND-1000. According with Agilent protocol, for a 4x44K microarray, we used 825 ng of each cRNAs.

4.19 Statistical analysis

P values were calculated using the ANOVA one way test led by MS Excel. P values $\leq$ 0.05 were considered to be statistically significant.

4.20 REFERENCES

1. Fujise, K., et al., *Integration of hepatitis B virus DNA into cells of six established human hepatocellular carcinoma cell lines.* Hepatogastroenterology, 1990. **37**(5): p. 457-60.
2. Lund, A., et al., *Assignment of human elongation factor 1alpha genes: EEF1A maps to chromosome 6q14 and EEF1A2 to 20q13.3.* Genomics, 1996. **36**(2): p. 359-61.
3. Madsen, H.O., et al., *Retropseudogenes constitute the major part of the human elongation factor 1 alpha gene family.* Nucleic Acids Res, 1990. **18**(6): p. 1513-6.
4. Powell, S.R., K.J. Davies, and A. Divald, *Optimal determination of heart tissue 26S-proteasome activity requires maximal stimulating ATP concentrations.* J Mol Cell Cardiol, 2007. **42**(1): p. 265-9.
5. Scholzen, T. and J. Gerdes, *The Ki-67 protein: from the known and the unknown.* J Cell Physiol, 2000. **182**(3): p. 311-22.
6. Dimri, G.P., et al., *A biomarker that identifies senescent human cells in culture and in aging skin in vivo.* Proc Natl Acad Sci U S A, 1995. **92**(20): p. 9363-7.
7. Mansilla, F., et al., *Deconstructing PTI-1: PTI-1 is a truncated, but not mutated, form of translation elongatin factor 1A1, eEF1A1.* Biochim Biophys Acta, 2005. **1727**(2): p. 116-24.
8. Scaggiante, B., et al., *Human cancer cell lines growth inhibition by GTn oligodeoxyribonucleotides recognizing single-stranded DNA-binding proteins.* Eur J Biochem, 1998. **252**(2): p. 207-15.
9. Poliseno, L., et al., *The energy profiling of short interfering RNAs is highly predictive of their activity.* Oligonucleotides, 2004. **14**(3): p. 227-32.
10. Poliseno, L., et al., *RNA-based drugs: from RNA interference to short interfering RNAs.* Curr Pharm Biotechnol, 2004. **5**(4): p. 361-8.